University of Calgary

PRISM Repository **https://prism.ucalgary.ca**

The Vault Open Theses and Dissertations

2014-09-04

Complex Formation of Pb(II) with Cysteine, Penicillamine and N-acetylcysteine

Sisombath, Natalie Sinh

Sisombath, N. S. (2014). Complex Formation of Pb(II) with Cysteine, Penicillamine and N-acetylcysteine (Master's thesis, University of Calgary, Calgary, Canada). Retrieved from https://prism.ucalgary.ca. doi:10.11575/PRISM/25383

http://hdl.handle.net/11023/1722

Downloaded from PRISM Repository, University of Calgary

UNIVERSITY OF CALGARY

Complex Formation of Pb(II) with Cysteine, Penicillamine and *N*-acetylcysteine

by

Natalie Sinh Sisombath

A THESIS

SUBMITTED TO THE FACULTY OF GRADUATE STUDIES

IN PARTIAL FULFILMENT OF THE REQUIREMENTS FOR THE

DEGREE OF MASTER OF SCIENCE

DEPARTMENT OF CHEMISTRY

CALGARY, ALBERTA

September 2014

© Natalie S. Sisombath 2014

Abstract

The mechanism of lead poisoning and interest in metal toxicity has been a growing area of study since the late 1950s. In order to gain insight on how toxic metals behave physiologically, simple molecules can first be used to model the environments.

Complex formation between Pb(II) and thiol-containing ligands *D*-penicillamine, *L*-cysteine and *N*-acetyl-*L*-cysteine were investigated in this study. The complexes formed were studied by ^{207}Pb, ^{13}C, ^{1}H NMR, UV-Vis, ESI-MS, and X-ray absorption spectroscopy. The results of the study provide spectroscopic finger prints for Pb(II) coordination environments relevant to biological systems. The study revealed that small structural changes between each ligand, plays a large role in the manner at which they bind to the lead(II) centre.

Acknowledgements

First, I would like to extend my appreciation to my supervisor, Dr. Farideh Jalilehvand, for her hard work and dedication. Your enthusiasm and curiosity in all aspects of my project pushed me to make my project successful and enjoyable. Thank you for time and kind words. I would also like to thank Prof. Roland Roesler, Prof. George Shimizu, and Prof. Ann-Lise Norman for their time serving on my committee.

I sincerely thank Qiao Wu, Wade White, Michelle Forgeron, Johnson Li and Dorothy Fox, who have all worked with me and guided me through out my time as a graduate student in the instrumentation facility. The greatest appreciation goes to the many friends I have made here, highlighting Ms. Kamila Bladek, who encouraged me, had helpful discussions with, and shared many coffees and lunches over the past two years. My graduate experience would not have been the same with out you, thank you.

Finally, I would like to acknowledge my biggest supporters, my parents, sister, future mother-in-law and Fiancé. Thank you for helping me succeed and get to where I am today, I could not do it with out your unconditional love and support.

Dedication

To my Fiancé,

my constant foundation and support, even cross-country.

Table of Contents

List of Tables

List of Figures

List of Symbols, Abbreviations and Nomenclature

Symbol	Definition
α	phase shift
ALA	aminolevulinate
ALAD	δ-aminolaevulinic acid dehydratase
B	magnetic field
β	stability constant
BB10	broad band 10 mm NMR probe
BLL	blood lead level
χ	EXAFS oscillation
C	concentration
c	speed of light
CN	coordination number
CSD	crystal structure database
COOP	cystal orbital overlap populations
DFT	density functional theory
δ	chemical shift
d	crystal lattice spacing
E	energy
eff	effective
ESI-MS	electroscpray ionization mass spectrometry
EXAFS	extended X-ray absorption fine structure
f_{eff}	effective amplitude function
FT	Fourier transform
γ	gyromagnetic ratio
GeV	giga electron volts
GSH	glutathione
ħ	Planck's constant
HNACOMe	*N*-acetyl-*L*-cysteine methyl ester
H_2Cys	cysteine
H_2NAC	*N*-acetyl-*L*-cysteine
H_2Pen	*D*-penicillamine
I	current
K	equilibrium constant
k	photoelectron wavevector
λ	wavelength
Λ	photoelectron mean free path
L	ligand
LAXS	large angle X-ray scattering
LMCT	ligand to metal charge transfer
μ	linear absorption coefficient
μ	magnetic moment
m	mass
M	metal
m_e	mass of an electron

mol	moles
N	coordination number
NBO	natural bond orbital
NMR	nuclear magnetic resonance
ϕ_{ij}	phase shift
θ	angle
R	distance
RBA	rear beam attenuator
RF	radiofrequency
ROS	reactive oxygen species
RT	room temperature
σ	disorder parameter
S_0^2	amplitude reduction factor
SSRL	Stanford synchrotron radiation lightsource
UV	ultraviolet
vis	visible
ω	Larmor frequency
XANES	X-ray absorption near edge structure
XAS	X-ray absorption spectroscopy
Z	atomic number
ZPP	zinc protoporphyrin

Chapter One : Introduction

1.1. Lead chemistry

1.1.1 Chemical properties

1.1.1.1 Stereochemistry

Lead occurs with four natural isotopes ^{204}Pb (1.4 %), ^{206}Pb (24.1 %), ^{207}Pb (22.1 %) and ^{208}Pb (52.4 %).[1] It can easily lose its two *6p* valence electrons to form the Pb^{2+} ion. The *6s* electrons are said to be stereochemically active when the position of ligands around Pb(II) create a void in the coordination sphere. Such Pb(II) coordination system is referred to as a *hemidirected* geometry, while ligands encompassed symmetrically around Pb(II) have a *holodirected* coordination geometry (Figure 1).[2] Shimony-Livny et al. performed a crystal structure database (CSD) survey to identify conditions that influence whether or not the lone pair is stereochemically active. Based on coordination number (CN) around Pb(II), it was found that only hemidirected coordination existed for CN 2 to 5, while only holodirected geometry was present for CN 9 and 10. Both geometries were found for CN 6 to 8. Compounds with higher CN showed a tendency for several Pb-O interactions, and rarely formed hemidirected geometries. Compounds with a stereochemically active lone pair typically had shorter Pb-X bond distances opposite the position of the void.[2]

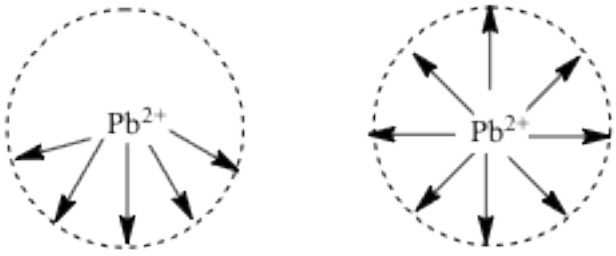

Figure 1: Hemidirected and holodirected coordination of lead(II).

The void in Pb(II) complexes with low coordination numbers and in heavier main group elements is commonly attributed to the "inert pair effect".[3–5] Traditionally, the inert property of the ns^2 electron pair could be described by relativistic effects. As electron velocity approaches the speed of light, especially in heavier elements with higher effective nuclear charge, increased mass of inner electrons is substantial.[6,7] Relativistic contraction of *s*-orbitals results in increased shielding of the nucleus and expansion of *d* and *f*-orbitals, as well as *p*-orbitals to a lesser extent.[8,9] More recent studies using density functional theory (DFT) have shed light on the asymmetric electron density that generates voids in Pb(II) complexes. Walsh and Watson performed DFT calculations on symmetric and asymmetric Pb(II) complexes, and investigated the underlying interactions using integrated crystal orbital overlap populations (COOP).[10] According to this study, lead(II) complexes with asymmetric distorted structures have a stereochemically active lone pair, which is the result of interactions between the Pb^{2+} cation and the coordinated ligand. Natural bond orbital (NBO) analyses supported the stabilization of Pb-*6p* orbitals in the presence of Pb-*6s* and ligand-*np* mixing, observing increased *p*-character in the lone pair only in hemidirected coordination.[2] Other factors influencing hemi- or holo-directed coordination geometry include ligand repulsion, high charge transfer, ionic bonding and repulsive interaction within ligands.[11] Along with coordination number, coordination geometries showed a dependence on the hardness or softness of donor atoms. Soft atoms are described as possessing diffuse, easily polarisable orbitals.[12] Oxygen and nitrogen donor atoms are defined as hard bases, where hardness is decreasing $O^{2-} > NH_3$; and sulfur donors are considered soft bases. In coordination compounds, Pb^{2+} is a Lewis acid, accepting electron pairs, while ligands are electron-donating Lewis bases. Acid-base interactions are strongest between soft-soft or hard-

hard pairs, rather than mixed hard-soft pairs.[12] Soft interactions generally result in covalent bonds while hard interactions usually result in ionic bonds.

1.1.1.2 Solution chemistry

In aqueous solution, ions are surrounded by water molecules (hydrated) to different extents, depending on ionic radius, charge density, and pH of the solution. A DFT study determined that six to eight H_2O molecules are coordinated to Pb^{2+} in aqueous solution, with a holodirected geometry above coordination number 6.[13,14] The structural arrangement of water around the Pb(II) ion is found as a result of direct lone pair donation from oxygen into molecular orbitals with mainly Pb *6p* and *5d* character. The Pb-O bond studied by extended x-ray absorption fine structure (EXAFS) and large angle x-ray scattering (LAXS)of the hydrated lead(II) ion in solution, possessed a bond distance of 2.54(1) Å.[14] The hydrated ion was found to be six-coordinate with hemi-directed coordination. Hydrolysis of metal ions occurs when the acidity of water protons in the first hydration sphere becomes high enough to form a hydroxo metal species and a hydronium ion in the second hydration shell (equation 1).[15] The hydrolysis constant for the first coordinated water molecule (K_{11}) is a common method of defining the extent of hydrolysis of a metal ion. The hydrolysis constant for divalent metal ions and the first coordinated proton (pK_{11}) has a direct correlation to the cationic charge (Z), the distance between the metal ion and the water molecule (r_{M-OH_2}), and the number of water molecules in the first hydration shell *n* (equation 2).

$$M^{Z+}(OH_2)\,(aq) + H_2O \leftrightarrow M(OH)^{(Z-1)+}(aq) + H_3O^+ \quad (1)$$

$$pK_{11} \propto \frac{Z^2}{(r_{M-OH_2}) \times n} \quad (2)$$

The pK_{11} value reported for Pb^{2+} is 8.0, meaning it is not as easily hydrolyzed as some trivalent metal cations, and results in aqua complexes with low hydroxo coordination numbers.[15] Two main Pb-OH oligomers $[Pb_4(OH)_4]^{4+}$ and $[Pb_6O(OH)_6]^{4+}$ have been previously studied by X-ray scattering and vibrational spectroscopy in aqueous solutions.[16,17] Both oligomers possess structures where the Pb(II) electron lone pairs point outwards, largely restricting higher degrees of hydration.[15] At low pH (< 5.25) the tetramer dominates in solution, while formation of the hexamer was found to be ca. pH 8.5. At neutral pH, formation of a trimer $[Pb_3(OH)_4]^{2+}$ precipitates.[18] All three oligomers appear in three distinct phases, and can be obtained in crystalline form under suitable conditions. Another study, however, suggests that mononuclear complexes are dominant over polynuclear species in aqueous solution, especially under typical environmental and biological conditions.[19] The speciation diagram in Figure 2 shows the lead(II)-hydroxo species present in solution over varied pH.

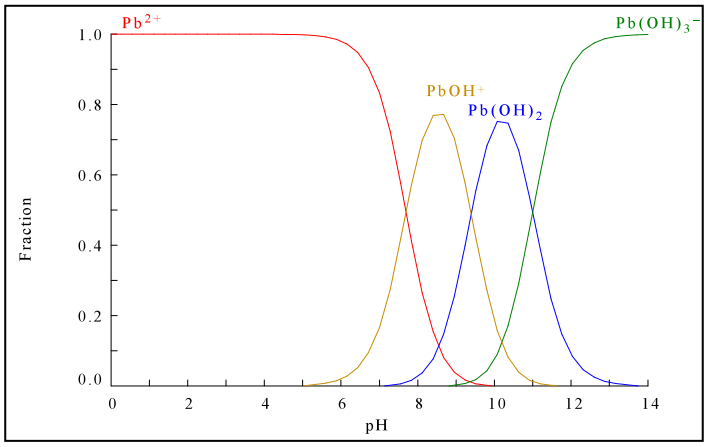

Figure 2: Speciation diagram for Pb^{2+} in aqueous solution over pH range 0 – 14, at $C_{Pb^{2+}} = 10$ mM (stability constants from Reference [20]).

At alkaline pH ~ 9 as studied in this thesis, Pb-hydroxo complexes do not compete with Pb(II) complexes formed with each ligand in aqueous solution. Stability constants reported for Pb(II) complexes with *D*-penicillamine and *L*-cysteine indicate that the metal centre has a high affinity for these ligands at the pH and concentration used in the current studies (pH > 9).[21] Potentiometric studies have identified stability constants for different Pb(II) species with *D*-penicillamine and *L*-cysteine, that can be used to predict Pb(II) complexes formed in solution (Figure 3).

(a)

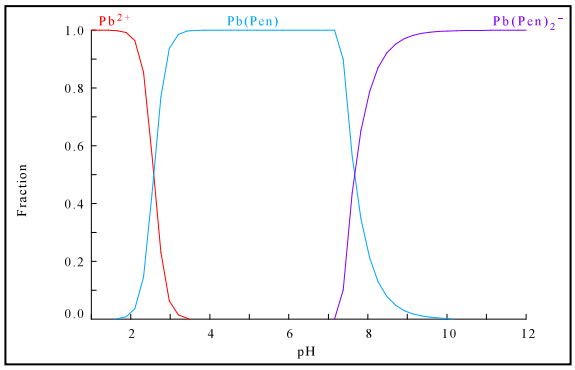

(b)

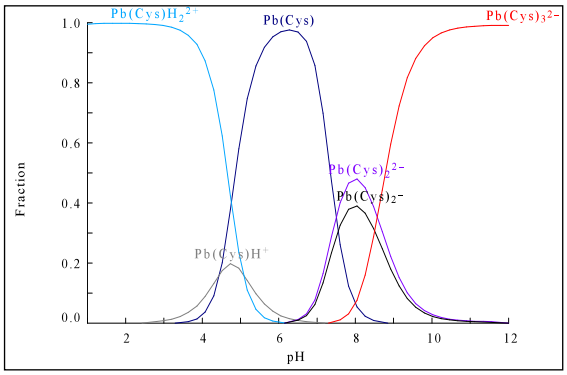

Figure 3: Distribution of (a) Pb(II)- *D*-penicillamine and (b) Pb(II)-cysteine complexes as a function of pH based on stability constants from reference [21].

Stability constants β, for 1:1 complexes are simply the formation constant of the reaction, where one ligand bonds with the metal (equation 3). Subsequently, stability constants become

more complicated upon presence of addition ligands; the product of multiple formation constants, as shown in equation 7 for a ML_2 species.

$$M + L \leftrightarrow ML \quad (3)$$

$$K_1(=\beta_1) = \frac{[ML]}{[M][L]} \quad (4)$$

$$ML + L \leftrightarrow ML_2 \quad (5)$$

$$K_2 = \frac{[ML_2]}{[ML][L]} \quad (6)$$

$$\beta_1 = K_1K_2 = \frac{[ML_2]}{[M][L]^2} \quad (7)$$

Formation of ML_n complexes is a step-wise process and depends on free ligand concentration $[L]_{free}$. The dynamic exchange of ligands with each other or with solvent largely depends on the lability of the Pb-L, and nature of the solvent. Unfortunately, Pb(II) is persistent in the environment, and lead(II) contamination has been a problem since it first came into use.[22–24,8]

1.1.2 Environmental and biological impact

Naturally occurring heavy metals collectively make up less than 1 % of the rock in Earth's crust, and are often known as trace metals.[22] While some trace metals are essential to the growth and function of living organisms, at elevated concentrations, heavy metals such as Ag, As, Cd, Hg and Pb are toxic and can cause harmful effects to biological systems.[3–5,25] Lead is among the first heavy metals used by civilization, dating back as early as 5000 B.C.[26] It was first used in components of tools, pots and pans; and pigments in ceramics and cosmetics.[27] It was

also the main element in piping used to transport water, which is still a major concern today.[8] Lead's physical properties such as high density, low melting point (ca. 327 °C), high boiling point (> 1700 °C), resistance to corrosion, air stability and malleability make it appealing for industrial use.[8,28] After the industrial revolution, lead became a part of numerous industrial processes like smelting, mining, electronics manufacturing, ceramics, paints and glazes.[29,30] As a result, elevated levels of lead were introduced into the environment. Emission into the atmosphere from human activity, usually as aerosols and fumes can be dispersed up to several thousand kilometres away. Surrounding water, soil, air and dust are contaminated with lead, and unlike most organic compounds that degrade over time, heavy metals persist and accumulate in the environment lasting up to several thousand years.[3,4,8,9,11,31,32] Perhaps one of the most well known uses of lead was in gasoline, in the form of tetraethyl lead. Tetraethyl lead, a powerful neurotoxin was used as an additive in gasoline as an "anti-knock" agent in the 1920s.[19,33]Like most organic compounds, it is capable of crossing lipid brain barriers, and rapidly affects the nervous system upon exposure.[34] Today, adults and children are still exposed to lead via drinking water, old paint dust, and imported products including food. There is no apparent threshold for a safe level of lead in the body, and children are more vulnerable to serious cognitive effects.[35–38] Though untreated lead poisoning can lead to severe encephalopathy in both children and adults, most symptoms can be treated and even reversed if detected early.[11,39,40]

Bioavailability and hence toxicity of lead is dependent on the route, quantity and form of exposure. Lead absorption most commonly occurs via ingestion and inhalation, especially in children who are accustomed to hand-to-mouth behaviours.[8,25] Once absorbed, lead is distributed in the bone, blood and soft tissues. Bone accommodates 80 – 95 % (in adults) the body burden of lead, and can have a 20 to 30 year half-life.[29] Prolonged storage in the skeleton causes lead

accumulation and redistribution into blood and soft tissues. Almost all of circulating lead is found in the erythrocytes and dispersed into soft tissues affecting key organs like the liver, kidney, lungs, brain, pancreas, muscle and heart.[8]Over the span of 20 years, the lower limit defining lead poisoning based on blood lead level (BLL) was dramatically decreased as toxic affects became more apparent. In 1970, persons with BLL $\geq$ 60 μg/dL were classified to have lead poisoning; this lower limit steadily decreased to 10 μg/dL by 1991. Lead poisoning is usually is treated by chelation therapy at a BLL 15 μg/dL or higher.[40]

Two major systems affected by lead poisoning causing known symptoms such as anaemia or psychosis are the Hematopoietic and Central Nervous systems respectively. Anaemia occurs with chronic high-level lead exposure when lead interferes with haemoglobin production by inactivation of key enzymes.[41] The central nervous system is most sensitive to toxic effects of lead, where intellect, memory, motor skills and attention are largely affected.[28] Many effects of lead intoxication are a result of its ability to replace essential minerals Zn^{2+} and Ca^{2+} found in active sites of enzymes, ultimately inhibiting their proper function.[42]

5-Aminolevulinate dehydratase (ALAD) or porphobilinogen synthase, is a zinc metalloenzyme in the heme biosynthetic pathway. It catalyzes the condensation of two aminolevulinate (ALA) to form the monopyrrole porphobiilnogen, a precursor of heme and other hemoproteins.[43–45]When inhibited by lead, anaemia and a build up of ALA results. ALAD contains a tetrahedral Zn active site, where Zn^{2+} is coordinated to three cysteinyl residues and a water molecule.[44,45] Lead readily replaces Zn^{2+}, taking a trigonal pyramidal coordination geometry, subsequently inhibiting its catalytic activity.[46,47] Ferrochelatase, which catalyzes the insertion of iron into protoporphyrin to form heme, is also inhibited by lead when Zn^{2+} is in surplus and replaces Fe, increasing zinc protoporphyrin (ZPP) concentrations.[29] Accordingly,

accumulation of ALA or ZPP can be used as biomarkers to clinically detect lead poisoning. Inhibition of ALAD and hence increased ALA concentrations are most profound, detectable in plasma or urine at BLL as low as 10 μg/dL and is commonly used to gauge the extent of lead poisoning in patients.[28] Additionally, lead poisoning can cause oxidative stress when antioxidant, glutathione (GSH) is inactivated upon binding to Pb^{2+}. Oxidative stress caused by lead leads to generation of reactive oxygen species (ROS), depletion of antioxidant reserves, and increased vulnerability to cell death.

Most effects of lead poisoning can be attributed to its coordination chemistry, and that it differs from the coordination of essential metals it replaces in the body. This affects protein folding, release of neurotransmitters, ionic transport, enzyme regulation, etc. Even in picomolar concentrations, Pb^{2+} can replace Ca^{2+}, having a negative effect on protein kinase C; a process which regulates long-term neural excitation and memory storage.[47] Understanding lead coordination chemistry, can certainly help to effectively prevent and treat lead poisoning. Specifically, studying the complex formation between Pb(II) and thiol-containing ligands as models for binding of peptides or proteins can give insight to the mechanism of lead poisoning.

1.1.3 D-penicillamine, L-cysteine and N-acetyl-L-cysteine

The ligands studied in this thesis contain thiol (SH), amine (NH_2) and/or carboxylate (COO^-) groups. *L*-cysteine and its derivatives *D*-penicillamine and *N*-acetyl-*L*-cysteine have been reported as effective chelates for heavy metals including cadmium, mercury, zinc and nickel. Chelation therapy has emerged as an effective method of treatment to increase excretion of toxic metals from the body, however, it still lacks metal specificity. Lead(II) has a high

affinity for thiol-containing residues in biological conditions, usually binding to 3 or more thiol groups in active sites. Each ligand shown in Figure 4 differs in structure by the ability to coordinate via NH_2 or COOH functional groups. Differences in binding to Pb(II) can hence be attributed to the structural changes.

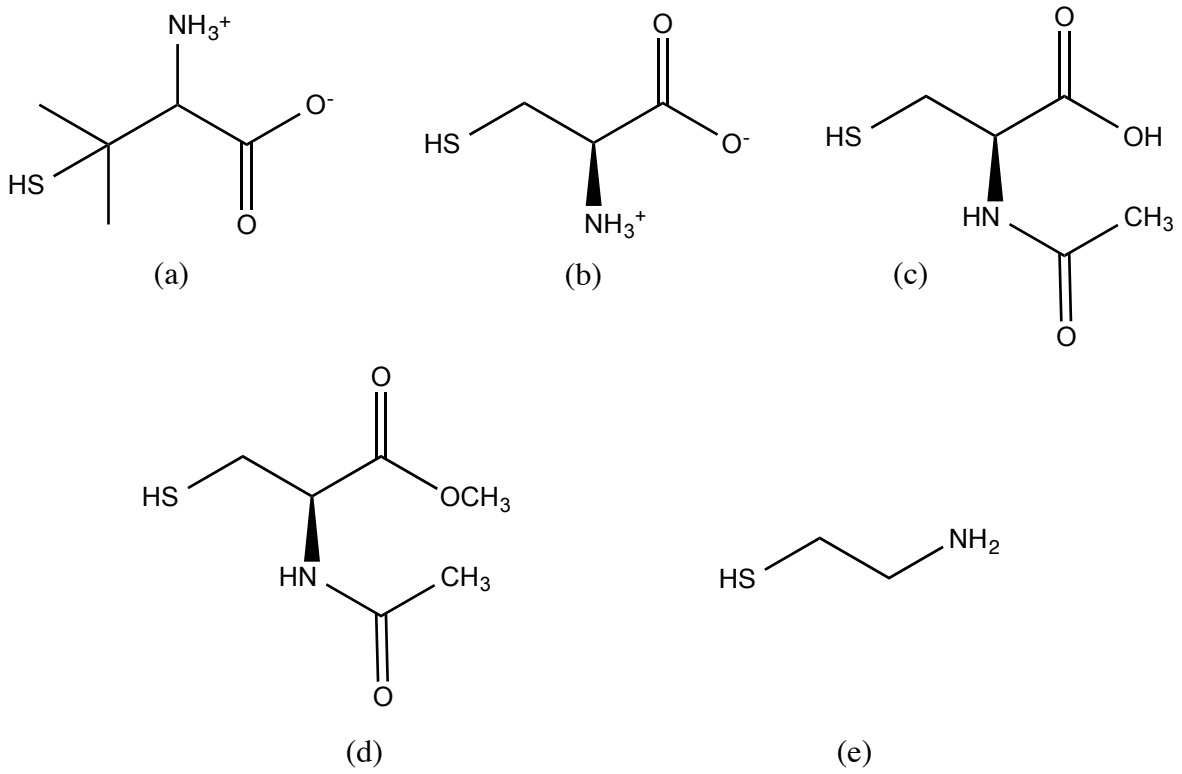

Figure 4: Structures of *D*-penicillamine (a), *L*-cysteine (b) *N*-acetyl-*L*-cysteine (c); *N*-acetyl-*L*-cysteine methyl ester (d) and cysteamine (e).

D-penicillamine has been used as an oral chelator for the treatment of Wilson's disease since the 1950s, a genetic copper storage disorder that causes liver and nervous system dysfunction.[48] *D*-penicillamine can effectively bind metal centres at three different binding sites, its detoxifying properties of *D*-penicillamine usually attributed to its tight binding to metal centres, via tridentate mode of coordination of all three sites. The crystal structure reported for

Pb(II)- *D*-penicillamine illustrated long range interactions between atoms on neighbour molecules, and contributes to the stability of the complex. In ligand design, C-alkylation will increase complex stability, as long as the alkyl groups added do not cause steric over-crowding that can interfere with binding.[49] For *D*-penicillamine, it is clear that the inductive effect of the two methyl substituents toward sulphur and nitrogen donor atoms has an overall stabilizing effect in chelate complexes.

Similarly, *L*-Cysteine has the ability to bind to a metal centre at any three coordination S, N or O donor sites, allowing for mono-, bi- or tri-dentate binding to metal centres. The thiol group in cysteine has numerous roles in biological functions of peptides and proteins, with increased reactivity when the thiolate (S^-) is formed. In biological systems, at neutral pH, the thiol group is found to be in its most active thiolate (S^-) form, therefore, our investigations in alkaline solutions emulate this. Cysteine is also essential in the production of glutathione (GSH), a vital tripeptide that plays an important role in maintaining redox balance in the cell.[50]

Cysteine has a promising role in nanomaterial applications in the synthesis of PbS nanostructures, and as a method for heavy metal removal or sensing.[51,52] Nanostructured polysaccharide materials have emerged for the use of heavy metal adsorption. Oxidized nanofibers can be grafted with cysteine via amide bonds between the cysteine amine and cellulose (polysaccharide) carboxylate.[53] A large surface-to-volume ratio is produced, creating many active sites where heavy metal adsorption can occur. Furthermore, Pb(II) specific nanochelants have been synthesized, successfully removing accumulated lead(II) in bone, organ and blood through oral administration to mice.[52] Environmentally friendly poly-α,β-*DL*-aspartic acid (PD) is commonly used in anticorrosion and electrochemical treatments as the biomaterial is able to coat nanoparticles and promote crystallization. When coupled with cysteine, PD

selectively removes Pb(II), without depleting essential metals Cu(II), Fe(II), Mn(II), Zn(II) and Ca(II). Over the past decade, PbS nanoparticles with varying morphologies have been synthesized for the development of opto-electronic devices. Complexation with cysteine as a precursor is a common method of modifying different types of nanoparticles that are created such as nanorods, nanotubes, nanocubes, starshapes, dendrites, etc.[54,55,56] The selectivity of cysteine towards Pb(II) also enable detection or sensing, and removal of the heavy metal from water.[57,58]

N-acetyl-*L*-cysteine (NAC), possesses antioxidant properties, supplies cysteine to GSH, and is an electrophile scavenger. It has been widely used in the treatment of congestive and obstructive heart diseases, available for binding only through the sulphur and oxygen atoms. Quantum Dot (QD)-induced cytotoxicity was treated using NAC-capped QDs.[59] Upregulation of Fas- a negative effect of ROS production, is completely inhibited when QDs are pre-treated with NAC. Stability constants reported for coordination to cadmium(II) show that NAC does not bind as strongly as *L*-cysteine or *D*-penicillamine, attributed to the absent nitrogen-coordination.

In this study, alkaline environments were required to study complex formation between Pb(II) and thiol-containing ligands in solution, to complete dissolve the 1:1 metal:ligand solid precipitates formed at lower pH. Alkaline conditions allow for complete deprotonation of ligand thiol groups, promoting formation of Pb(II) complexes with higher thiolate coordination. All samples were freshly prepared before characterization, as decomposition of solutions occurred within 24 hours, via precipitation. Only one stereo isomer for each ligand (*L*-cysteine, *N*-acetyl-*L*-cysteine, and *D*-penicillamine) was used in the preparation of solutions.

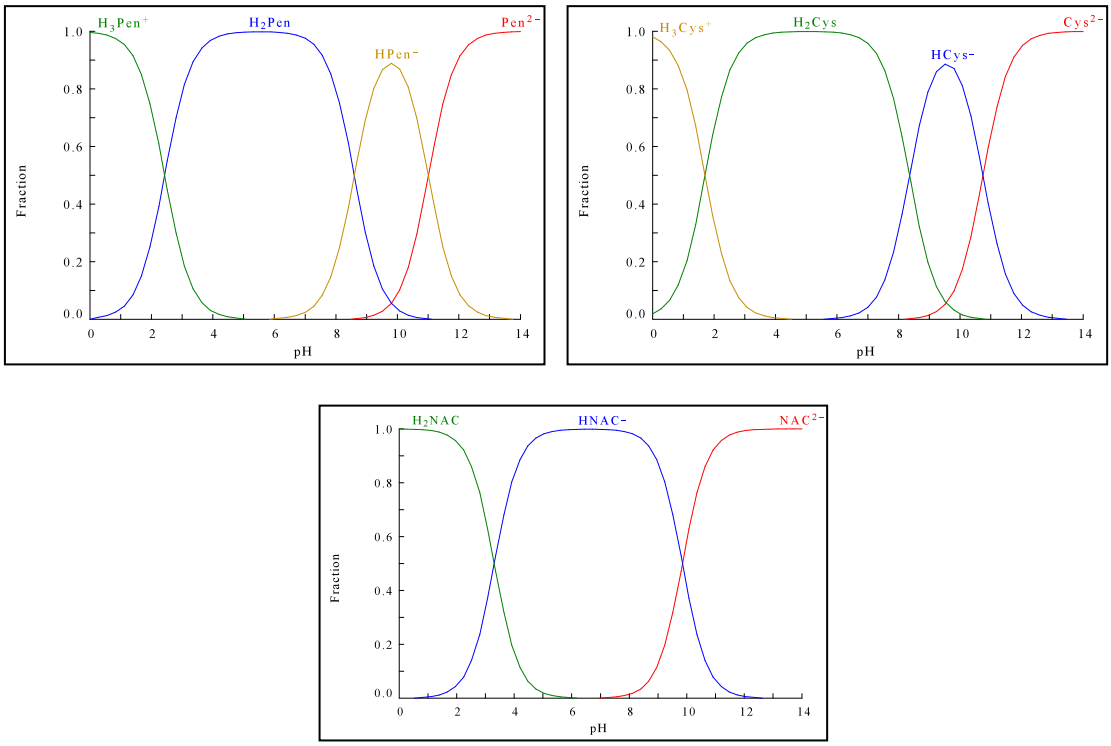

Figure 5: Speciation diagram of *D*-penicillamine (top, left), *L*-cysteine (top, right) and *N*-acetyl-*L*-cysteine (bottom) from pH 0 to 14.

Over a range of stoichiometric L:M values (2.0 to 10.0) and $[Pb(II)]_{total}$, the nature of Pb(II) complexes formed will vary. It is through X-ray absorption and NMR spectroscopy that we can investigate the various binding modes of Pb(II) in solution, to further understand the coordination preferences of the toxic metal under varying conditions.

1.2 Characterization techniques used to study lead(II) systems

1.2.1 Synchrotron based X-ray absorption spectroscopy

Synchrotron radiation, is the light emitted from high energy charged particles accelerated on a curved path. In 1945, it was first detected by physicists in the Research Laboratory of the General Electric Company in 1947. By the 1960s, the usefulness of synchrotron radiation was realized and sources were quickly developed and put into use in European and American laboratories. The evolution of synchrotron facilities grew in many facets, namely expanding disciplines from physics to chemistry and biological sciences. Initially, sources were built among existing particle accelerators, before fully dedicated synchrotron sources were being constructed using bending magnets in the 1970s. During this evolution period, insertion devices (wigglers and undulators) were introduced to increase the brightness of the X-ray source. By the 1980s, synchrotron sources had seen extensive progress towards stability, power, control, tuning, and became recognized for many applications that it remains utilized for today.[60] Today's synchrotron sources encompass user-friendly beam lines, supplying simultaneous radiation for numerous experimental set ups using a combination of wigglers and undulators and several other insertion devices to focus and control the beam.

The main components of synchrotron radiation sources include an electron gun, linear accelerator (linac), booster, storage ring, and beam lines (Figure 6). Electrons are continuously expelled from an electron gun, operated by thermo-electric heating of a cathode surface (usually tungsten) to very high temperatures. The electrons are then accelerated through a vacuum (linear

accelerator) before entering the booster for further acceleration. The energetic electrons are then injected into the main storage ring.

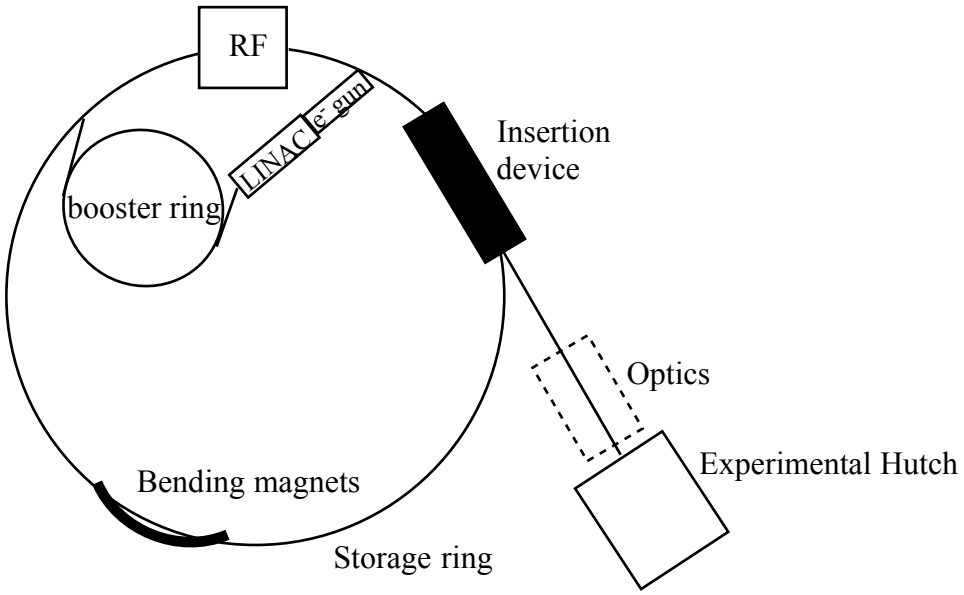

Figure 6: Components of a synchrotron radiation source.

The storage ring holds a continuous beam of electrons traveling close to the speed of light, under vacuum; consisting of several components to maintain electrons with high speeds. Bending magnets create the curved path required to produce synchrotron radiation tangential to its path, making the curvatures of the storage ring. Straight sections are comprised by insertion devices to produce radiation with higher flux and brightness. By forcing the electron beam paths to oscillate between sets of alternating magnets, undulators and wigglers increase beam intensity by more than 1000-fold. While undulators create highly intense beams with narrow energy ranges, wigglers provide continuous radiation like bending magnets, but much more intense. Finally, radio frequency (RF) cavities maintain the speed of electrons within the storage ring by accelerating circulating bunches of electrons using oscillating electromagnetic fields.

1.2.1.1 X-ray absorption spectroscopy (XAS) theory

The X-ray energy required for excitation of a core electron into a higher energy unoccupied orbital of an absorbing atom, is known as the binding energy. Sudden absorption of energy by a 1s electron (in the K-shell) is called a K-edge absorption, while excitation from a 2p electron (L-shell) is called an L-edge etc. Because each element has distinct binding energies, this makes XAS an element specific technique, allowing it to be a direct probe of the local environment around an absorbing atom. After a core electron in the absorbing atom is excited into a continuum, a core hole is created, which can be filled by an electron from a higher orbital. Upon relaxation, a photon is released (X-ray fluorescence), which can also be measured specifically for each element (Figure 7). Emission lines are given names based on the relaxation into shells K, L or M. In Extended X-ray Absorption Fine Structure (EXAFS) and X-ray Absorption Near-Edge Spectroscopy (XANES) measurements, the ejected photo electron can be backscattered by neighbouring atoms.

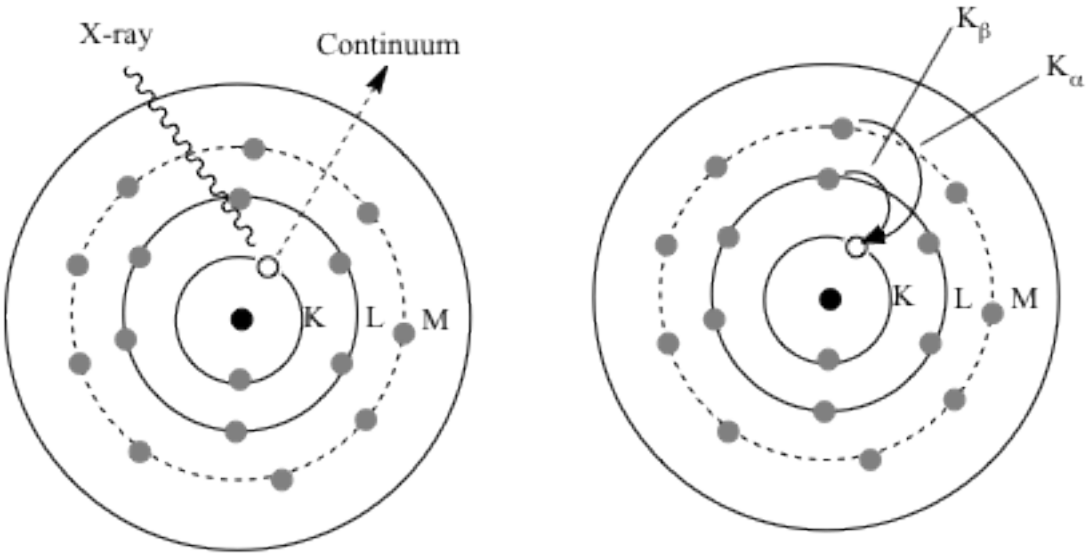

Figure 7: The photoelectric effect. Core electron is excited to continuum (left) and a photo electron is ejected upon relaxation of an electron from a higher shell (right).

The energy of the X-ray source is tuned to scan before, during and after the binding energy of a core electron for a specific element. When the incident X-ray reaches the binding energy E_0, the core electron can be excited to a higher unoccupied orbital, giving rise to a sharp absorption edge corresponding to a *1s* → *np* allowed transition.[60] Core electrons that are ejected with sufficient energy as a photo electron wave will encounter neighbouring atoms, and get back-scattered. The out-going and back-scattered waves will *constructively* and *destructively* interfere with one another. The resulting interference pattern is a fine structure oscillation that can be described by the EXAFS function $\chi(E)$, where μ, is the measured absorbance, and μ_0 is the absorbance of an isolated atom.

$$\chi(E) = \frac{[\mu(E) - \mu_0(E)]}{\mu_0(E)} \qquad (8)$$

Regions of XAS spectra with respect to the energy scale are described as: the pre-edge, where the energy E, is much lower than the threshold energy E_0; the near-edge or X-ray absorption near edge (XANES) region, where the energy is between 10 eV below and 30 eV above the edge; and the extended X-ray absorption fine structure (EXAFS) region, where the energy is 30 to 1000 eV above the edge as shown in Figure 8.

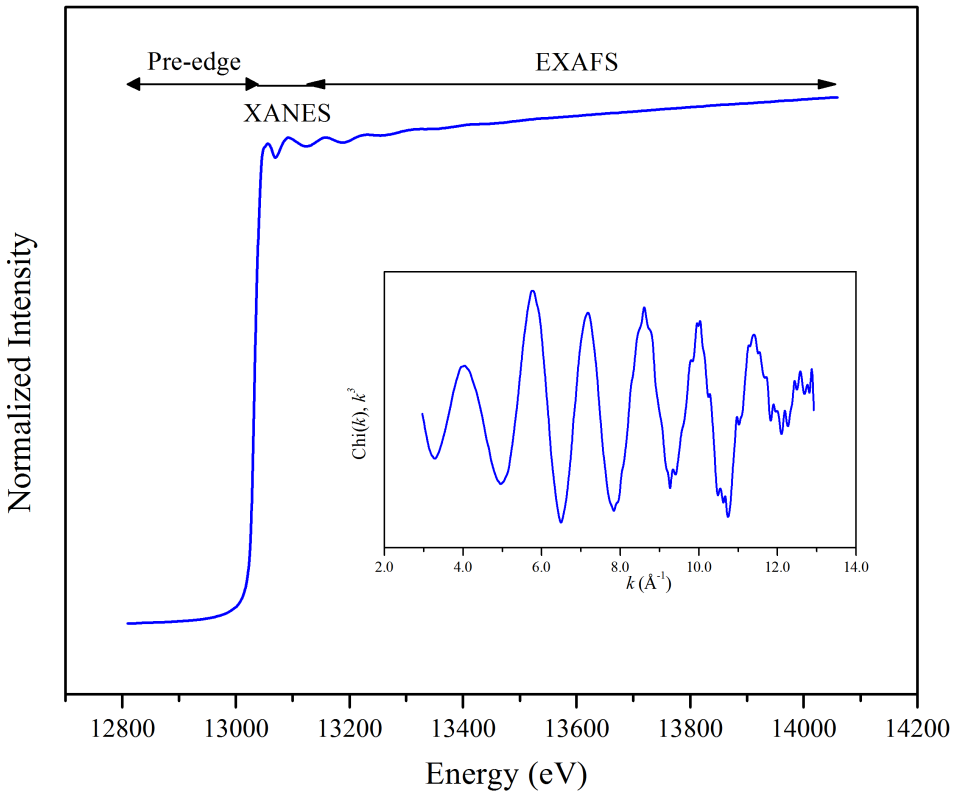

Figure 8: XAS spectrum of a Pb L_{III}-edge solid sample of $[Pb(aet)_2]$. Inset showing the extracted k^3-weighted EXAFS oscillation.

1.2.1.2 XAS measurement and experimental set up

XAS can be measured in two different ways: (1) in transmission and (2) in fluorescence modes. The absorption of the X-ray beam by the sample can be monitored in transmission mode, by measuring the intensity of the radiation before (I_0) and (I_1) after the sample, or in fluourescence mode by monitoring the intensity of the incident beam and the emitted fluorescence radiation.

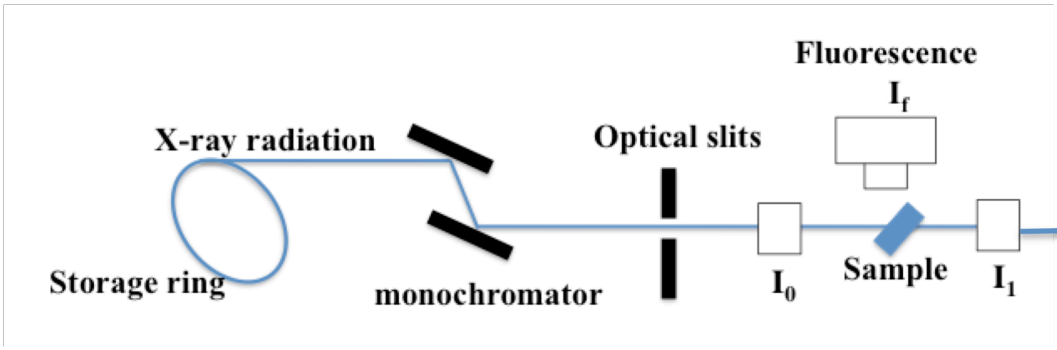

Figure 9: Schematic setup for transmission (I_0 and I_1) and fluorescence (I_f) measurements.

Synchrotron radiation emitted from the bending magnet or insertion device is directed into experimental work stations called hutches. For XAS measuremeants, the X-rays will go through a series of slits, a monochromator, detector, and sample. A double crystal monochromator is used to tune the beam energy. According to Bragg's Law, where n is an integer value, λ is the wavelength, d is the lattice spacing of the crystals and θ is the angle of reflection:

$$n\lambda = 2d\sin\theta \qquad (9)$$

Higher harmonics are eliminated by tilting the second monochromator crystal relative to the first one (detuning), a process which reduces the intensity of the incident radiation, I_0. Using

a lead foil between I_1 and I_2, internal calibration of the X-ray energy is performed. Slits are used to adjust the beam size.

Gas-filled ion chambers are generally used to detect the intensity of the incoming radiation and measures the current (*I*). Ion chambers are filled with inert gases such as He, N_2, Ar or Kr depending on the X-ray energy used in the experiment. Finally, the current detected is converted to voltage using amplifiers, and monitored on a computer. The gases inside the ion chamber are chosen to absorb approximately 10% of the X-rays in I_0, 20 to 40 % in I_1, and a third ion chamber I_2 will absorb any remaining X-rays after I_1.

For samples with concentration above ~20 mM, the XAS measurements can be performed in transmission mode; such spectrum can be plotted as $\log(I_0/I_1)$ versus X-ray energy where $\mu(E)$ is the linear absorption coefficient and *t* is the sample thickness.

$$\log\frac{I_0}{I_1} = \mu(E)t \qquad (10)$$

For dilute samples (< 20 mM), XAS spectra can be collected by measuring a secondary effect, fluorescence. The intensity of fluorescence radiation emitted from a sample is proportional to the linear absorption coefficient $\mu(E)$. To collect fluorescence radiation from the sample, a fluorescence detector is positioned at a 90° angle and sample placed at a 45° angle to the incident beam as shown in Figure 9. When using a Lytle detector, a filter made from an element Z-1 or Z-2 from the absorber element can be used to minimize scattered radiation. A set of Soller slits is also used behind the filter to scatter the emission from the filter to prevent the emission from being detected as emission from the sample.

1.2.1.3 The EXAFS oscillation

The kinetic energy of the photo electron is typically expressed as the *photoelectron waven vector, k* ($Å^{-1}$), the conversion made using equation (11), where m_e is the electron mass, $(E-E_0)$ is the kinetic energy of the photoelectron and $\hbar$ is Planck's constant.

$$k = \sqrt{\frac{2m_e(E-E_0)}{\hbar^2}} \qquad (11)$$

The experimental EXAFS function, $\chi(E)$ is extracted by pre-edge subtraction, normalization, and subtracting $\mu_0(E)$, known as the spline. Through normalization, any thickness or concentration effects are removed. Energy conversion to k-space is done by setting the threshold energy E_0 as the first inflection point of the absorption edge. An EXAFS oscillation is usually weighted due to dampening at high k-values. In the XANES region, the excitation of core electrons into higher unoccupied orbitals occurs, as well as multiple scattering of the photo electron when it leaves the absorber; it provides information about the oxidation state of the absorber, and structural geometry around it. EXAFS oscillations can be considered as a sum of sinus waves, each with amplitude and phase. Therefore, the scattering of the photoelectron in the EXAFS region can be expressed using the following equation:

$$\chi_i(k) = \sum_j \frac{N_j S_0^2(k)}{kR_j^2} \left| f_{eff}(k) \right|_j e^{-2k^2\sigma^2} e^{\left[\frac{-2R_j}{\Lambda(k)}\right]} \sin\left[2kR_j + \phi_{ij}(k)\right] \qquad (12)$$

where:

N_j is the number of backscatterers in the *j*th shell

S_0^2 is the amplitude reduction factor

k is the photoelectron wave vector ($Å^{-1}$)

R_j is the distance between the absorber and the backscattering atom

$f_{eff}(k)$ is the effective amplitude function, related to the type of backscattering atoms and defines the shape of the EXAFS oscillation for the jth shell

σ^2 is the Debye-Waller parameter (mean square variation in bond distance)

$\Lambda(k)$ is the mean free path of the photoelectron

$\phi_{ij}(k)$ is the phase shift

The EXAFS equation describes the amplitude of the oscillations, while the term $\sin[2kR_j + \phi_{ij}(k)]$ describes the phase and frequency of the oscillation; the latter is related to the distance between the absorber and the backscattering atom. The fine structure can provide information about the absorber atom, including: (1) coordinated atoms; (2) average bond distances (± 0.02 Å); (3) coordination number (CN) (± 20 %); and (4) mean variation around bond distances (σ^2).

1.2.1.4 EXAFS data refinement

To obtain local structure information around the absorbing atom, EXAFS curve fitting is performed Using a model compound such as a crystal structure with similar absorber and backscatter atoms, a theoretical EXAFS oscillation can be created. A program called "FEFF" then calculates the contribution of each scattering path to the theoretical EXAFS oscillation.[61] Multiple paths can be combined to make a theoretical EXAFS oscillation from the following equation[62]:

$$\chi_{theor}(k) = \sum_{j}^{N} \mathrm{Im}\{\chi_j(k)\} \qquad (13)$$

where N is the number of paths and $\chi_j(k)$ is the EXAFS oscillation of the jth scattering path. Least-squares fitting algorithms are used to minimize the mean square error (χ^2) of experimental EXAFS oscillations and theoretical EXAFS oscillation described by the equation:

$$\chi^2 = \int_{k=0}^{\infty} [(weightingfactor)(\chi_{\exp}(k) - \chi_{theor}(k))]^2 dk \qquad (14)$$

1.2.2 Nuclear magnetic resonance spectroscopy

NMR spectroscopy probes the precession of magnetic nuclei in an external magnetic field B_0, and the relaxation to equilibrium after perturbation in an applied magnetic field B_1. The rate of precession, or the Larmor frequency ω_0, can be expressed in terms of the magnetic field B_0 and the gyromagnetic ratio γ, which is directly proportional to the signal strength of a nucleus in NMR:

$$\omega_0 = -\gamma B_0 \qquad (15)$$

By combining together spins of protons and neutrons in the nucleus, nuclei with an odd sum of protons and neutrons will possess a nuclear spin quantum number $I \geq ½$, and are NMR active. As shown in Table 1, besides commonly used ^{1}H and ^{13}C NMR spectroscopy, the 207-Pb isotope is NMR active, with a relatively good receptivity and natural abundance with respect to ^{13}C.

Table 1: Nuclear isotopes and associated spins, gyromagnetic ratio, and NMR frequency.

Isotope	Ground-state spin	Natural Abundance (%)	Gyromagnetic ratio ($x10^6$ rad s^{-1} T^{-1})	NMR frequency at 11.74T (MHz)
^{1}H	½	100	267.52	-500
^{13}C	½	1.1	67.28	-126
^{207}Pb	½	22.1	55.8	-105

^{207}Pb NMR spectroscopy has a wide chemical shift range (~17 000 ppm), dependent on factors such as, neighbouring atoms, number of atoms, strength of donation, through space (solvent) interactions etc.; the latter all affect the Larmor frequency, and hence the chemical shift observed for any nucleus. The wide chemical shift range enhances the ability to detect subtle changes in the chemical environment around the Pb nucleus. However, detecting the position of the ^{207}Pb NMR in such a wide range is challenging. ^{207}Pb NMR data, and other heavier nuclei (^{113}Cd, ^{199}Hg) to date, have shown a general trend, where increased polarizability of donor atoms tends to decrease the shielding on the chemical shift in order of least shielding S < N < O. The chemical dependence of ^{207}Pb NMR shifts has yet to be systematically evaluated as extensively as other nuclei such as ^{13}C or ^{1}H but, has the potential to become a useful biological application comparable to the success of ^{113}Cd NMR.[63–65] There have also been some ^{207}Pb NMR studies modeling the binding of Ca^{2+} and Zn^{2+} containing proteins by Pb(II), showing it is a reliable technique for both complex and simple systems.

1.2.3 Electrospray ionization mass spectrometry

Electrospray ionization mass spectrometry (ESI MS) is a gas-phase technique that can give insight on kinetically stable complex ions formed characteristic of, but not directly correlated to species in solid or solution phases. ESI-MS is an ionization source based on the electrostatic spraying of volatile samples through a capillary held at a high voltage (kV). Positive or negative ions can be detected in ESI, but neutral species are not. Unlike harder ionization techniques such as electron impact or chemical ionization that cause a high degree of fragmentation, ESI is a soft technique that causes little fragmentation of sample ions. Gas-phase ions are formed from charged droplets containing both positive and negative ions. As the droplet (solvent) evaporates, ions become closer together, increasing Coulombic repulsion, until reaching the Rayleigh limit and separating into smaller droplets. This process continues until single ions or clusters are formed (Figure 10) and are forced toward the detector by a charged plate. Depending on the ion-mode, a charged plate will attract anions/cations, while repelling cations/anions respectively. Low sample concentrations are required to reduce inter-atomic collisions inside the source and mass separator. Ion suppression is a common occurrence in ESI MS, where competitive ionization of solvent or matrix can completely interfere with the detection of analyte ions.

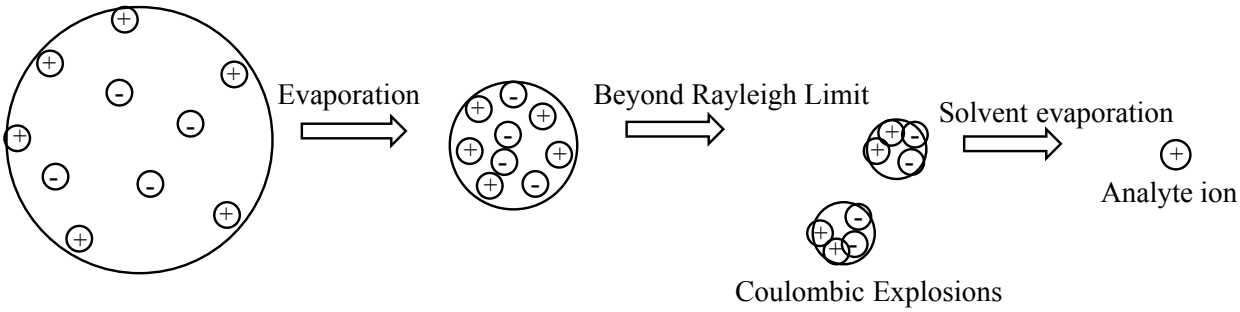

Figure 10: Evaporation of solvent to form charged analyte after the Rayleigh limit has been reached.

Once ions are formed, they are introduced into the mass analyzer and are separated based on their mass-to-charge (*m/z*) ratios. Time of flight (Tof) mass analysers separate ions by accelerating them through a constant electric field, with potential V. Ions of different mass will have different velocities according to the equation below, where *z* is the ionic charge, *e* is the elementary charge, *m* is mass and *v* is the velocity (m/s). Heavier ions will have the slowest velocities and are the last ones to reach the detector.

$$zeV = \frac{mv^2}{2} \qquad (16)$$

The natural abundance of lead's isotopes make it possible to identify analyte ions containing Pb(II) using its isotopic pattern. The distinctive isotopic pattern of ^{206}Pb (24.1 %), ^{207}Pb (22.1 %) and ^{208}Pb (52.4 %) is shown in Figure 11.

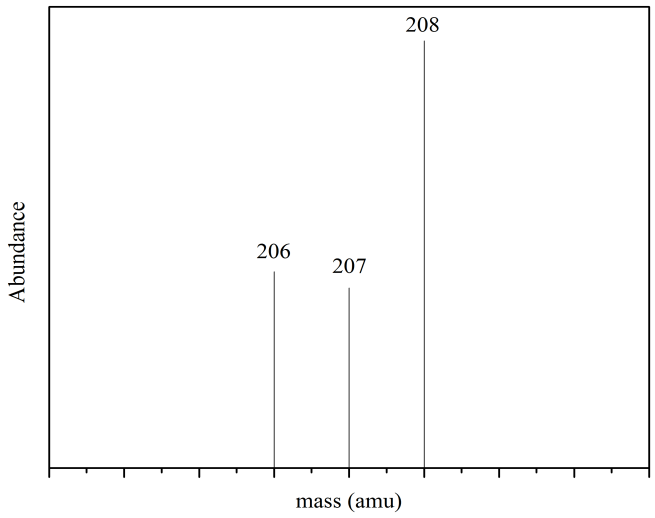

Figure 11: Schematic ESI spectrum showing the natural abundance of Pb isotopes.

1.3 Objectives

The development of X-ray absorption spectroscopy (XAS) and multinuclear NMR has provided a valuable tool to study specific metal centres at the atomic level. The main focus of this work is to probe the fundamental coordination chemistry of lead(II) and its interactions with simple thiol-containing molecules. In this project, three lead(II) systems have been studied and characterized in aqeuous solution at two different $[Pb^{2+}]_{total}$ concentrations.

This research presents the study of lead and its interactions with ligands *L*-cysteine, *N*-acetyl-*L*-cysteine and *D*-penicillamine. Lead(II)-ligand complexes have been studied in solution by XAS, NMR and UV-Vis spectroscopy. Solid-state ^{207}Pb NMR spectroscopy was also utilized to gain more spectroscopic information on the known structure of the lead(II)-cysteamine system. Ultimately, these findings can advance the development of ligand synthesis for effective and selective binding of lead(II) used in chelation therapy.

Chapter Two: Complex formation of Lead(II) and *D*-penicillamine

2.1 Introduction

Penicillamine has long been used as a detoxifying agent, mainly for the treatment of Wilson's disease, and has also been orally administered for lead poisoning.[66–75] Although it is clinically administered, it is also associated with unpleasant side effects or adverse reactions. Side effects incurred are generally the result of insufficient selectivity of penicillamine, hence depletion of essential elements in the body.[67,76,77] For these reasons, supplements are usually prescribed during treatment with penicillamine.[11,28] It has been understood to strongly prefer tridentate chelation to the Pb(II) centre in both crystalline form and in solution. In crystalline form, the stability of the 1:1 metal-to-ligand complex has been attributed to weak interactions between neighbouring ligand molecules and the effects of its two methyl groups.[49,75,78]

The crystal structure of Pb(II)-penicillamine reveals close Pb-S, Pb-N and Pb-O distances similar to other thiol containing Pb(II) complexes with Pb-N or Pb-O interactions.[78,79] Formation constants of the Pb(II)-penicillamine system have also been reported and compared to other thiol-containing ligands, as well as stability constants of penicillamine with other heavy metals.

EXAFS, ^{207}Pb NMR and UV-Visible spectroscopic techniques were used to investigate lead(II)-penicillamine complexes in aqueous, alkaline solution, by varying the ligand-to-metal ratio from 2.0 – 10.0 at pH 9.6 – 11.0. Alkaline conditions were required to dissolve the precipitate that formed in solution and enable solution-state studies in UV-Vis, NMR, ESI-MS and EXAFS.

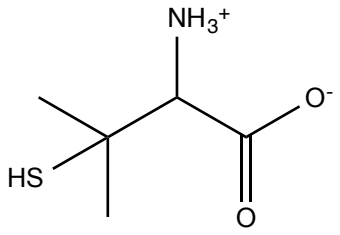

Figure 12: Zwitterion form of *D*-penicillamine.

2.2 Experimental section

2.2.1 Sample preparation

All samples were synthesized under an inert argon atmosphere with oxygen-free boiled water to avoid oxidation of thiol groups. A Thermo Scientific Orion Star pH meter, calibrated to standard buffers (pH 7.0 and 10.0) was used to monitor the pH of solutions. Lead(II) perchlorate trihydrate $Pb(ClO_4)_2 \cdot 3H_2O$, *D*-penicillamine, and sodium hydroxide were purchased from Sigma Aldrich and used without further purification. Enriched ^{207}PbO (94.5 %)^{208}Pb(5.5 %) was obtained from Cambridge Isotope Laboratories.

2.2.1.1 Preparation of Pb(II)-penicillamine solutions

Solutions were prepared by dissolving penicillamine (0.1 – 5 mmol) in 5 mL of deoxygenated water. Upon addition of $Pb(ClO_4)_2 \cdot 3H_2O$ (0.05 or 0.5 mmol), a white precipitate is formed at pH 2.4. The pH was increased using sodium hydroxide (1 M), until the solid dissolved above pH 9, giving a clear, colourless solution. Eight aqueous solutions with $[Pb^{2+}]_{total}$ = 10 or 100 mM and H_2Pen:Pb(II) molar ratios 2.0, 3.0, 4.0 and 10.0 were prepared with pH adjusted to 9.6. Table 2 presents the composition of solutions for Pb(II)-Penicillamine (A-H). Solutions A

and E (H_2Pen:Pb(II) 2.0) were adjusted to pH 10.3 and 11.0 respectively to completely dissolve the solid precipitate.

Table 2: Composition of Lead(II)-Penicillamine solutions.

Solution	$[Pb^{2+}]_{total}$ (mM)	$[H_2Pen]_{total}$ (mM)	H_2Pen/Pb^{2+}	pH
A	10	20.0	2.0	10.3
B	10	30.0	3.0	9.6
C	10	40.0	4.0	9.6
D	10	100.0	10.0	9.6
E	100	200.0	2.0	11.0
F	100	300.0	3.0	9.6
G	100	400.0	4.0	9.6
H	100	1000.00	10.0	9.6

2.2.2 EXAFS data collection

Pb L_{III}-edge X-ray absorption spectra for solutions A – D and F were collected at Beamline 7-3 and for solutions E, G, and H at Beamline 2-3 at the Stanford Synchrotron Radiation Lightsource (SSRL) with a 500 mA ring current and 3 GeV injector. Higher-order harmonics were rejected by placing a Rh-coated harmonic rejection mirror after a Si(220) double crystal monochromator at Beamline 7-3. The data was collected at room temperature in fluorescence mode for solutions A – D and transmission mode for solutions E – H. The X-ray energy was calibrated by collecting the absorption spectrum of a Pb foil placed between ion

chamber I_1 and I_2 and assigning the first inflection point to 13035.0 eV. Ion chambers I_0, I_1, and I_2 were filled with nitrogen gas (N_2). A 30 element Ge solid-state detector array was used to measure L_α X-ray fluorescence emitted from dilute samples.

Solutions were placed in 5 mm thick Teflon sample holders with 5 μm polypropylene film windows. Three scans were measured for Pb(II)-penicillamine solutions E - H, and 10 - 20 scans collected for solutions A - D. All spectra were compared to ensure no radiation damage occurred during measurement. Each Ge detector channel for each scan was examined before averaging for monochromator glitches and data quality.

2.2.3 EXAFS data analysis

EXAFS oscillations were extracted using the using the WinXAS 3.11 program by performing a background subtraction using a first-order polynomial, followed by normalization of the edge step. Threshold energies that varied between E_0 = 13034.4 – 13040.6 eV were converted into k space (Å^{-1}), where $k = [(8\pi^2 m_e/h^2)(E-E_0)]^{1/2}$. The crystal structure of *D*-penicillaminatolead(II) was used in the *ATOMS* program to create the input file using the *FEFF 7.0* program.[62,80] A six-segment spline was subtracted to remove the atomic background contribution. Least-squares refinements were performed using k^3-weighted raw data (k = 2.8 – 11.8 Å^{-1}). Structural parameters such as distance R, Debye-Waller factor σ^2 and sometimes coordination number N, were refined by least-squares curve fitting of k^3-weighted experimental EXAFS oscillations, while fixing the amplitude reduction factor (S_0^2) at 0.9 and allowing ΔE_0 to float. The amplitude reduction factor of 0.9 was obtained from the EXAFS data analysis of the penicillaminatolead(II) complex.[81] The amplitude reduction factor 0.9 was obtained from the

EXAFS data analysis of the penicillaminatolead(II) complex, and the number of scatterers N, were fixed to appropriate values. The accuracy of bond distances is estimated to be within ± 0.04 Å.

2.2.4 NMR spectroscopy

A Bruker Avance II 400 MHz spectrometer was used to collect ^{1}H and ^{13}C NMR spectra at room temperature (~300 K). ^{207}Pb NMR spectra were collected using a Bruker AMX 300 MHz spectrometer equipped with a 10 mm broadband probe and solid-state capability for solutions A – D. A Bruker Avance 400 MHz spectrometer was used to collect ^{207}Pb NMR spectra for solutions E – H. ^{207}Pb-enriched PbO (94.5 %) was utilized in the synthesis of solutions A – D to enable detection of ^{207}Pb-NMR resonances at lower Pb^{2+} concentration, since samples decomposed within 24 hours after they were prepared.

The ^{207}Pb chemical shift was externally calibrated relative to 1.0 M $Pb(NO_3)2$ in D_2O at -2962.1 ppm relative to $Pb(CH_3)_4$.[82] The ^{207}Pb NMR data were acquired using a 30° pulse, 66.7 kHz sweep-width, 1 second delay between scans, and 16000 data points. Approximately 10000 - 50000 scans were co-added. Spectra were processed using exponential line broadening 10 % of the line width at half-maximum.

^{1}H NMR spectra were collected using a 30° pulse; 6.4 kHz sweep width, 32000 data points and a 0.5 second delay between scans. 16 – 32 scans were co-added and spectra were internally referenced using the HOD/H_2O peak at 4.80 ppm.[83] ^{13}C NMR spectra were collected using a 30° pulse, 26.2 kHz sweep width, 32000 data points and a 1 second delay between scans.

1500 - 7200 scans were co-added and spectra were externally calibrated using CH_3OH in D_2O set to 49.15 ppm.[83]

2.2.5 Electronic spectroscopy

UV-Vis absorption spectra for solutions A – D $C_{Pb(II)}$= 10 mM were measured at room temperature using a Cary 300 UV-Vis double-beam spectrometer. Samples were measured in 1 mm thick quartz cells and a 1.5 absorbance Agilent rear-beam attenuator (RBA) was used in the reference position. The UV-Vis spectrum of penicillamine $[H_2Pen]_{total}$ = 1 mM was measured in a 1 cm thick quartz cell (pH 9.3) .

2.2.6 Mass spectrometry

Electrospray ionization mass spectrometry (ESI MS) spectra were collected on an Agilent 6520 Q-Tof in positive and negative-ion modes by direct infusion of Pb(II)-penicillamine solutions A and D. The capillary voltage was set to 4 kV and skimmer volage at 65 V. A continuous injection flow rate of 0.2 mL min^{-1} and drying gas flow rate of 7 L min^{-1} at 200 °C were used.

2.3 Results and discussion

2.3.1 Electrospray ionization mass spectrometry

ESI-MS spectra were collected for solutions A and D ($[Pb^{2+}]$ = 10 mM). The spectra for both solutions, identified similar Pb(II)-penicillamine complexes formed in both positive and negative ion modes. The isotopic distribution of naturally occurring lead allows facile assignment of Pb(II)-containing ions in the ESI-MS spectra. In positive-ion mode, peaks associated with Pb(II)-pencillamine complexes were observed for $[Pb(HPen)]^+$ (*m/z* 356.02), $[Pb(Pen)Na]^+$ (*m/z* 378.00), $[Pb(H_2Pen)(HPen)]^+$ (*m/z* 505.07), and $[Pb_2(Pen)_2Na^+]^+$ (*m/z* 733.01) species. Ions detected were the product of fragmentation, protonation or adduct formation in the gas-phase, which can resemble the species found in Pb(II)-pencillamine solutions A and D. In the negative-ion mode, one lead(II)-containing species was detected at *m/z* 503.05 for a $[Pb(Pen)(HPen)]^-$ complex. No more than two penicillamine ligands bound to the Pb(II) centre were detected. Although ESI-MS provides the total charge and possible ionized binding sites in each complex, the types of atoms coordinated to the Pb(II) centre cannot be determined by ESI-MS alone.

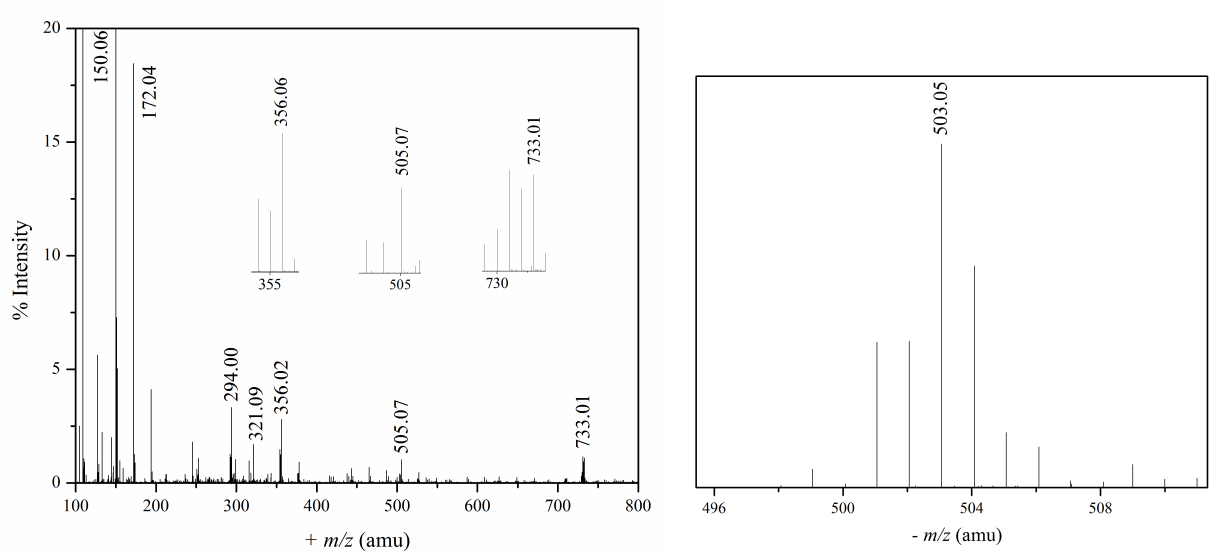

Figure 13: ESI-MS spectrum in the positive-ion mode for Pb(II)-penicillamine solution A ($H_2Pen/Pb^{2+} = 2.0$); *m/z* 150.06 has been set to 100% intensity (left); negative-ion mode for Pb(II)-penicillamine solution D.

Table 3: Assignment of ions detected in ESI-MS spectra (+) mode for Pb(II)-penicillamine solutions A and D.

***m/z* (amu)**	**assignment**	***m/z* (amu)**	**assignment**
150.06	$[H_2Pen + H^+]^+$	356.02	$[Pb(H_2Pen) - H^+]^+$
172.04	$[Na^+ + H_2Pen]^+$	378.00	$[Na^+ + Pb(H_2Pen) - 2H^+]^+$
194.02	$[2Na^+ + H_2Pen - H^+]^+$	505.07	$[Pb(H_2Pen)_2 - H^+]^+$
294.00	$[2Na^+ + H_2Pen + ClO_4]^+$	514.11	$[3Na^+ + 2(H_2Pen) - 2H^+]^+$
321.09	$[Na^+ + 2(H_2Pen)]^+$	536.09	$[4Na^+ + 3(H_2Pen) - 3H^+]^+$
343.07	$[2Na^+ + 2(H_2Pen) - H^+]^+$	733.01	$[Na^+ + Pb_2(H_2Pen)_2 - 4H^+]^+$

2.3.2 Electronic absorption spectroscopy

The UV-Vis spectra of solutions A – D, persistently showed an intense absorption in the far-UV region (< 260 nm) and a less intense absorption at ca. 299 nm (Figure 14). The absorption maximum is consistent with reported ligand-to-metal charge transfer (LMCT) bands due to S^- 3p → Pb(II) 6p and Pb(II) intra-atomic transitions Pb(II) 6s → 6p. The molar absorptivity of solution A ($\varepsilon\iota \sim 3980\ M^{-1}cm^{-1}$) is noticeably smaller than for solutions C – D ($\varepsilon\iota \sim 4800\ M^{-1}cm^{-1}$), although still in the range of molar absorption expected for S^- 3p → Pb(II) 6p transitions. To give insight on the type of coordination occurring, the absorption maxima (λ_{max}) of solutions A – D can be compared to maxima observed for other Pb(II) systems. Maxima are reported for Pb(II) complexes with cysteine-containing peptides CP-CCCC and CP-CCCH ((λ_{max} = 330 nm, PbS_3)[84], CadC mutants (325 nm, $PbS_2(N/O)$)[86], glutathione (335 nm, PbS_3), zinc-binding proteins (337 nm, PbS_3), and wild-type CadC protein (350 nm, PbS_3). Pb(II)-penicillamine solutions A – D showed a blue-shift compared to systems with three cysteine residues coordinated to the lead(II) centre. The λ_{max} is comparable to the reported absorption band of 310 nm for a Pb(II) complex with a synthetic peptide containing two cysteine and two histidine residues with PbS_2N_2 coordination.[46] This comparison suggests there are two thiolate interactions with the Pb(II) centre. Overlapping absorption bands for Pb(II)-penicillamine solutions B – D, also imply similar bis-thiolate Pb(II) coordination in all Pb(II)-penicillamine solutions.

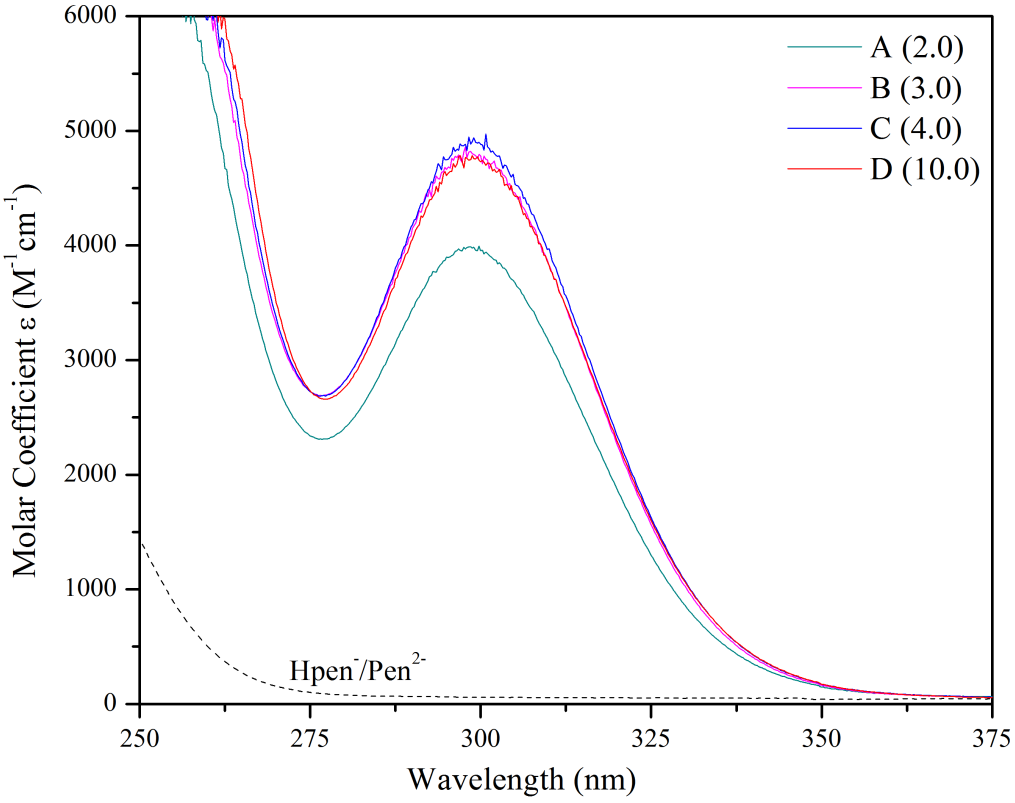

Figure 14: UV-Vis spectra of Pb(II)-penicillamine solutions A – D ($[Pb^{2+}]$ = 10 mM), compared with free penicillamine (pH 9.6; $[H_2Pen]_{total}$ = 1 mM).

The lower molar absorption of solution A, could be attributed to the presence of other Pb(II) species in solution, with less thiolate coordination, and different absorption maxima (λ_{max}). At a slightly more alkaline pH (10.3) compared to solutions B – D (pH 9.6), the loss of intensity is likely due to a degree of hydrolyzed species such as $[Pb(Pen)OH]^-$, where an OH^- replaces a penicillamine ligand, or $Pb(OH)_3$, a Pb(II) species commonly observed in alkaline environments with λ_{max} = 239 nm ($\varepsilon\iota$ = 2500 $M^{-1}cm^{-1}$). Although the penicillaminatolead(II) crystal structure is an example of a mono-thiolate Pb(II) complex, the solid does not dissolve until pH ~ 11, and is not likely to be the cause of the decreased intensity of the absorption band for Pb(II)-penicillamine solution A.

2.3.3 ^{13}C NMR and ^{1}H NMR Spectroscopy

All of the ^{13}C NMR spectra for free penicillamine (pH 9.6) and Pb(II)-pencillamine solutions A – D in D_2O, are shown in Figure 15. Due to fast exchange on the NMR time scale, an average signal is observed for both coordinated and free penicillamine in solutions A – D. Relative to free penicillamine, carbon sites C_1, C_2 and C_3 showed a downfield chemical shift. The largest downfield shift was observed for C_1, which corresponds to the binding of the carboxylate group (COO^-), to the Pb(II) ion. Due to fast exchange on the NMR time scale, an average signal is observed for both coordinated and free penicillamine in solutions A – D. Relative to free penicillamine, carbon sites C_1, C_2 and C_3 showed a downfield chemical shift. Due to the equilibrium between coordinated and free penicillamine in solutions A – D, as the amount of unbound penicillamine increases, the downfield shift of carbon sites $C_1 – C_3$ is less pronounced compared to free penicillamine. A similar effect was observed in the ^{1}H-NMR spectra of Pb(II)-penicillamine solutions A – D compared to free penicillamine, where the largest $\Delta\delta$ was observed for H_1 $\Delta\delta$ (^{1}H) = 0.38 ppm. Both ^{13}C and ^{1}H NMR support that all three binding sites are bound to the Pb(II) centre, and tridentate coordination is maintained in these solutions, similar to the crystal structure.[78,79]

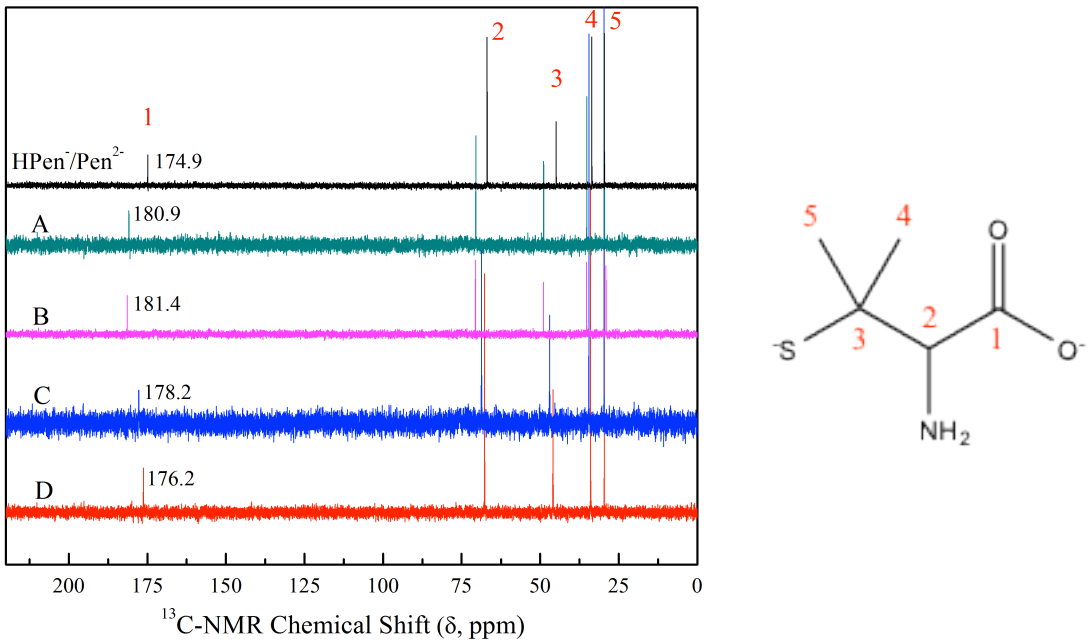

Figure 15: ^{13}C NMR spectra of 0.1 M penicillamine in D_2O (pH 9.6) and Pb(II)-pencillamine solutions (99.9 % D_2O, $[Pb^{2+}]$ = 10 mM); schematic numbering of carbon sites for penicillamine.

Table 4: Changes in ^{13}C NMR chemical shifts ($\Delta\delta(^{13}C)$) for Pb(II)-pencillamine solutions A - D to free penicillamine.

	$\Delta\delta(^{13}C)$, ppm		
Solution	**C_1**	**C_2**	**C_3**
A	6.0	3.6	4.0
B	6.5	3.7	4.0
C	3.1	1.8	2.1
D	1.4	0.8	1.0

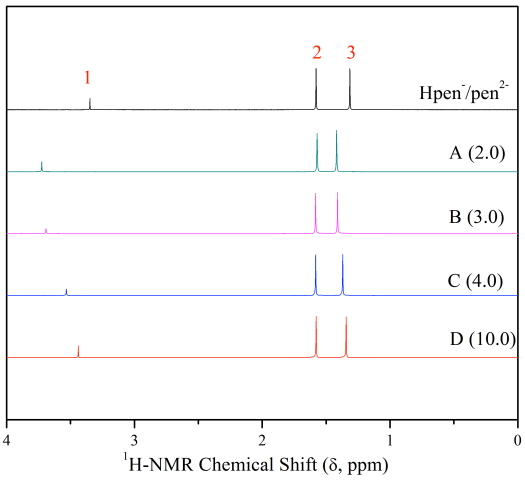

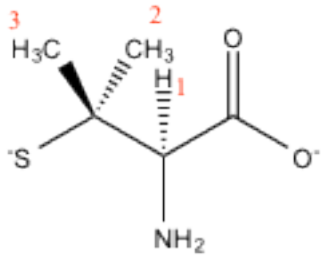

Figure 16: ^1H NMR spectra of 0.1 M penicillamine in D_2O (pH 9.6) and Pb(II)-pencillamine solutions (100 % D_2O, $[Pb^{2+}]$ = 10 mM); schematic numbering of protons for penicillamine.

2.3.4 ^{207}Pb NMR Spectroscopy

Despite the advantages of ^{207}Pb NMR, and biological interest of lead(II)-thiolate systems, only few ^{207}Pb NMR chemical shifts have been reported for Pb(II)-thiolate complexes. Some lead(II)-thiolate complexes containing oxygen and nitrogen donors include: lead(II) thiobenzoate $[Pb(SOCPh)_3]$ where ph = phenyl (1422 – 1463 ppm)[85], Bis(*N*-cyclohexyl-phenylacetothiohydroxamato) lead(II) (1506 – 1555 ppm)[86], $[PATH\text{-}Pb]ClO_4$ (2357 ppm)[87],

solid-state $[(2,6\text{-}Me_2C_6H_3S)_2Pb(pyCOH)]_2$ where py = pyridine (δ_{iso} = 2733 ppm) and PbS_2N_2S' (δ_{iso} = 2873; S′ = bridging thiolate), PbS_2N (δ_{iso} = 2852 ppm)[88], and in Pb(II)-peptides (2577 – 2853 ppm), showing the sensitivity of ^{207}Pb chemical shifts to the coordination environment. All ^{207}Pb NMR spectra collected for solutions A – H were comprised of a single resonance (Figure 17), indicating a single, dominant lead(II) species, or more than one in a dynamic equilibrium, which was faster than the NMR time-scale. The resonance signal observed for solution E (1826 ppm) was distinctly sharper compared to solutions A – D and F – H. All other peaks observed for Pb(II)-penicillamine solutions were also moderately narrow ($\Delta\nu_{1/2} \sim 100 – 200$ Hz). Slight broadening of signals for solutions A – D and F – H can be attributed to slower exchange between different Pb(II)-penicillamine species in solution at room temperature. Comparing solutions A and E of similar molar ratios (H_2Pen:Pb = 2.0), the broadening of the signal for solution A may again be due to formation of minor amounts of $Pb(Pen)(OH)^-$ as discussed earlier in the electronic spectra. The range of observed resonances is relatively small (1806 – 1871 ppm for A – D; 1826 – 1873 ppm for E - H), as the total ligand concentration is increased, suggesting that the Pb(II) environment is not changing to a great extent in these solutions. Moreover, solutions (C and G) and (D and H) have similar chemical shifts, even though the free ligand concentration ($[H_2Pen]_{free}$) are different. In contrast to the solid-state shift δ_{iso} = 902 ppm (measured by Qiao Wu), where Pb(II) has strong (S,N,O) interactions in the crystal structure, the solution-state resonances are shifted ca. > 900 ppm downfield. The downfield shift is likely due to the formation of a bis thiolate Pb(II) complex such as $[Pb(Pen)(HPen)]^-$, where two ligands are bound to the Pb(II) centre. Compared to reported Pb(II) complexes with PbS_2O_2 (1506 – 1555 ppm), $PbSN_2$ (2357 ppm) and PbS_2N_2 coordination (2733 ppm)[88], the bis-thiolate Pb(II)-penicillamine complex dominates in solutions A – H, particularly in solution E (1825 ppm),

where a narrow signal is observed, and minimal amount of free penicillamine is present. The [Pb(*S,N,O*-pen*)S*-HPen]$^-$ species detected in the negative-ion mode in ESI-MS at *m/z* -503.5 supports this premise. As the free ligand concentration and hence $[H_2Pen]_{total}$ increases, it is possible that a three coordinate [Pb-(*S*-Pen)$_3$]$^{4-}$ complex is formed in minor amounts, resulting in the gradual downfield shift that is observed.

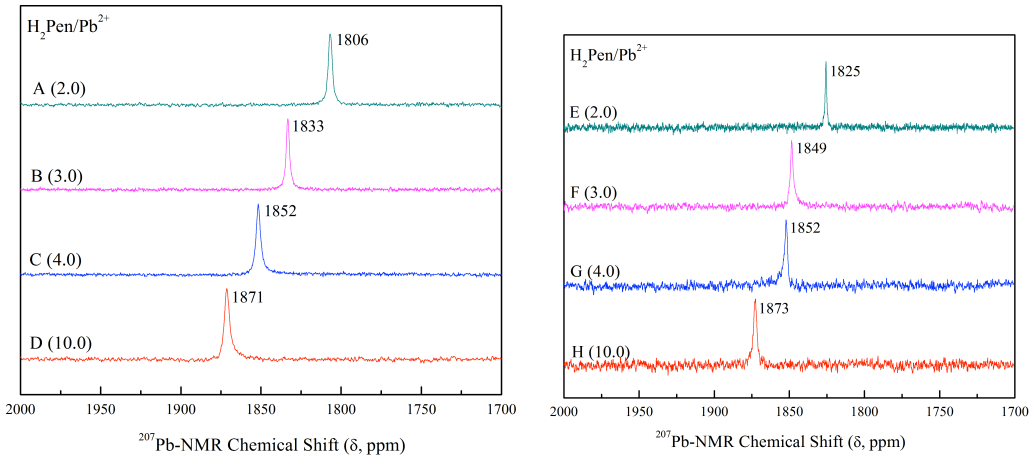

Figure 17: ^{207}Pb NMR spectra of Pb(II)-penicillamine solutions A – D ([Pb^{2+}] = 10 mM; enriched ^{207}Pb) and E – H ([Pb^{2+}] = 100 mM) in 10 % D_2O.

2.3.5 EXAFS of Pb(II)-penicillamine solutions

The X-ray absorption spectra for Pb(II)-penicllamine solutions A – D were collected in both transmission and fluorescence modes simultaneously. Although low quality data from a few Ge-detector channels were removed during the averaging process, transmission data was less noisy and used for further data analysis.

The EXAFS oscillations and corresponding Fourier Transforms (FT) for Pb(II)-penicillamine solutions A – D are shown in Figure 18. The oscillations for all solutions were overlapping and fitted to three different models as shown in Table 5. Although none of the models had a substantially better fit, comparing residuals, Model I revealed the most consistent Pb-(N/O) bond distances (2.38 – 2.44 Å). A short Pb-(N/O) distance obtained for Pb(II)-penicillamine solution A may be due to a minor amount of $[PbPen(OH)]^-$ formed in the more alkaline solution (pH 10.3). Pb-(N/O) bond distances obtained from Models I and II (2.36 – 2.39 Å) is shorter than expected for a 4-coordinate Pb(II)-thiolate complex.[79,87,89–91] High disorder parameters obtained for Pb-(N/O) distances, suggests a large variance of the Pb-(N/O) bond lengths around the local structure of Pb(II)-penicillamine complexes. Similarly, experimental EXAFS oscillations of solutions E – H were overlapping (Figure 22). Slightly longer Pb-(N/O) distances are revealed for models I and II, while model III obtains Pb-(N/O) distances longer than expected (Table 6). Disorder parameters remained high for Pb(II)-penicllamine solutions E – H for Pb-(N/O) bond lengths. The difficulty of determining low-Z scatterers such as Pb-(N/O) in the presence of heavier Pb-S scattering is a limitation of EXAFS data analysis.[84,92] For all Pb(II)-penicillamine solutions A – H, Pb-S bond distances consistently emerged in the range

2.62 – 2.67 Å, with reasonable Debye-Waller factors, indicating small variation in the Pb-S bond length. Model I with an overall Pb-$S_2(N/O)_2$ is supported by the slight downfield shift of resonances observed in ^{207}Pb NMR, spectra of Pb(II)-penicillamine solutions A – H.

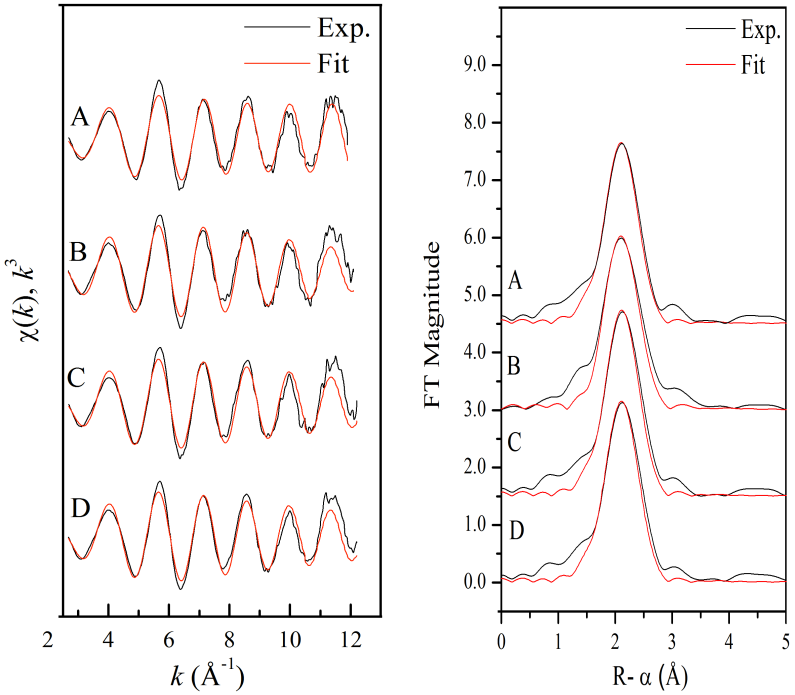

Figure 18: Pb L_{III}-edge k^3-weighted EXAFS oscillations (left); and corresponding (non phase-shift corrected) Fourier Transforms (right) for Pb(II)-penicillamine solutions A – D (Table 5) with Model I fittings.

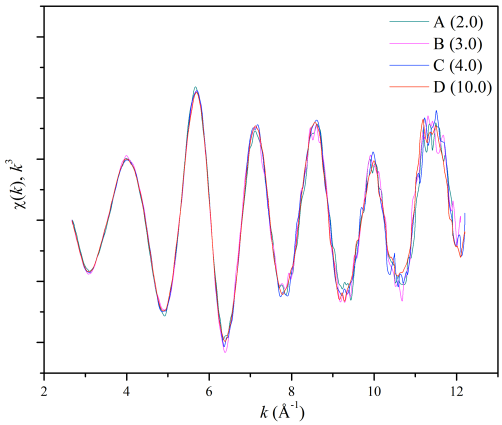

Figure 19: Pb L_{III}-edge k^3-weighted EXAFS oscillations compared for Pb(II)-penicillamine solutions A – D.

Table 5: Least-squares curve fitting results for the Pb L_{III}-edge k^3 EXAFS for Pb(II)-Penicillamine solutions A – D (See Figure 18).

		2 Pb-(N/O)			Pb-S			
Solution	**Model**	***R* (Å)**	**σ^2(Å^2)**	***N***	***R* (Å)**	**σ^2(Å^2)**	**ΔE_0**	**Residual**
A	I	2.38	0.024	2*f*	2.62	0.0051	-4.0	26.5
	II	2.40	0.0103	1*f*	2.63	0.0014	-2.4	28.2
	III	2.36	0.018	1.7	2.62	0.0041	-4.4	26.8
B	I	2.43	0.020	2*f*	2.64	0.0056	-2.2	29.6
	II	2.46	0.0079	1*f*	2.66	0.0020	1.8	31.1
	III	2.39	0.020	1.7	2.64	0.0040	-2.6	29.0
C	I	2.43	0.020	2*f*	2.64	0.0053	-1.2	23.7
	II	2.41	0.0068	1*f*	2.65	0.0010	0.01	23.0
	III	2.40	0.0097	1.3	2.65	0.0026	-1.0	22.8
D	I	2.44	0.020	2*f*	2.64	0.0057	-2.9	29.1
	II	2.44	0.0076	1*f*	2.65	0.0021	1.0	28.2
	III	2.39	0.018	1.8	2.63	0.0045	-3.0	26.7

f = fixed value; Fitting range: 2.8 – 12.3 Å^{-1}; $S_0^2 = 0.9f$; $R \pm 0.04$ Å; $\sigma^2 \pm 0.002$ Å^2; residual value reflects the deviation between theoretical and experimental EXAFS oscillations.

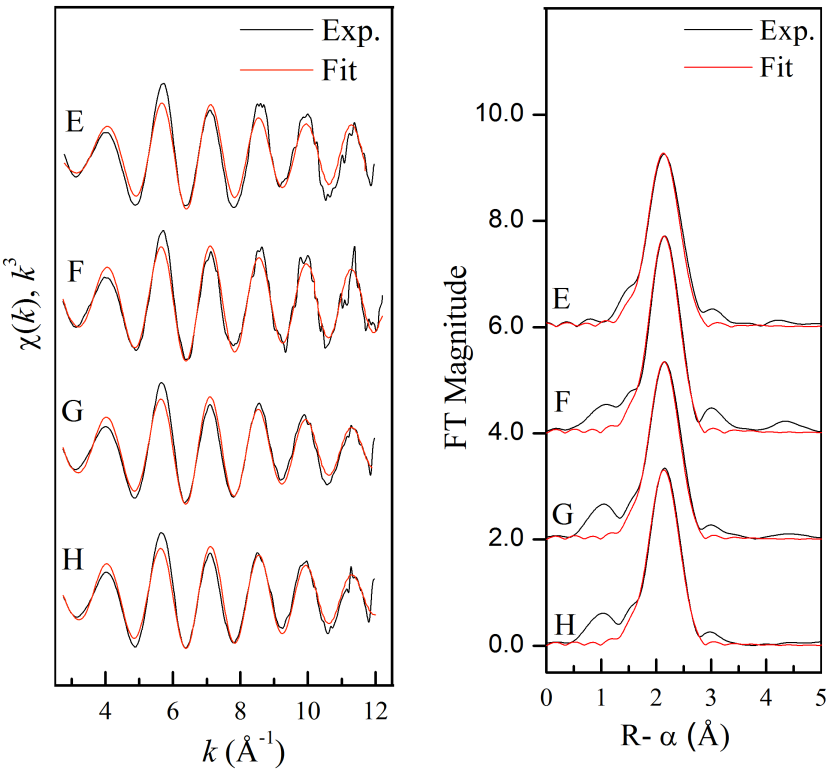

Figure 20: Pb L_{III}-edge k^3-weighted EXAFS oscillations (left); and corresponding (non phase-shift corrected) Fourier Transforms (right) for Pb(II)-penicillamine solutions E – H (Table 6) with Model I fittings.

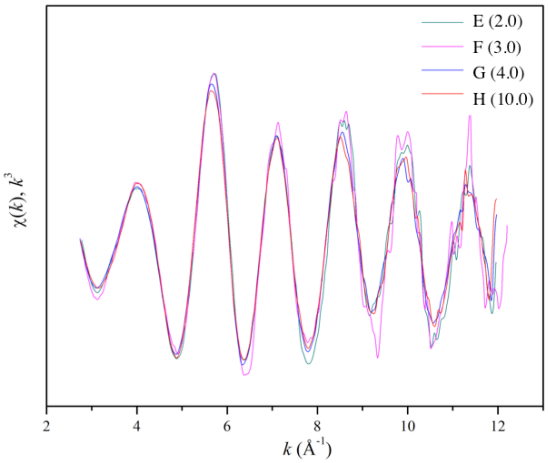

Figure 21: Pb L_{III}-edge k^3-weighted EXAFS oscillations compared for Pb(II)-penicillamine solutions E – H.

Table 6: Least-squares curve fitting results for the Pb L_{III}-edge k^3 EXAFS for Pb(II)-Penicillamine solutions E – H (See Figure 20).

		2 Pb-(N/O)			Pb-S			
Solution	**Model**	***R* (Å)**	**σ^2(Å^2)**	***N***	***R* (Å)**	**σ^2(Å^2)**	**ΔE_0**	**Residual**
E	I	2.45	0.025	2 *f*	2.65	0.0051	-0.8	15.9
	II	2.46	0.0084	1 *f*	2.67	0.0024	3.3	20.0
	III	2.50	0.036	2.4	2.40	0.0061	-1.3	16.0
F	I	2.45	0.023	2 *f*	2.65	0.0046	0.1	26.6
	II	2.44	0.0079	1 *f*	2.66	0.0015	3.1	27.5
	III	2.48	0.029	2.3	2.64	0.0052	-0.5	26.7
G	I	2.47	0.019	2 *f*	2.65	0.0058	0.7	23.8
	II	2.45	0.0077	1 *f*	2.67	0.0028	3.6	25.6
	III	2.58	0.031	2.9	2.64	0.0076	-1.3	23.7
H	I	2.46	0.020	2 *f*	2.65	0.0058	0.5	23.8
	II	2.46	0.0072	1 *f*	2.67	0.0034	4.5	26.1
	III	2.59	0.036	2.9	2.64	0.0077	-1.6	23.8

f = fixed value; Fitting range: 2.8 – 12.3 Å^{-1}; S_0^2 = 0.9 *f*; *R* ± 0.04 Å; σ^2 ± 0.002 Å^2; residual value reflects the deviation between theoretical and experimental EXAFS oscillations.

2.4 Conclusions

The structural investigation of the Pb(II)-penicillamine complex formation in alkaline aqueous solution using ESI-MS, UV-Vis , multinuclear (^{207}Pb, ^{13}C, ^{1}H) NMR and EXAFS spectroscopy, suggest there is a dominant complex formed over a range of H_2Pen/Pb^{2+} = 2.0 – 10.0). Solutions A – D and E – H had overlapping k^3-weighted EXAFS spectra and ^{207}Pb NMR chemical shifts over a narrow range (1806 – 1873 ppm) which indicates an insignificant change in Pb(II) speciation and local structure around the Pb(II) centre. Regardless of the free ligand concentration, solutions A - H likely contain one major Pb(II)-penicillamine complex, $[Pb(Pen)(HPen)]^-$ as detected in ESI-MS for Pb(II)-penicillamine solutions A and D. In previous studies, the stability of penicillamine chelation to Pb(II) has been attributed to the tridentate coordination of the ligand, in a 1:1 ligand-to-metal behaviour. The study in this chapter however, shows that in aqueous solution (pH 9.6 – 11), penicillamine can interact with Pb(II) with a 1:2 metal-to-ligand molar ratio, maintaining the tridentate coordination of one penicillamine molecule. A second pencillamine ligand is proposed to bind in a mono-dentate fashion, giving an over all Pb-*S_2NO* coordination geometry (Figure 22). The bis-thiolate Pb(II)-penicillamine complex proposed is supported by UV-Vis spectroscopy with λ_{max} = 299 nm ($\varepsilon\iota \approx 4800\ M^{-1}cm^{-1}$) and ^{207}Pb NMR $\delta(^{207}Pb) \approx 1826$ ppm. In addition, downfield shifts of carbon and proton sites in ^{13}C and ^{1}H NMR support coordination of all three binding sites to the Pb(II) centre. Average Pb-(N/O) and Pb-S distances for all eight solutions (A – H) were found to be 2.44 Å ± 0.04 Å and 2.64 Å ± 0.02 Å respectively. These results improve the understanding of Pb(II) speciation with

a long-used chelating agent *D*-penicillamine, and can be used as a tool to improve rational design of future chelating agents.

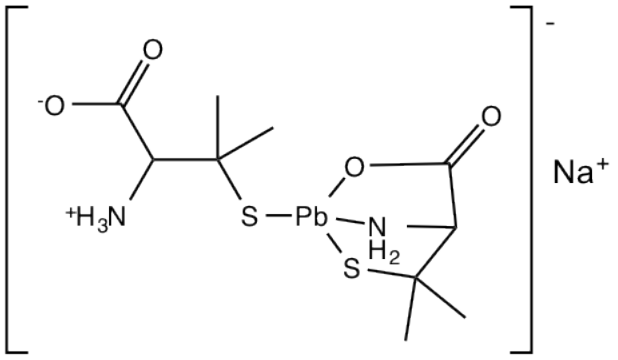

Figure 22: Proposed structure for a lead(II) *D*-penicillamine complex Na[Pb(Pen)(HPen)] formed in aqueous solution at alkaline pH.

Chapter Three: Complex formation of Lead(II) and *N*-acetyl-*L*-cysteine

3.1 Introduction

N-acetyl-*L*-cysteine (NAC) is a derivative of *L*-cysteine and a precursor for glutathione (GSH). NAC is a well-known anti-oxidant, which counteracts oxidative stress and supplies cysteine for GSH synthesis in biological environments.[93,94] It has been clinically used both as anti-oxidants and chelators in the treatment of congestive and obstructive heart diseases, paracetemol intoxication, and has been proposed as a therapeutic agent for AIDS, as it showed inhibition of HIV-1 replication. NAC has also been used in sensor designs, where it was used to detect Hg(II) and other metal ions based on fluorescence quenching.

The structure of protonated NAC (H_2NAC) containing thiol (SH) and carboxyl (COOH) binding groups, is shown in Figure 23. Upon deprotonation of its binding sites, NAC has the ability to act as a chelator forming bidentate complexes, or monodentate complexes with heavy metals such as cadmium, mercury, zinc and nickel.[93,95,96] Generally, bidentate chelation is more effective when amino (NH_2) and thiolate (S^-) pairs are bound to metal centres, compared to carboxylate (COO^-) and thiolate pairs. Furthermore, comparison of stability constants reported for Cd(II) with sulphur-containing ligands cysteine or penicillamine , revealed that NAC does not bind as strongly.

In this chapter, Pb(II)- *N*-acetylcysteine complex formation is studied in alkaline (pH 9.1) solution, since the carboxyl (pK_a ~ 3.3) and thiol (pK_a ~ 9.5) groups of *N*-acetylcysteine are deprotonated, and the precipitate is completely dissolved.

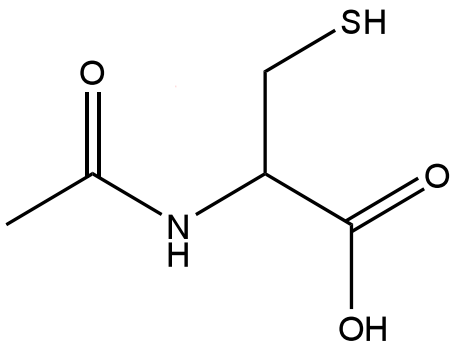

Figure 23: Structure of H_2NAC.

3.2 Experimental section

All samples were synthesized under an inert argon atmosphere with oxygen-free boiled water. A Thermo Scientific Orion Star pH meter, calibrated to standard buffers (pH 7.0 and 10.0) was used to monitor the pH of solutions. Lead(II) perchlorate trihydrate $Pb(ClO_4)_2 \cdot 3H_2O$, *N*-acetyl-*L*-cysteine, and sodium hydroxide were purchased from Sigma Aldrich and used without further purification. Enriched ^{207}PbO (94.5 %) obtained from Cambridge Isotope Laboratories was used by dissolving the solid in 0.1 M $HClO_4$ acid.

3.2.1 Preparation of Pb(II)-N-acetylcysteine solutions

Solutions were prepared by dissolving H_2NAC (0.1 – 5 mmol) in 5 mL of deoxygenate water. After the addition of $Pb(ClO_4)_2 \cdot 3H_2O$ (0.5 or 0.5 mmol), a white precipitate is formed upon addition of sodium hydroxide. The pH was increased using 1M sodium hydroxide until the solid dissolved (pH 9.1), giving a clear, light yellow solution. Ten aqueous solutions with $[Pb^{2+}]_{total}$ = 10 or 100 mM and H_2NAC:Pb(II) ligand-to-metal molar ratios 2.0, 3.0, 4.0, 5.0 and

10.0 were prepared with pH adjusted to 9.1. Table 3-1 presents the composition of Pb(II)- *N*-acetylcysteine solutions A – J.

Table 7: Composition of Lead(II)-*N*-acetylcysteine solutions (pH 9.1).

Solution	$[Pb^{2+}]_{total}$ (mM)	$[H_2NAC]_{total}$ (mM)	H_2NAC/Pb^{2+}
A	10	20	2.0
B	10	30	3.0
C	10	40	4.0
D	10	50	5.0
E	10	100	10.0
F	100	20	2.0
G	100	30	3.0
H	100	40	4.0
I	100	50	5.0
J	100	100	10.0

3.2.2 Methods

Full details of EXAFS data collection and analysis, NMR, UV-Vis and ESI-MS measurements were described in Chapter 2.

^{207}Pb NMR spectra were collected using a Bruker AMX 300 spectrometer equipped with a 10 mm broadband probe and solid-state capability for Pb(II)-*N*-acetylcysteine solutions A – F. A Bruker Avance 400 MHz spectrometer was used to collected ^{207}Pb NMR spectra for Pb(II)-*N*-acetylcysteine solutions G – L. ^{207}Pb-enriched PbO (94.5 %) was utilized in the preparation of Pb(II)-*N*-acetylcysteine solutions A – F to enable faster detection of ^{207}Pb NMR resonance

before sample decomposition. Samples were checked regularly to ensure precipitation did not occur during NMR measurements. Approximately 4000 – 71000 scans were co-added. 16 scans were co-added for ^{1}H NMR spectra, and 1500 – 7200 scans co-added for ^{13}C NMR spectra.

3.3 Results and discussion

3.3.1 Electrospray ionization mass spectrometry

ESI-MS spectra were collected in positive and negative-ion modes by direct infusion of Pb(II)-cysteine solutions A, B and E ($[Pb^{2+}]$ = 10 mM). ESI-MS spectra of these three solutions identified 1:1, 2:2, 1:2 and 1:3 ligand-to-metal Pb(II)- *N*-acetylcysteine complexes in the gas phase, which may correspond to species found in solution. Several mass ion peaks were observed; as described in Table 8. Only complexes with metal-to- ligand ratios 1:1 and 1:2 were detected in solution A, and a low-intensity signal for a 2:2 complex. Pb(II)-*N*-acetylcysteine complexes with 1:1, 1:2 and 1:3 metal-to-ligand species detected in solutions B and E suggest that $Pb(NAC)_3$ is adequately formed when $H_2NAC/Pb^{2+} \geq 3.0$. No ions associated with Pb(II)-*N*-acetylcysteine complexes were detected in the negative-ion mode. Similar ESI results were found for the Pb(II)-GSH system. Our results differ from the Pb(II)-*N*-acetylcysteine species detected in a previous study, where 1:1, 2:1, 2:2, 3:2 ligand-to-metal complexes were observed, at lower free ligand concentrations.

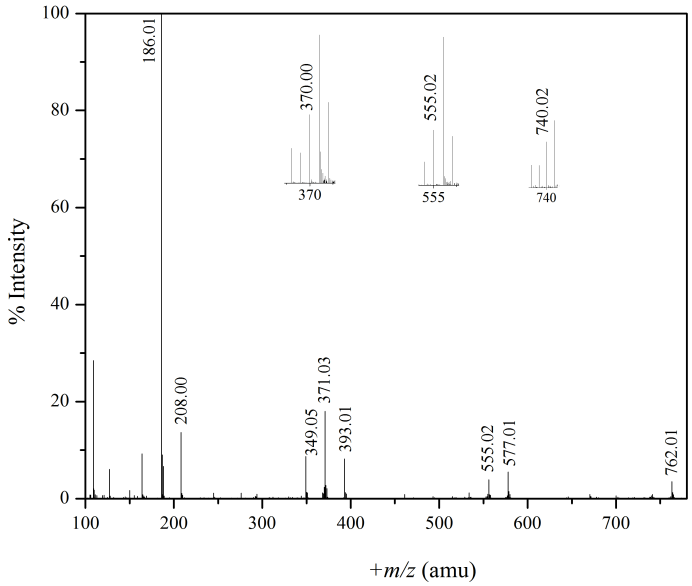

Figure 24: ESI-MS spectrum in the positive-ion mode for solution E (H_2NAC/Pb^{2+} = 10.0); *m/z* = 186.01 amu has been set to 100 % intensity.

Table 8: Assignment of ions detected in ESI-MS spectra; (+) mode for Pb(II)- *N*-acetylcysteine solutions A, B and E.

***m/z* (amu)**	**assignment**	***m/z* (amu)**	**assignment**
186.01	$[Na^+ + H_2NAC]^+$	555.02	$[Na^+ + Pb(H_2NAC)_2 - 2H^+]^+$
208.00	$[2Na^+ + (H_2NAC) - H^+]^+$	577.01	$[2Na^+ + Pb(H_2NAC)_2 - 3H^+]^+$
349.05	$[Na^+ + (H_2NAC)_2]^+$	738.99*	$[Pb_2(H_2NAC)_2 - 3H^+]^+$
370.00	$[Pb(H_2NAC) - H^+]^+$	740.02	$[2Na^+ + Pb(H_2NAC)_3 - 3H^+]^+$
371.03	$[2Na^+ + (H_2NAC)_2 - H^+]^+$	762.01	$[3Na^+ + Pb(H_2NAC)_3 - 4H^+]^+$
393.01	$[3Na^+ + (H_2NAC)_2 - 2H^+]^+$		

*Only detected in Pb(II)-N-acetylcysteine solution A.

3.3.2 Electronic absorption spectroscopy

Two transitions were observed in the UV-Vis spectra of solutions A – E below 275 nm and between 318 – 335 nm (Figure 25). The transitions have been assigned to a combination of S^- 3p→ Pb^{2+} 6p ligand-to-metal charge transfer (LMCT) and intraatomic Pb^{2+} 6s → 6p transitions. For Pb^{2+}-$(GSH)_3$ and other Pb(II) complexes with Pb-S_3 coordination environments, bands with λ_{max} ca 330 nm have been reported as well. The LMCT bands for solutions A and B (H_2NAC/Pb^{2+} = 2.0 and 3.0) were shifted to lower wavelengths (318 and 330 nm respectively) with lower molar absorptivities ($\varepsilon\iota_{max}$ = 3500 and 3600 $M^{-1}cm^{-1}$) relative to Pb(II)-*N*-acetylcysteine solutions C – E (H_2NAC/Pb^{2+} = 4.0 and 10.0). Maximum absorption of Pb(II)-*N*-acetylcysteine solutions B – E were similar to that of Pb(II) complexes with cysteine-containing peptides (λ_{max} = 330 nm), glutathione (λ_{max} = 335 nm), and zinc-binding proteins (λ_{max} = 337 nm)[97], all containing PbS_3 coordination environments. Previous studies show that a red-shift of the LMCT band from 330 to 315 nm corresponds to an increase in number of coordinated cysteine residues from two to three. The molar absorptivity of solutions A and B can be attributed to bis-thiolate Pb(II) complex formation with lower molar absorptivity than PbS_3 complexes in these solutions. Overlapping absorption bands of solutions C – E imply similar Pb(II) speciation in all these solutions. For comparison, the UV-Vis spectrum of a Pb(II)-*N*-acetylcysteine methyl ester solution ($HNACOMe/Pb^{2+}$ = 5.0, pH 7.4) is also shown in Figure 25. *N*-acetylcysteine methyl ester can only bind through its thiol site, and has the same λ_{max} = 335 nm as Pb(II)-*N*-acetylcysteine solutions A – H.

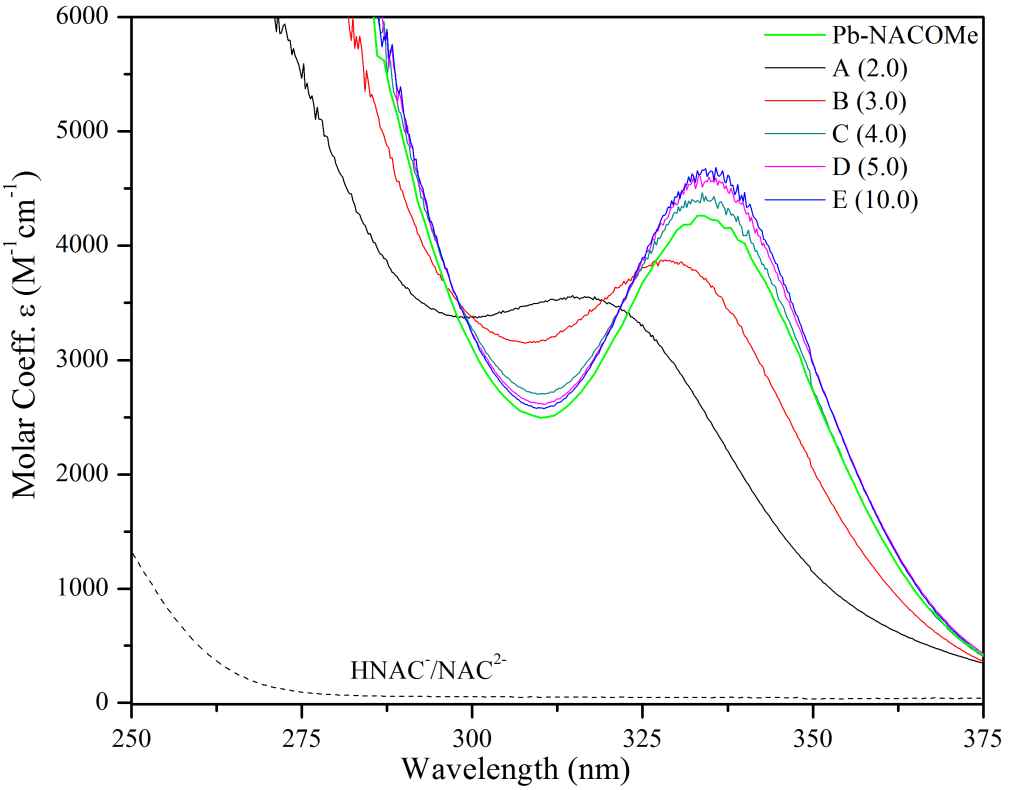

Figure 25: UV-Vis spectra of Pb(II)-*N*-acetylcysteine solutions A – E ([Pb^{2+}] = 10 mM), and free *N*-acetylcysteine (pH 9.1; [H_2NAC] = 1mM).

3.3.3 ^{13}C NMR and ^{1}H NMR spectroscopy

The ^{13}C NMR spectra for free *N*-acetylcysteine (pH 9.1) and Pb(II)- *N*-acetylcysteine solutions A – E in D_2O are shown in Figure 26. Due to fast ligand exchange on the NMR time scale, one set of resonances are observed for both coordinated and free *N*-acetylcysteine in Pb(II)- *N*-acetylcysteine solutions A – E. Compared to free *N*-acetylcysteine, carbon site C_3 bound to the thiolate group showed the largest downfield chemical shift ($\Delta\delta$ ^{13}C = 3.1 ppm), (Table 9) indicating deprotonation and coordination of the thiol group to the Pb(II) centre. The carboxylate (COO^-) group is not likely coordinated, as the $\Delta\delta$ (^{13}C) compared to free *N*-

acetylcysteine is only slightly deshielded (Δδ, ^{13}C = 0.5 ppm) , even in solution A. The C_1 atom of the carboxylate group is only slightly deshielded relative to free *N*-acetylcysteine (Δδ, ^{13}C = 0.5 ppm). The Δδ (^{13}C) observed is considerably smaller than that observed for Pb(II)-penicillamine solutions(Δδ, ^{13}C = 1.4 – 6.0 ppm). The minor shift in ^{13}C NMR signals for carbon site C_1 in solutions A - E suggest that *N*-acetylcysteine is only weakly coordinating to Pb(II) through its COO^- group, if at all. It is believed that the coordination of thiolate groups to Pb^{2+} is more thermodynamically favourable than carboxylate coordination. The chemical shift of carbon C_2 is shifted slightly downfield compared to free *N*-acetylcysteine, likely due to inductive (resonance) effects, and not coordination of the amide group (NH), as the neighbouring acyl-group ($-COCH_3$) prevents *N*-acetylcysteine from binding through the NH site.

Similarly, the chemical shift of proton H-2 bonded to the same carbon atom as the thiolate group, was largely deshielded for Pb(II)- *N*-acetylcysteine solutions A - E compared to free *N*-acetylcysteine (Figure 27), indicating coordination to the Pb(II) centre via S^-. In contrast, deshielding of proton H-1 is only noticeable for Pb(II)-*N*-acetylcysteine solution A, an indication that weakly coordinated COO^- can be bound to the Pb(II) centre.

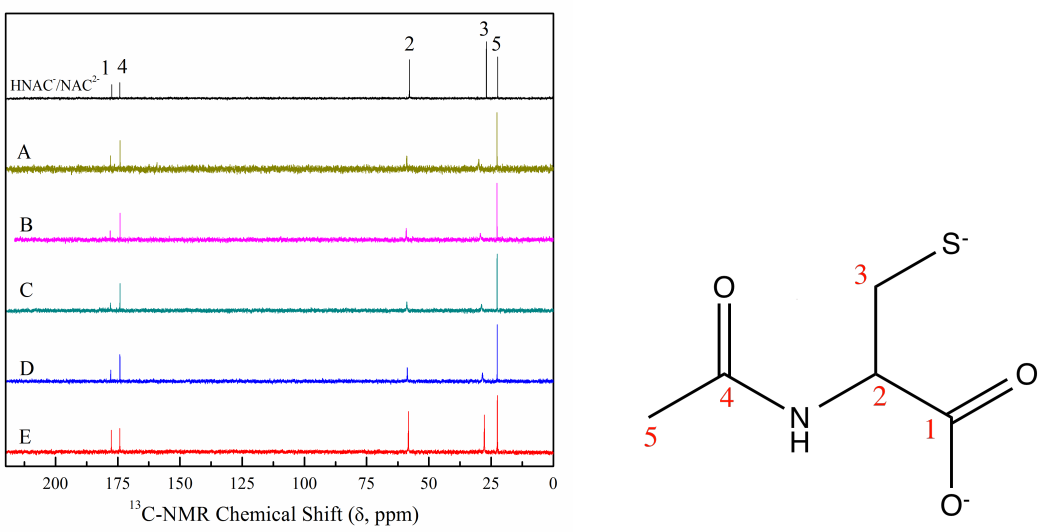

Figure 26: ^{13}C NMR spectra of 0.1 M *N*-acetylcysteine in D_2O (pH 9.1) and Pb(II)- *N*-acetylcysteine solutions A - E(99.9 % D_2O, $[Pb^{2+}]$ = 10 mM); schematic numbering of carbon sites for *N*-acetylcysteine.

Table 9: Comparing ^{13}C NMR chemical shifts for Pb(II)- *N*-acetylcysteine solutions to free *N*-acetylcysteine (Figure 26).

	Δδ (^{13}C, ppm)	
Solution	**C_1**	**C_3**
A	0.5	3.1
B	0.6	2.4
C	0.5	2.0
D	0.4	1.6
E	0.2	0.8

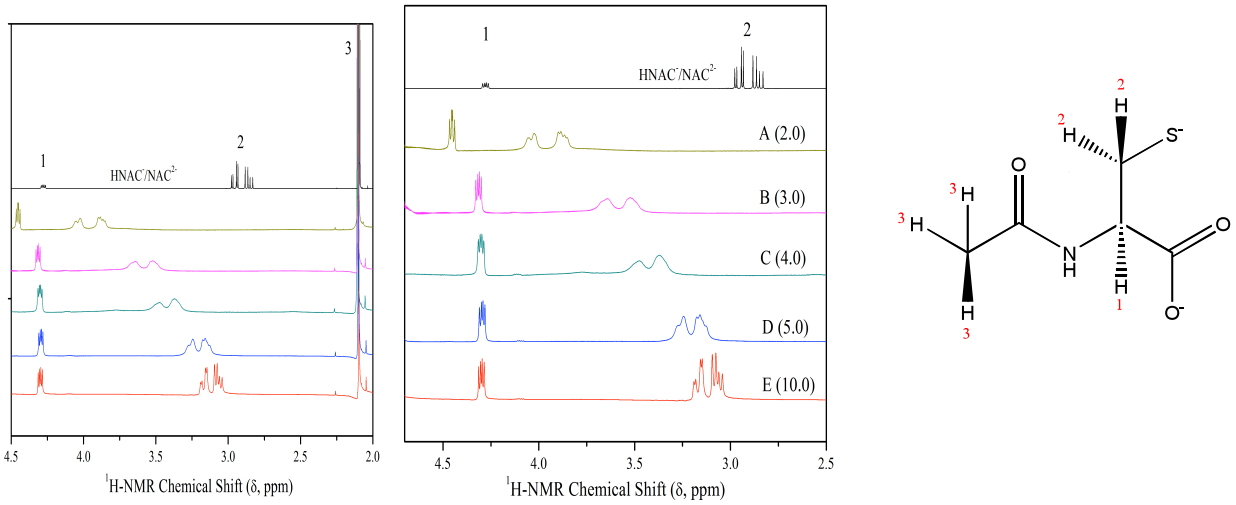

Figure 27: ^1H NMR spectra of 0.1 M *N*-acetylcysteine in D_2O (pH 9.1) and Pb(II)- *N*-acetylcysteine solutions (99.9 % D_2O, $[Pb^{2+}]$ = 10 mM); and schematic numbering of protons for *N*-acetylcysteine.

3.3.4 ^{207}Pb NMR spectroscopy

^{207}Pb chemical shifts have been reported for some lead(II)-thiolate systems, containing carboxylate groups, similar to *N*-acetyl-*L*-cysteine, such as Pb(II) complexes with PbS_3O_3 (1422 – 1463 ppm)[85], and PbS_2O_2 (1506 – 1555 ppm)[98] coordination environments. ^{207}Pb chemical shifts of Pb(II) complexes with only lead(II)-thiolate interactions have also been reported in the range 2577 – 2853 ppm for Pb(II)-peptide complexes with overall PbS_3 coordination environments.[63,81,99] Reported chemical shifts of different Pb(II)-thiolate systems, make evident, the sensitivity of ^{207}Pb resonances are to the chemical environment around the Pb(II) centre. The ^{207}Pb NMR spectra collected for Pb(II)- *N*-acetylcysteine solutions A – J contained single resonances, indicating a single, dominating lead(II) species, or more than one Pb(II) complex in a dynamic equilibrium, faster than the NMR time-scale. ^{207}Pb chemical shifts of Pb(II)- *N*-acetylcysteine solutions containing $H_2NAC:Pb^{2+}$ molar ratios 3.0 – 10.0 were observed over a very small range (> 30 ppm) for both sets of Pb(II)- *N*-acetylcysteine solutions. No ^{207}Pb NMR resonances were detected for solutions A and B ($[Pb^{2+}]$ = 10 mM), likely due to a slow ligand exchange between different Pb(II)- *N*-acetylcysteine complexes, that significantly broadened the signals.[100] Resonances for Pb(II)- *N*-acetylcysteine solutions C, D (H_2NAC/Pb^{2+} = 4.0, 5.0; $[Pb^{2+}]$ = 10 mM) and G (H_2NAC/Pb^{2+} = 3.0; $[Pb^{2+}]$ = 100 mM) were especially broadened ($\Delta\nu_{½}$ ~ 1000 – 16000 Hz) compared to other Pb(II)- *N*-acetylcysteine solutions ($\Delta\nu_{½}$ ~ 10 – 300 Hz), indicating slower ligand exchange between different Pb(II)- *N*-acetylcysteine species at these free ligand concentrations. Pb(II)- *N*-acetylcysteine solutions F and J had especially sharp resonances, indicating a dominant Pb(II)-*N*-acetylcysteine species. The narrow range in which

the ^{207}Pb NMR resonances are observed for both sets of Pb(II)- *N*-acetylcysteine solutions (C – E and G – J) with H_2NAC/Pb^{2+} molar ratios ≥ 3.0, is an indication that a dominant Pb(II)- *N*-acetylcysteine species is present. Both ^{207}Pb resonances for Pb(II)- *N*-acetylcysteine solutions E and J containing similar H_2NAC/Pb^{2+} molar ratios, but differing $[H_2NAC]_{free}$ concentrations (70 and 700 mM), appear at almost identical chemical shifts 2792 and 2791 ppm, a difference of 1 ppm considered negligible on the large ^{207}Pb NMR scale (~17 000 ppm).

The ^{207}Pb chemical shift of Pb(II)- *N*-acetylcysteine solution F containing $H_2NAC:Pb^{2+}$ molar ratio 2.0 was observed at 2886 ppm, appearing further downfield compared to solutions G – J. Its chemical shift comparable to Pb(II) complex $[(C_6H_5)_4As][Pb(SC_6H_5)_3]$ (2868 ppm).[101,102] However, the overall deshielding of the Pb(II) environment for Pb(II)-NAC solution F compared to solutions G – J can be attributed to additional thiolate coordination, since oxygen-donor atoms cause a general shielding effect in ^{207}Pb NMR. Therefore, at this molar ratio ($H_2NAC:Pb^{2+}$ = 2.0), it is proposed that a geometry giving in an overall PbS_3 coordination exists in this Pb(II)- *N*-acetylcysteine solution. ^{207}Pb NMR resonances for binuclear Pb(II) complexes in the solid-state have been reported at δ_{iso} = 2873 ppm for a PbS_2N_2S' coordination environment, where S′ is a bridging thiolate.[88] As a result of the proposed binuclear Pb(II) complex, lack of signal may have been observed for solution A, due to the dynamic exchange between binuclear Pb(II)- *N*-acetylcysteine complexes with an overall Pb-(*S*-NAC)$_3$ coordination, and mononuclear Pb(II) complexes with Pb-(*S*-NAC)$_3$ coordination. Simple lead(II)-thiol systems have been known to form oligonuclear species with bridging thiolates, resulting in dimeric M_2L_3 species, however upon dilution, disappear and remain as 1:1 metal-to-ligand complexes in solution.[103] Similarly, the broadened signal for Pb(II)- *N*-acetylcysteine solution G is likely due to the presence of

mononuclear and binuclear Pb(II) complexes as well, as adequate ligand becomes available to form the mononuclear three-coordinate PbS_3 environment in this solution.

^{207}Pb NMR spectrum measured for an aqueous solution of Pb(II)-*N*-acetylcysteine methyl ester (NACOMe) with thiol as the only functional group (HNACOMe/Pb^{2+} = 5.0, pH 7.4), showed a sharp resonance at 2847 ppm. In the vicinity of the signal for Pb(II)-NAC solution F, the sharp signal suggests one dominating species in solution, and is due to formation of a Pb(II)-(*S*-NACOMe)$_3$ complex. Owing to the ester functional group in NACOMe, unlike *N*-acetylcysteine, the carboxylate in NACOMe no longer participates in metal-binding and only acts as a monodentate (thiolate) ligand. To prevent hydrolysis of the ester group, the Pb(II)-NACOMe solution was kept at physiological pH (7.4), with excess ligand concentration ($[HNACOMe]_{total}$ = 500 mM) to increase the probability of thiolate coordination to the Pb(II) centre.

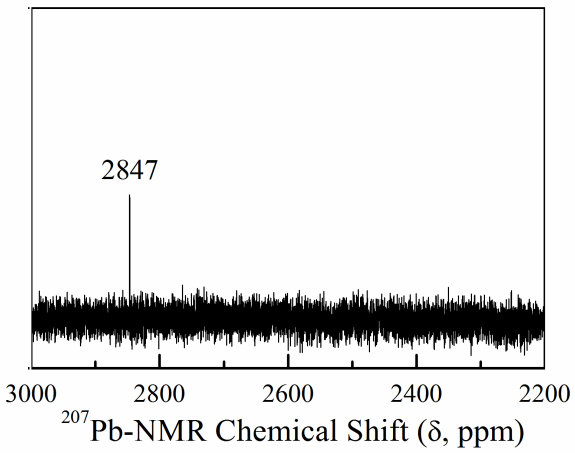

Figure 28: ^{207}Pb NMR spectrum of Pb(II)-*N*-acetylcysteine methyl ester solution [Pb^{2+}] = 100 mM, [HNACOMe] = 500 mM; pH 7.4 in 10 % D_2O.

The resonance observed is comparable to the previously reported ^{207}Pb chemical shift of 2793 ppm for the Pb(II)-$(GSH)_3$ complex that has an overall PbS_3 coordination geometry.[81] It is

reasonable to predict that a mononuclear tri-thiolate Pb(II)- *N*-acetylcysteine complex with trigonal-pyramidal geometry dominates in Pb(II)- *N*-acetylcysteine solutions E and H – J, where narrow resonances were observed with similar chemical shifts.[102]

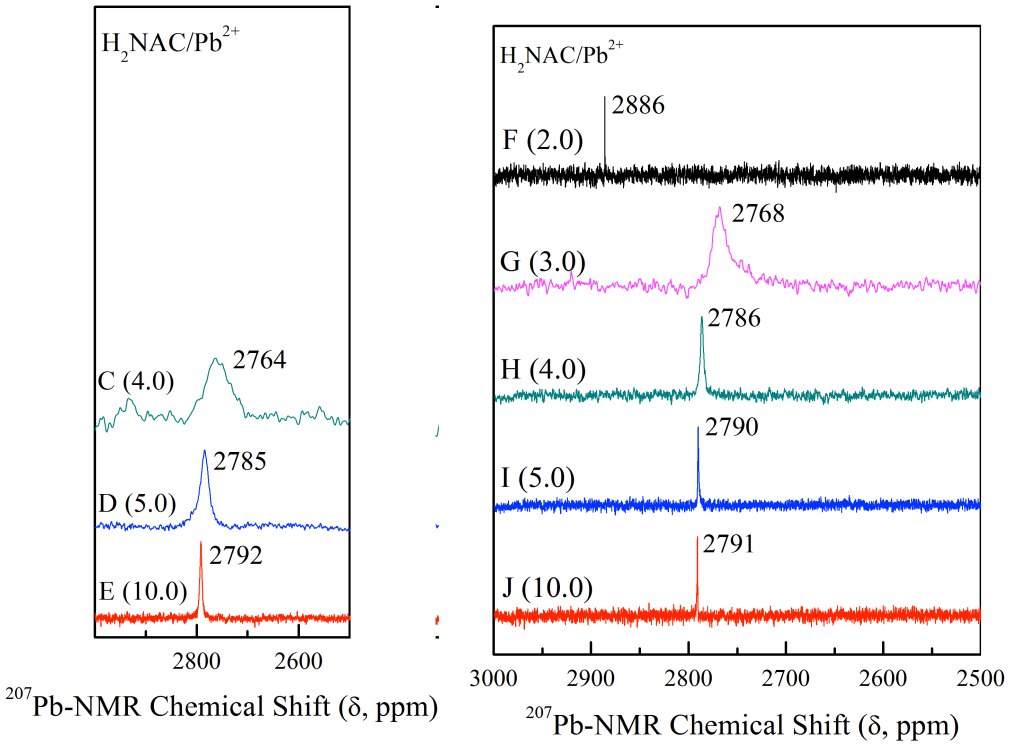

Figure 29: ^{207}Pb NMR spectra of Pb(II)- *N*-acetylcysteine solutions C – E ([Pb^{2+}] = 10 mM; enriched ^{207}Pb) and F - J ([Pb^{2+}] = 100 mM) in 10 % D_2O.

3.3.5 EXAFS spectroscopy

The EXAFS oscillations and corresponding Fourier Transforms (FT) for Pb(II)- *N*-acetylcysteine solutions A – J are shown below. The oscillations for Pb(II)-*N*-acetylcysteine solutions A and F; and B – E and G – J were overlapping (Figure 30). The FT magnitude increased from solutions with H_2NAC/Pb^{2+} molar ratios 2.0 (A and F) to 3.0 (B and G). The decrease in FT magnitude suggests dampened Pb-S oscillations for Pb(II)-*N*-acetylcysteine

solutions A,F and B,G, likely due to the varying bond distances of each Pb-S bond in these solutions. The varied Pb-S bond distances can be attributed to different Pb-S distances expected for terminal compared to bridging Pb-S bonds. When experimental EXAFS spectra of solutions A and F were modeled with three Pb-S bonds, an average Pb-S bond distance of 2.67 ± 0.02 Å was obtained, comparable to a tris(2-mercapto-1-phenylimidazolyl)hydroborato complex (2.67 Å).[84] Again, slightly longer Pb-S distances obtained for Pb(II)- *N*-acetylcysteine solutions A and F can be attributed to the variation in Pb-S distances (terminal vs. bridging) due to the presence of binuclear Pb(II) complexes. All other Pb(II)-*N*-acetylcysteine solutions consistently emerged with average Pb-S bond distances of 2.65 ± 0.02 Å. When the H_2NAC/Pb^{2+} molar ratio is increased from 2.0 to 3.0, the disorder parameter (σ^2) for the Pb-S pathway decreased from 0.0180 – 0.0117 $Å^2$ to more reasonable values 0.0060 - 0.0082 $Å^2$. The average Pb-S distance for all Pb(II)-*N*-acetylcysteine solutions A - J of 2.65 ± 0.02 Å is comparable to the Pb-S bond distance obtained from an EXAFS study of Pb(II) with zinc-binding peptides (2.66 Å), which revealed that Pb(II) preferably binds in a three-coordinate $Pb-S_3$ mode with a trigonal-pyramidal geometry.[84,104,105] It is unlikely that Pb(II) binds to *N*-acetylcysteine with a coordination number higher than three, as an EXAFS study showed that the average Pb-S bond length expected for a PbS_4 coordination environment is ~2.8 Å.[84]

Although two different models was utilized to fit the EXAFS oscillations (I) only Pb-S path, and (II) Pb-S and Pb-O paths, ^{207}Pb NMR does not support a Pb(II)-*N*-acetylcysteine complex with an overall PbS_2O coordination geometry. The deshielded chemical shifts observed from 2768 – 2886 ppm agree with a dominant Pb(II)-N-acetylcysteine complex with an overall PbS_3 coordination.

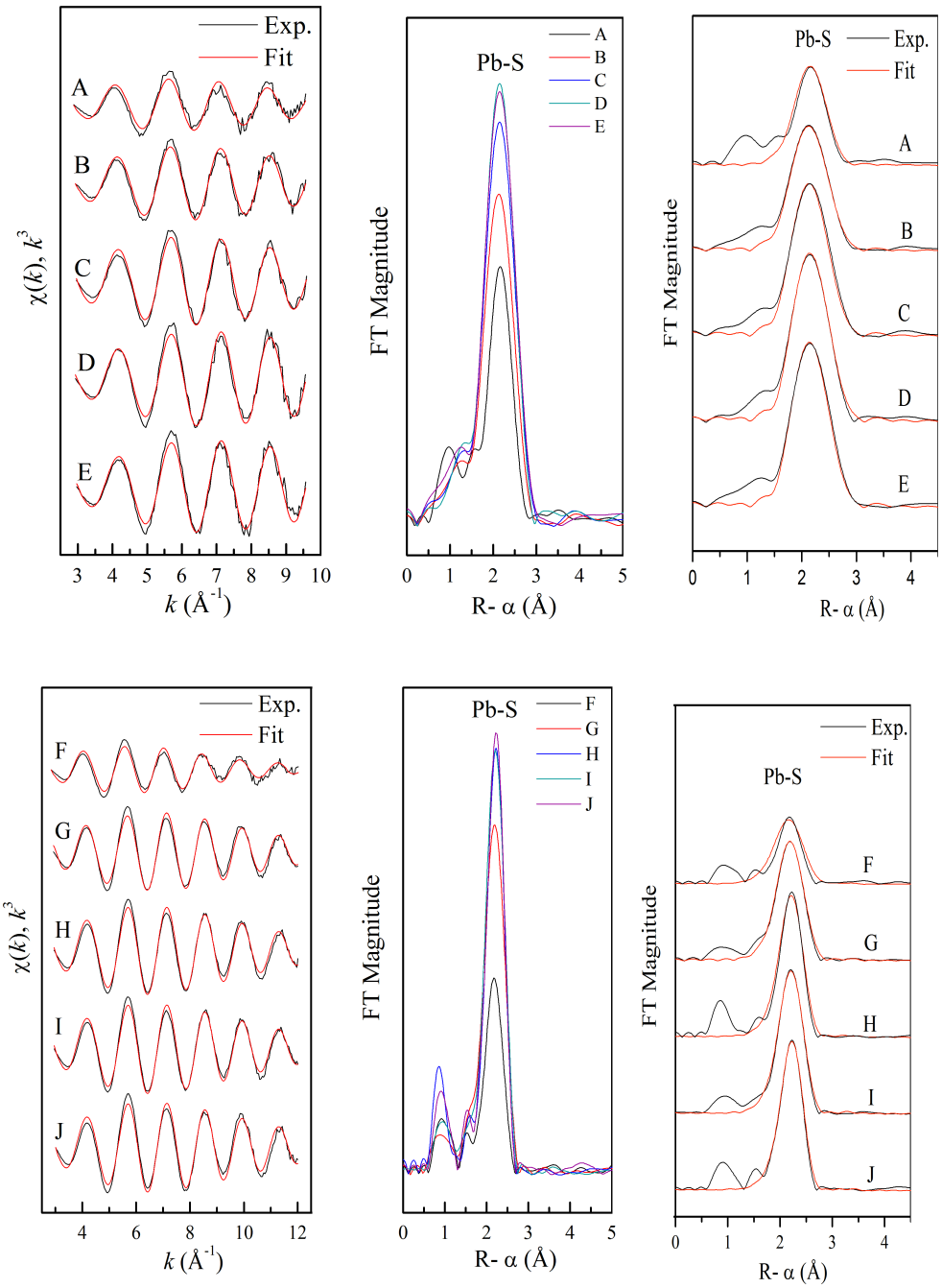

Figure 30: Pb L_{III}-edge k^3-weighted EXAFS oscillations (left); and corresponding (non phase-shift corrected) Fourier Transforms (centre); and FT fitting results for Pb(II)- *N*-acetylcysteine solutions A – E (top) and F – J (bottom) with fittings for Model II.

Table 10: Least-squares curve fitting results for the Pb L_{III}-edge k^3 EXAFS for Pb(II)- *N*-acetylcysteine solutions A – J.

		Pb-O			Pb-S			
Solution	Model	*N*	*R* (Å)	σ^2 (Å^2)	*N*	*R* (Å)	σ^2 (Å^2)	Residual
A	**I**	1.0 *f*	2.45	0.0180	2.0 *f*	2.67	0.011	36.2
	II				2.8	2.68	0.014	36.1
B	**I**	1.0 *f*	2.43	0.0070	2.0 *f*	2.68	0.0061	20.8
	II				3.0	2.65	0.0082	21.0
C	**I**	1.0	2.41	0.0024	2.0 *f*	2.69	0.0044	18.3
	II				3.0	2.65	0.0064	18.1
D	**I**	1.0 *f*	2.38	0.0046	2.0 *f*	2.67	0.0024	18.0
	II				3.0	2.65	0.0053	18.1
E	**I**	1.0 *f*	2.41	0.0017	2.0 *f*	2.68	0.0034	19.8
	II				3.0	2.65	0.0057	19.7
F	**II**				3.0	2.67	0.011	28.7
G	**II**				3.0	2.65	0.0070	16.3
H	**II**				3.5	2.65	0.0066	16.9
I	**II**				3.8	2.65	0.0066	15.8
J	**II**				3.8	2.65	0.0065	21.7

f = fixed value; Fitting range: 2.8 – 12.2 Å^{-1}; S_0^2 = 0.9 *f*; *R* ± 0.02 Å; σ^2 ± 0.002 Å^2; residual value reflects the deviation between theoretical and experimental EXAFS oscillations.

3.4 Conclusions

The investigation of the Pb(II)-*N*-acetylcysteine system in alkaline aqueous solution via ESI-MS, UV-Vis, heteronuclear NMR and EXAFS spectroscopic techniques, suggest there is dominantly Pb-S_3 coordination over the H_2NAC/Pb^{2+} molar ratio range 3.0 – 10.0 and $[Pb^{2+}]$ = 10 and 100 mM. Ions detected in positive-ion mode of ESI-MS show no more than three *N*-acetylcysteine ligands bound to the Pb(II) centre at higher free ligand concentration in Pb(II)- *N*-acetylcysteine solution E ($[NAC^{2-}]$ = 70 mM), similar to the findings for the Pb(II)-GSH system.[106] UV-Vis spectra showed maximum absorption between 318 – 335 nm, characteristic of that expected for $S^- \rightarrow Pb^{2+}$ ligand-to-metal charge transfers (LMCT).[84,97,106] The maximum absorption of the band (λ_{max}) was red-shifted as the $H_2NAC:Pb^{2+}$ molar ratio was increased from 2.0 to 10.0, indicating that the coordination environment had changed from two (Solution A) to three (Solutions B – E) lead(II)-thiolate interactions. It is proposed that a binuclear Pb(II)-N-acetylcysteine with overall PbS_2S' is present in Solution A with $H_2NAC:Pb^{2+}$ = 2.0, and a mononuclear PbS_3 complex dominates after $H_2NAC:Pb^{2+}$ = 3.0 – 10.0. ^{13}C and ^{1}H NMR investigations indicated the thiolate (S^-) group is mainly bound to Pb(II), with weak carboxylate binding. Moreover, the narrow range (< 30 ppm) ^{207}Pb resonances appear, signify the Pb(II) coordination environment does not change drastically over Pb(II)-*N*-acetylcysteine solutions C – J.

The coordination number and average bond distances of Pb(II)-*N*-acetylcysteine solutions A - J investigated by EXAFS spectroscopy, revealed average Pb-S bond distances of 2.65 ± 0.02 Å for $[Pb^{2+}]$ = 10 and 100 mM, and $H_2NAC:Pb^{2+}$ = 3.0 – 10.0 molar ratios. EXAFS spectra of

Pb(II)-*N*-acetylcysteine solutions B – D and F - J were well-modeled by three Pb-S bonds, with acceptable disorder parameters (σ^2 = 0.0051 – 0.0117 Å^2). Slightly high DWFs obtained for Pb(II)-*N*-acetylcysteine solutions A and F, were indicative of non-equivalent Pb-S bond distances, supporting the possibility of a binuclear Pb(*S*-NAC)$_3$ species in solution. Decreased FT magnitudes for solutions A and F were due to destructive interference of Pb-S oscillations possessing varied Pb-S bond lengths, attributed to bridging or terminal Pb-S bonds; while the increase in FT magnitude from solutions A and F to E and J, indicate more consistent Pb-S bond distances for higher H_2NAC/Pb^{2+} mole ratios, and, a dominant Pb(II)-*N*-acetylcysteine species.

The findings of this chapter, propose that Pb(II)-*N*-acetylcysteine solutions A – J possess a Pb-S_3 coordination environment, even at H_2NAC/Pb^{2+} molar ratio 2.0. At this low ratio, it is proposed that two Pb^{2+} ions are bridged by neighbouring thiolate (S^-) groups of *N*-acetylcysteine ligands (Figure 31). Upon availability of increased ligand ($H_2NAC/Pb^{2+} \geq 3.0$), a Pb(II)-*N*-acetylcysteine complex with Pb-(*S*-NAC)$_3$ dominates in aqueous solution at pH 9.1. These results enhance the understanding of Pb(II) speciation with *N*-acetylcysteine over varied ligand-to-metal molar ratios, characterized by their UV-Vis absorption maxima, and ^{207}Pb chemical shifts. Characterization methods may be valuable to applications, where the ligand *N*-acetylcysteine can be designed for detection of the Pb^{2+} ion, and the UV-Vis absorption can indicate the degree of thiolate coordination to the Pb(II) centre.[107–110]

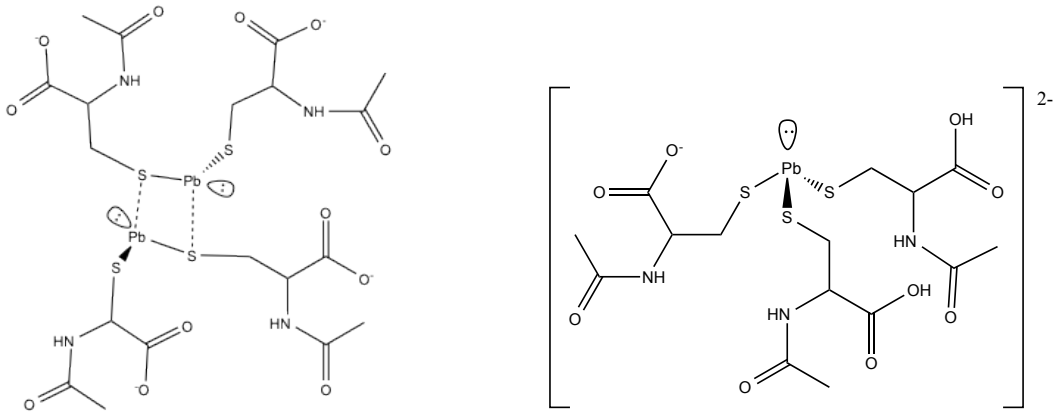

Figure 31: Proposed structures for lead(II)-*N*-acetylcysteine complexes formed in aqueous solution with H_2NAC/Pb^{2+} = 2.0 (left) and > 3.0 (right).

Chapter Four: Complex formation of Lead(II) and *L*-cysteine

4.1 Introduction

To understand the binding of lead(II) to cysteine residues in biomolecules, the speciation of Pb(II) with *L*-cysteine can be studied. *L*-cysteine is one of two amino acids containing a sulphur-moiety. Cysteine has the ability to bind at three coordination sites forming mono-, bi- or tri-dentate complexes, making it a potential chelating agent. Its carboxyl (COOH) group is deprotonated ($pK_a \sim 1.8$), while thiol (SH) and amino (NH_3^+) groups deprotonate simultaneously ($pK_a \sim 8.5$).[103,111] Its derivative *D*-penicillamine, a strong chelator, binds to Pb(II) in a terdentate fashion, and cysteine was thought to be as strongly chelating as penicillamine.[67] However, it was found to complex slightly lower amounts of Pb(II) with log formation constant 12.21 compared to 14.3 for penicillamine.[112] Furthermore, cysteine complexes with metal centres have a tendency to bind in a bidentate fashion.[111,113] In this chapter, Pb(II)-cysteine complex formation is studied in alkaline (pH 9.1 – 10.4) solution, at which solid precipitate was dissolved. At this pH, the probability for thiolate (S^-) formation is increased, promoting formation of higher Pb(II)-cysteine complexes in solution. Unlike penicillamine, cysteine does not possess methyl groups that can cause steric hindrance in solvation of water, or complexation of ligands.[23] Investigation of Pb(II)-cysteine speciation over varied ligand-to-metal ratio (2.0 – 10.0) and $[Pb(II)]_{total}$ (10 and 100 mM) will give valuable insight to cysteine binding to Pb(II) in biological sites.

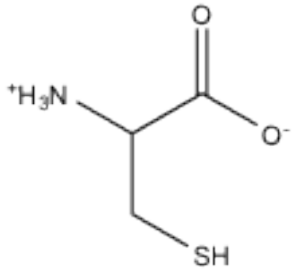

Figure 32: Zwitterionic structure of cysteine.

4.2 Experimental section

4.2.1 Sample preparation

All samples were synthesized under an inert argon atmosphere with oxygen-free boiled water. A Thermo Scientific Orion Star pH meter, calibrated to standard buffers (pH 7.0 and 10.0) was used to monitor the pH of solutions. Lead(II) perchlorate trihydrate $Pb(ClO_4)_2 \cdot 3H_2O$, *L*-cysteine and sodium hydroxide were purchased from Sigma Aldrich and used without further purification. Enriched ^{207}PbO (94.5 %) was obtained from Cambridge Isotope Laboratories.

4.2.1.1 Preparation of Pb(II)-cysteine solutions

Solutions were prepared by dissolving H_2Cys (0.1 – 5 mmol) in 5 mL of deoxygenated water. After the addition of $Pb(ClO_4)_2 \cdot 3H_2O$ (0.5 or 5 mmol), a white precipitate was formed. The pH was increased using 1M sodium hydroxide until the solid dissolved (pH 9.1 or 10.4), giving a clear, colourless solution. Two sets of aqueous solutions with $[Pb^{2+}]_{total}$ = 10 or 100 mM and H_2Cys:Pb(II) ligand-to-metal molar ratios 2.0, 3.0, 4.0, 5.0, 8.0, and 10.0 were prepared with pH adjusted to 9.1 or 10.4. Table 11 presents the composition of Pb(II)-cysteine solutions A – M.

Table 11: Composition of Lead(II)-cysteine solutions.

Solution	$[Pb^{2+}]_{total}$ (mM)	$[H_2Cys]_{total}$ (mM)	H_2Cys/Pb^{2+}	pH
A	10	20	2.0	10.4
B	10	30	3.0	9.1
C	10	40	4.0	9.1
D	10	50	5.0	9.1
E	10	80	8.0	9.1
F	10	100	10.0	9.1
G	10	150	15.0	9.1
H	100	200	2.0	10.4
I	100	300	3.0	9.1
J	100	400	4.0	9.1
K	100	500	5.0	9.1
L	100	800	8.0	9.1
M	100	1000	10.0	9.1

4.2.2 Methods

Full details of EXAFS data collection and analysis, NMR, UV-Vis and ESI-MS measurements were described in Sections 2.2.3 – 2.2.5 in Chapter 2.

Three to four scans were measured for solutions H – M and 12 – 13 scans collected for solutions A – F in EXAFS data collection. Individual scans for each sample were compared to ensure no radiation damage occurred during measurement.

^{207}Pb NMR spectra were collected using a Bruker AMX 300 spectrometer equipped with a 10 mm broadband probe and solid-state capability for solutions A – G. A Bruker Avance 400 MHz spectrometer was used to collected ^{207}Pb NMR spectra for solutions H – M. ^{207}Pb-enriched PbO (94.5 %) was utilized in the preparation of solutions A – G to enable faster detection of ^{207}Pb NMR resonance before sample decomposition. Approximately 12844 – 51200 scans were co-added. 16 scans were co-added for ^{1}H NMR spectra, and 500 – 3000 scans co-added for ^{13}C NMR spectra.

UV-Vis absorption spectra for solutions A – G $C_{Pb(II)}$= 10 mM were measured at room temperature. ESI-MS spectra were collected in positive and negative-ion modes by direct infusion of Pb(II)-cysteine solutions A, B and F.

4.3 Results and discussion

4.3.1 Electrospray ionization mass spectrometry

ESI-MS spectra were collected for Pb(II)-cysteine solutions A, B and F in positive and negative-ion modes. The ESI-MS spectra of these three solutions identified Pb(II)-cys complexes with metal:ligand mole ratios 1:1, 1:2, 1:3 and 2:2 in the gas phase, which may correspond to species found in solution. In positive-ion mode, several Pb(II)-cys mass peaks were observed as described in Table 12. In Pb(II)-cys solution A, only the 1:1 and 1:2 metal-to-ligand mole ratio complexes were detected, the 1:1 complex detected in positive-ion mode, and the low-intensity mass peak 1:2 complex detected in the negative-ion mode. In Pb(II)-cys solutions B and F, all three metal-to-ligand mole ratios 1:1, 1:2 mass peaks and a low-intensity 1:3 mass peak were

observed, suggesting that the H_2Cys/Pb^{2+} mole ratio 3.0 is sufficient to form a Pb-$(Cys)_3$ species. An ESI-MS investigation of amino acids with heavy metals, identified Pb(II)-cysteine complexes with metal-to-ligand mole ratios 1:1, 1:2, and 2:2, but not 1:3 from solutions prepared using equimolar (0.5 mmol) metal and ligand quantities.[109] No more than two cysteine ligands bound to the Pb(II) centre were observed, suggesting that cysteine binds with Pb(II) with 1:1, 1:2 or 1:3 metal-to-ligand mole ratios, even when additional ligand is available.

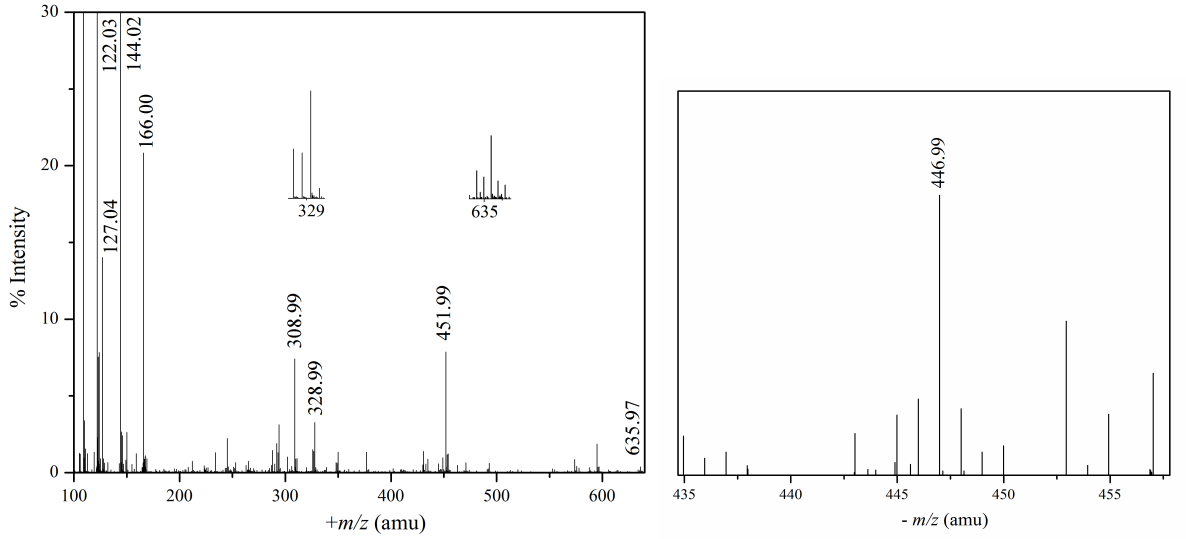

Figure 33: ESI-MS spectrum in the positive-ion mode (left) for Pb(II)-cysteine solution F (H_2Cys/Pb^{2+} = 10.0); *m/z* = 122.03 amu has been set to 100 % intensity and; negative-ion mode (right).

Table 12: Assignment of ions detected in ESI-MS spectra; (+) mode for Pb(II)-cysteine solutions A, B, and F.

***m/z* (amu)**	**assignment**	***m/z* (amu)**	**assignment**
122.03	$[H_2Cys + H^+]^+$	327.99	$[Pb(H_2Cys) - H^+]^+$
144.02	$[Na^+ + H_2Cys]^+$	349.97	$[Na^+ + Pb(H_2Cys) - 2H^+]^+$
166.00	$[2Na^+ + H_2Cys - H^+]^+$	635.97	$[3Na^+ + Pb(H_2Cys)_3 - 4H^+]^+$
308.99	$[3Na^+ + 2H_2Cys - 2H^+]^+$		

4.3.2 Electronic absorption spectroscopy

Two transitions were observed in the UV-Vis spectra of Pb(II)-cys solutions A – G: an intense band ca. 260 nm and a less intense band at $\lambda_{max} \sim 298 – 300$ nm. The transitions have been assigned to a combination of S^- 3p → Pb^{2+} 6p ligand-to-metal charge transfer (LMCT) and intra-atomic Pb^{2+} 6s → 6p transitions. LMCT bands have been reported for Pb(II)-complexes with PbS_2N_2[114] and $PbS_2(N/O)$[115] coordination geometry at 310 and 325 nm respectively. The absorption maxima of Pb(II)-cys solutions A – G, are almost identical to those found for Pb(II)-penicillamine solutions, as seen in Chapter 2 with $\lambda_{max} = 299$ nm. Additionally, Pb(II)-cysteine solution A has a comparable molar extinction coefficient $\varepsilon\iota_{max} \approx 4546$ $cm^{-1}M^{-1}$ to Pb(II)-penicillamine solutions ($\varepsilon\iota_{max} \approx 4900$ $cm^{-1}M^{-1}$). UV-Vis spectra for Pb(II)-penicillamine solutions were concluded to represent bis-thiolate lead(II) environments with an overall $PbS_2(N/O)_2$ coordination similar to that found for the Pb(II) complex with CP-CCHH, a finger peptide containing two cysteine and two histidine residues.[114] A decreasing intensity of a specific

absorption band, generally indicates less complex formation in solution, in this case a bis-thiolate Pb-$(cys)_2$ complex. The most apparent decrease in intensity is observed for Pb(II)-cysteine solutions D – G, with H_2Cys/Pb^{2+} mole ratios 3.0 – 15.0. Pb(II)-cysteine solution G with highest free ligand concentration, has the lowest intensity. Absorption maxima of Pb(II) complexes with glutathione and *N*-acetylcysteine, appeared at higher wavelengths (317 – 335 nm). As the LMCT band ca. 298 nm becomes less prominent for Pb(II)-cysteine solutions A – G, a subtle shoulder emerges around 337 nm, slightly increasing as free ligand concentration is increased. This may indicate that at $[Pb^{2+}]_{total}$ = 10 mM, formation of PbS_3 can be formed, although minor. LMCT bands have been reported for Pb(II) complexes with PbS_3 coordination environments for cysteine-containing peptides CP-CCCC and CP-CCCH with λ_{max} = 330 nm[14], zinc-binding proteins (337 nm), and wild-type CadC protein (350nm)[38].

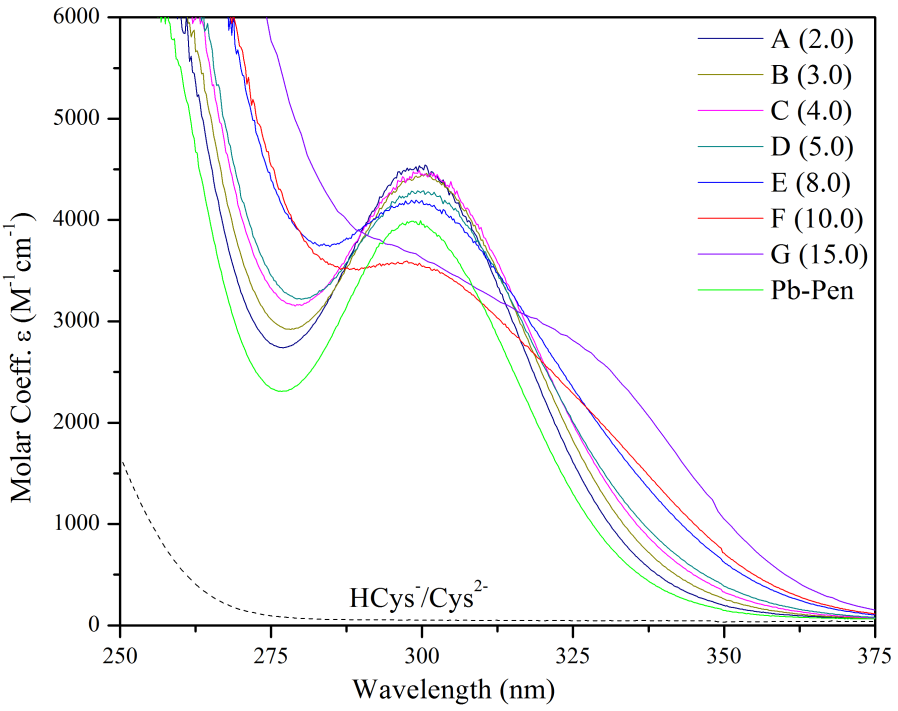

Figure 34: UV-Vis spectra of Pb(II)-cysteine solutions A – G ($[Pb^{2+}]$ = 10 mM), and free $HCys^-/Cys^{2-}$ (pH 9.1; $[H_2Cys]$ = 1 mM).

4.3.3 ^{13}C NMR and ^{1}H NMR spectroscopy

The ^{13}C NMR spectra for free $HCys^{-}/Cys^{2-}$ (pH 9.1) and Pb(II)-cysteine solutions A – F in D_2O are shown in Figure 35. As the free ligand concentration is increased, resonances observed for Pb(II)-cysteine solutions shift toward ^{13}C NMR resonance of free cysteine, due to the increase concentration of unbound ligand in each solution. A comparison of ^{13}C NMR shifts for each Pb(II)-cysteine solution to free cysteine (pH 9.1) is shown in Table 13. A downfield shift of all carbon sites for Pb(II)-cysteine solution A compared to free ligand, indicates that the carboxylate (COO^{-}), thiolate (S^{-}), and amine (NH_2) groups are all coordinated to the Pb(II) centre. A dramatic decrease in $\Delta\delta$ (^{13}C, ppm) is observed for carbon C_1 in Pb(II)-cysteine ligand concentration is increased by 10 mM, suggesting a large degree of reduced carboxylate coordination at H_2Cys/Pb^{2+} molar ratio 3.0. Less drastic decreases in $\Delta\delta$ (^{13}C, ppm) for carbons C_2 and C_3 indicate coordination via thiolate and amine sites is still expected. As H_2Cys/Pb^{2+} molar ratio is increased to 10.0, much of the resonances resemble free ligand chemical shifts, however, C_3 remains with the largest $\Delta\delta$ (^{13}C, ppm) compared to free ligand, and is likely still bound to the Pb(II) centre at high ligand concentration.

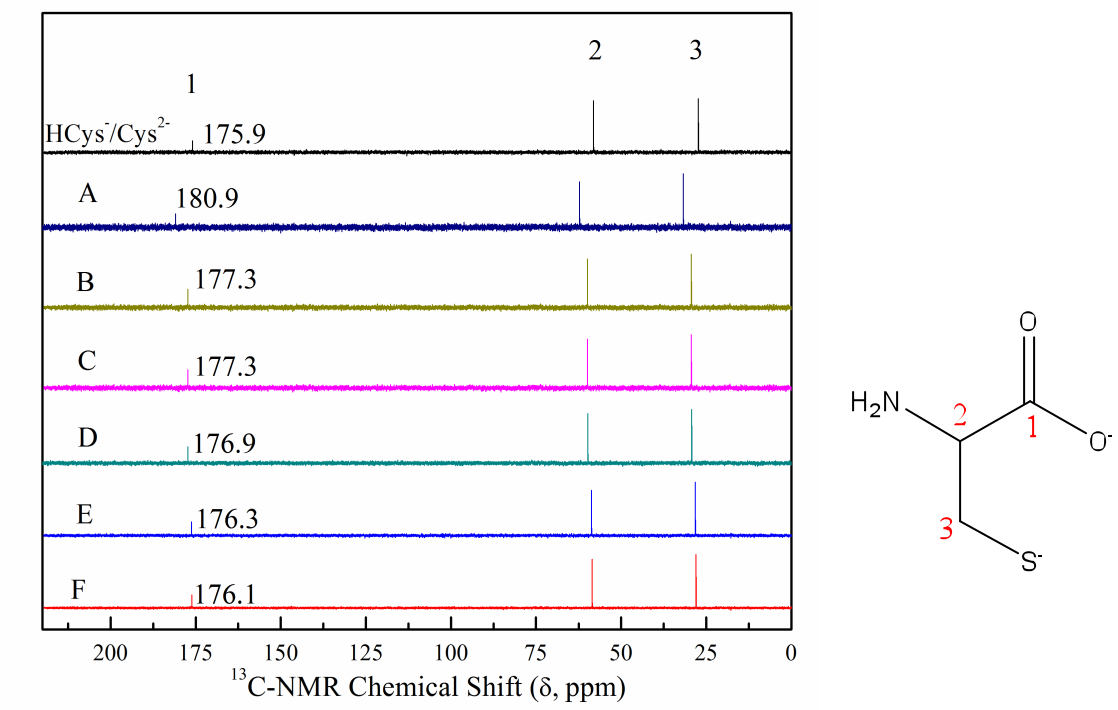

Figure 35: ^{13}C NMR spectra of 0.1 M H_2Cys in D_2O (pH 9.1) and Pb(II)-cysteine solutions A – F (99.9 % D_2O), $[Pb^{2+}]$ = 10 mM); schematic numbering of carbon sites for Cys^{2-}.

Table 13: Comparing ^{13}C NMR chemical shifts for Pb(II)-cysteine solutions A – F to free $HCys^-$ /Cys^{2-}.

	Δδ (^{13}C, ppm)		
Solution	C_1	C_2	C_3
A	5.0	4.1	4.4
B	1.4	1.8	2.0
C	1.4	1.7	2.0
D	1.0	1.3	1.5
E	0.4	0.6	0.9
F	0.2	0.4	0.7

Similarly, ^1H NMR spectra of Pb(II)-cysteine solutions A – F showed downfield shifts for three proton sites as shown in Figure 36. Magnetically non-equivalent protons H_a and H_b each appeared between 3.5 – 3.0 ppm for Pb(II)-cysteine solutions A – F. Proton H_c appeared furthest downfield, as it neighboured two electron with-drawing groups COO^- and NH_2. A high-field NMR study of cysteine and lead(II), reported that in alkaline solution, a trans-rotamer of cysteine is strongly favoured, which is restricted to bidentate coordination via S^- and NH_2 coordination sites. The trans-rotamer is likely favoured in alkaline solution, as repulsion of COO^- and S^- groups are minimized in this conformation. Therefore, if cysteine binds to Pb(II) with a 2:1 ligand-to-metal molar ratio, prone to being in the trans-conformation, there is a high possibility of bidentate Pb-$(S,N)_2$ coordination, similar to $Pb(aet)_2$.

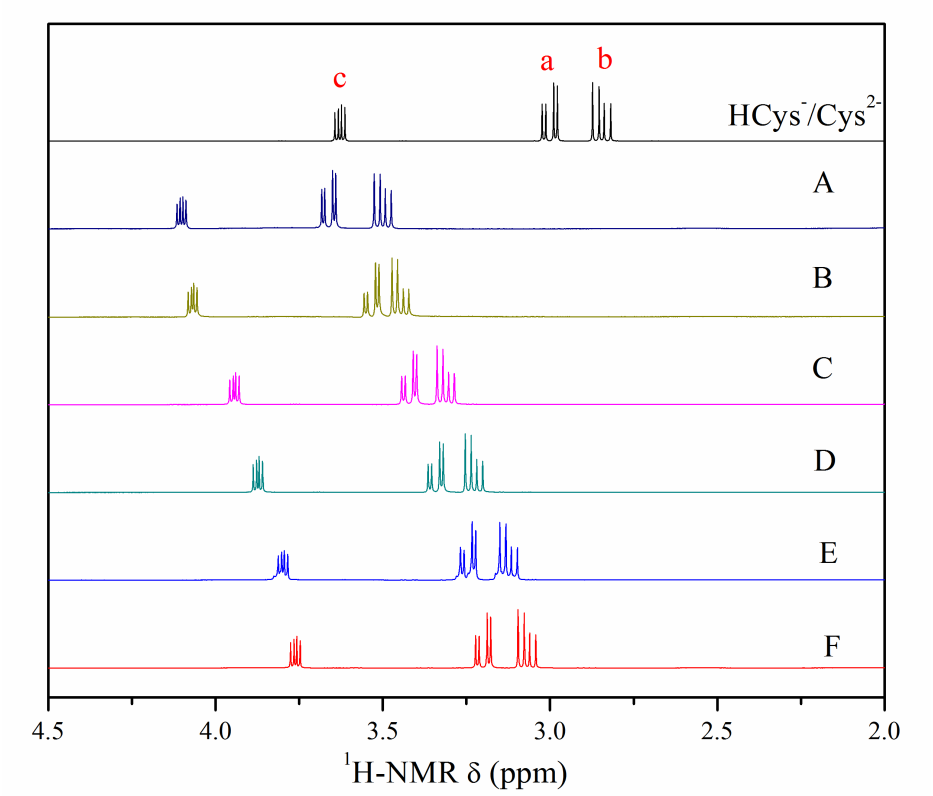

Figure 36: ^{1}H NMR spectra of 0.1 M H_2Cys in D_2O (pH 9.1) and Pb(II)-cysteine solutions A – F (99.9 % D_2O), [Pb^{2+}] = 10 mM); schematic numbering of protons for Cys^{2-}.

Table 14: ^{1}H NMR chemical shifts for Pb(II)-cysteine solutions A – F ([Pb^{2+}] = 10 mM) and chemical shifts compared to free ligand Δδ.

Solution	δ (^{1}H, ppm)		
	H_a	H_b	H_c
free $HCys^{-}/Cys^{2-}$	2.85	3.00	3.63
A	3.50	3.66	4.10
B	3.45	3.53	4.07
C	3.31	3.42	3.94
D	3.23	3.34	3.87
E	3.12	3.25	3.80
F	3.07	3.14	3.76

4.3.4 ^{207} Pb NMR spectroscopy

Reported ^{207}Pb chemical chemical shifts have previously been discussed in Chapters 2 and 3 for some lead(II)-thiolate systems that also contain carboxylate and amine groups ranging from 1422 – 2853 ppm.[63,85,99,100,116] The general trend seen in ^{207}Pb NMR and lead(II)-thiolate systems, is that nuclear shielding decreases with increasing polarizability of the coordinating atom, such that S < N < O is ordered least to most shielding. Hence, applying ^{207}Pb NMR to study changing Pb(II) environments can be advantageous. Recalling ligands from chapters 2 and 3, penicillamine and *N*-acetylcysteine, two derivatives of cysteine, one with steric hindrance (via *3,3*-dimethyl groups) and one with only two binding sites COO^{-} and S^{-} respectively. The

sensitivity of ^{207}Pb NMR to subtle changes in its chemical environment, will allow us to examine the speciation of Pb(II)-cysteine solutions.

The ^{207}Pb NMR spectra collected for Pb(II)-cysteine solutions A – M contained single resonances (Figure 37). ^{207}Pb chemical shifts of Pb(II)-cysteine solutions A – M, containing H_2Cys/Pb^{2+} molar ratios 2.0 – 10.0 were observed over a wide range (2005 – 2507 ppm) compared to the two previous lead(II)-thiolate systems discussed in chapters two and three: Pb(II)-penicillamine (1806 – 1873 ppm) and Pb(II)-*N*-acetylcysteine (2764 – 2886 ppm). A chemical shift range of $\Delta\delta$ (^{207}Pb, ppm) ~ 500 (Pb(II)-cysteine) compared to $\Delta\delta$ (^{207}Pb, ppm) < 50 ppm (Pb(II)-penicillamine and *N*-acetylcysteine), indicates the Pb(II) environment is changing significantly over Pb(II)-cysteine solutions A – M.

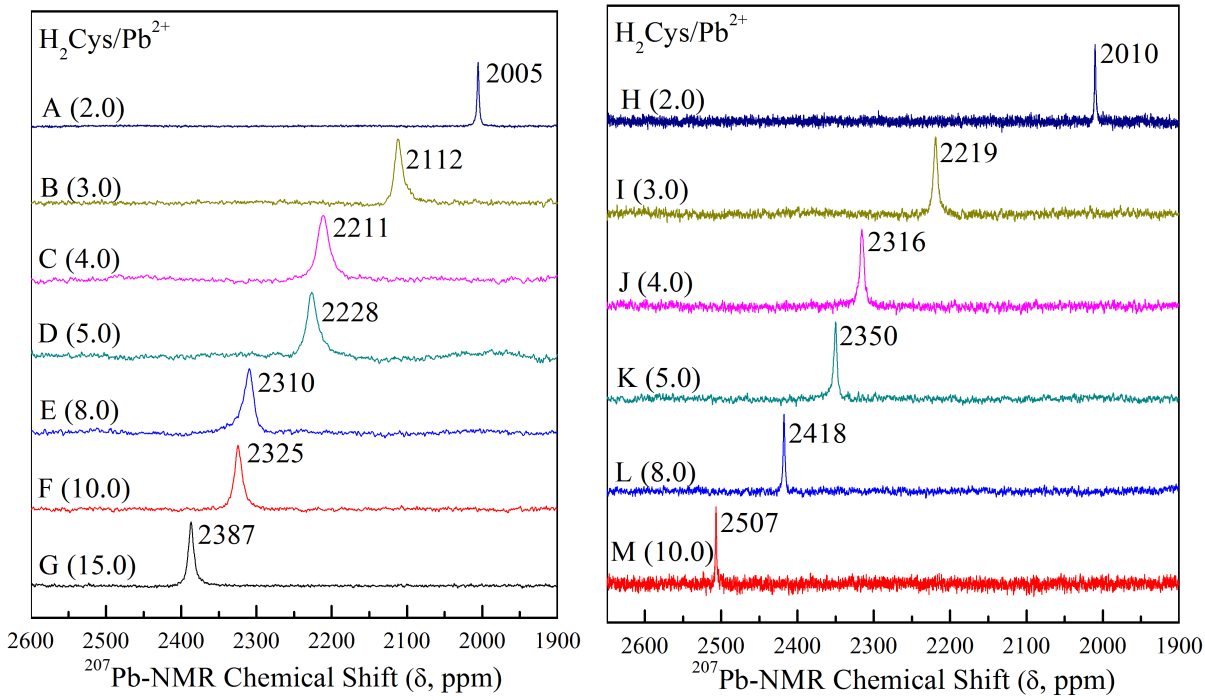

Figure 37: ^{207}PbNMR spectra of Pb(II)-cysteine solutions A – G $[Pb^{2+}]$ = 10 mM and H – M $[Pb^{2+}]$ = 100 mM.

Analogous to Pb(II)-penicillamine solutions with $H_2Cys/Pb^{2+} = 2.0$, resonances for Pb(II)-cysteine solutions A and G appear narrowest, and most shielded compared to solutions with higher H_2Cys/Pb^{2+} mole ratios. Compared to Pb(II)-pencillamine (~1825 ppm), Pb(II)-cysteine solutions A and G are ~200 ppm deshielded. The deshielding is proposed to be due to a Pb(II)-cysteine with a thiolate coordination to the lead(II) centre that replaces the carboxylate group, to give an overall PbS_2N_2 geometry, as suggested earlier by ^{13}C and ^{1}H NMR.

As freePb(II)-cysteine solutions B – G and I – M chemical shift values of similar molar ratios between each set become less parallel.^{207}Pb chemical shifts of solutions H – M progress downfield, quicker than for Pb(II)-cysteine solutions A – G. This trend is consistent with the amount of free ligand $[HCys^-/Cys^{2-}]_{free}$ present in Pb(II)-cysteine solutions. As more free ligand is available in solutions F – M than A – E, three-coordinated Pb(II)-cysteine complexes form more readily, that are causing a downfield progression. If solutions A and G are proposed to be a mixture of PbS_2NO and PbS_2N_2 coordination, then addition of another lead(II)-thiolate interaction, will cause deshielding and downfield movement of the average Pb(II) chemical shift.

To further investigate the behaviour of Pb(II)-cysteine complexes in solution, ^{207}Pb NMR of Pb(II)-aminoethanethiolate (aet) samples were measured in both solid and solution-state. The crystal structure of Pb(II)-$(aet)_2$ was reported by Fleischer and Schollmeyer (2004), but no ^{207}Pb NMR spectra were obtained due to the labile nature (and low solubility) of simple thiolates in solution, and difficulty of separating sidebands in solid-state Pb NMR. Fortunately, solid-state ^{207}Pb NMR spectra of the lead(II) bis$(aet)_2$ solid was successfully measured, using spin rates 5.0, 6.0 and 7.0 kHz. By determining overlapping sidebands in all three spectra, the isotropic chemical shift $\delta_{iso} = 2100$ ppm was assigned to the PbS_2N_2 coordination geometry (Figure 39).

Additionally, a solution-state ^{207}Pb NMR spectrum was measured by dissolving $Pb(aet)_2$ crystals in aqueous solution (10 % D_2O), and adding 1 equimolar of free cysteamine to solution, to prevent precipitation of the stable $Pb(aet)_2$ crystals. The ^{207}Pb chemical shift obtained from this solution (Figure 40) detected a single resonance at 2212 ppm. The ~100 ppm $\Delta\delta$ (^{207}Pb, ppm) present, is due to the slight increase in ligand concentration (aet/Pb^{2+} = 3.0) allowing the formation of $Pb(S\text{-}aet)_3$ in solution. The pH of the Pb(aet) solution was measured at pH 10.1, as prepared (not adjusted), since precipitation occurred if the pH was lowered.

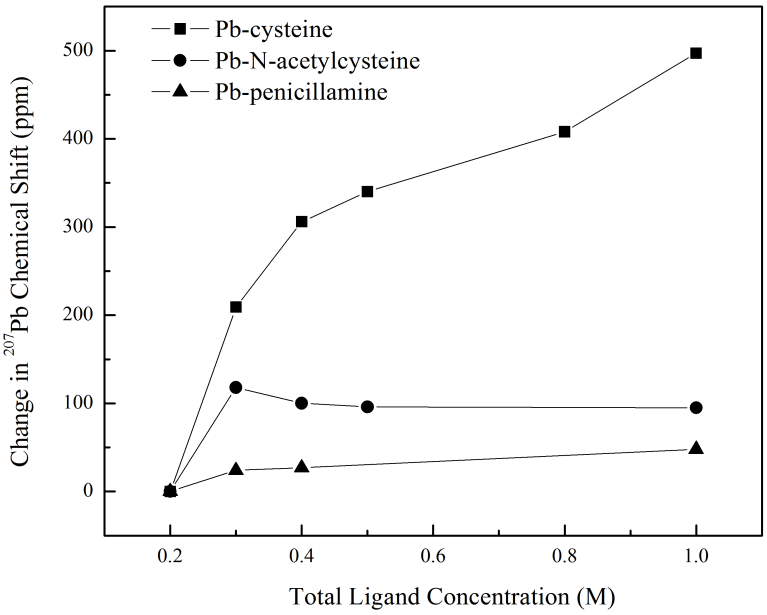

Figure 38: Comparing the change in ^{207}Pb chemical shift with increased ligand concentration for solutions with [Pb^{2+}] = 100 mM for Pb(II) systems with cysteine, penicillamine and *N*-acetylcysteine.

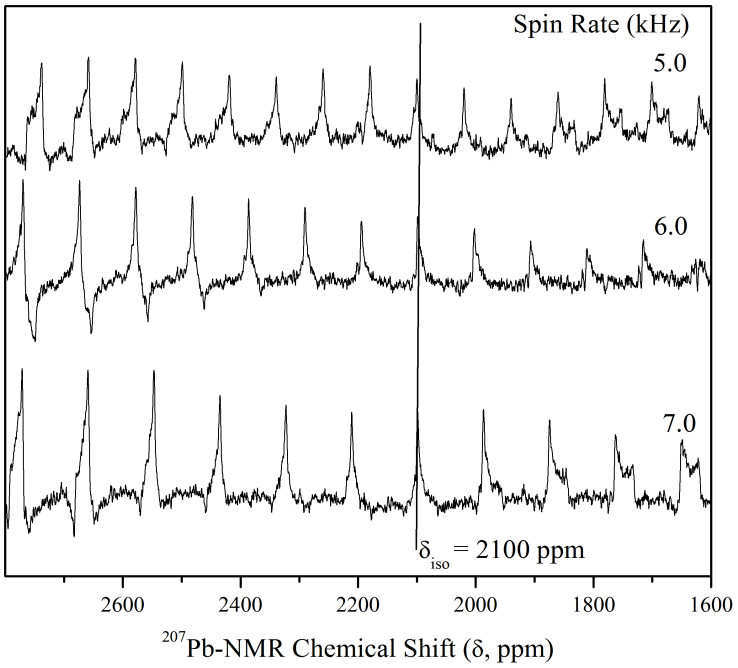

Figure 39: ^{207}Pb variable amplitude MAS NMR spectra of lead(II)-bis-(aminoethanethiolate)$_2$ solid.

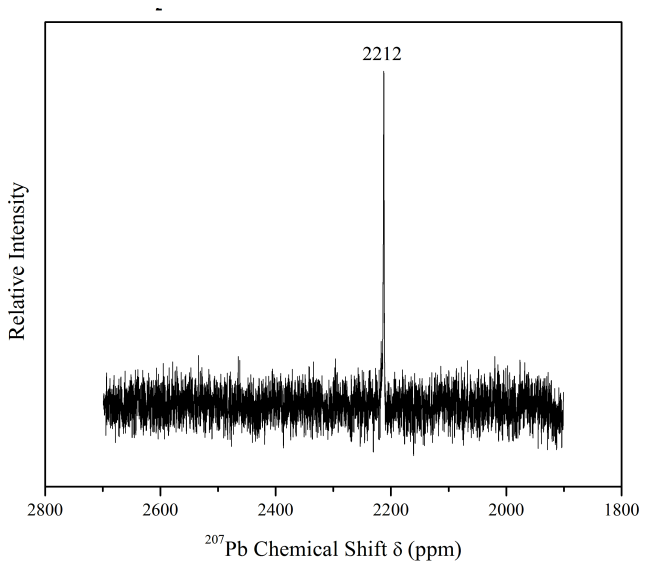

Figure 40: Solution-state ^{207}Pb NMR spectrum of Pb(II)-(aet) solution with aet/Pb^{2+} = 3.0 and [Pb^{2+}] = 76 mM, pH 10.1.

The steady downfield shift of ^{207}Pb resonances of Pb(II)-cysteine solutions A – M can be justified by the dynamic equilibrium between three main Pb(II)-cysteine complexes. Starting downfield from Pb(II)-penicillamine chemical shifts, Pb(S,N,O-cys)S-cys and Pb(S,N-cys)$_2$ complexes dominate solutions A and H. As H_2Cys/Pb^{2+} increases, Pb(II)-cysteine complexes with Pb(S,N-cys)$_2$ are dominant (2219 ppm), with the formation of Pb(S-cys)$_3$ in solutions B and I, as supported by Pb(aet)$_3$ solution with δ_{Pb} = 2212 ppm. Finally, at highest H_2Cys/Pb^{2+} molar ratios ($\leq$ 4.0), Pb(II)-cysteine complexes with Pb(S-cys)$_3$ form in larger amounts, while Pb(S,N-cys)$_2$ complexes will persist in these solutions. Broadened signals observed in Pb NMR spectra of solutions B – G support that a mixture of Pb(II)-cysteine complexes is in equilibrium at lower free ligand concentrations. Pb(II)-cysteine solution G was measured to determine if H_2Cys/Pb^{2+} molar ratio 15.0 at $[Pb^{2+}]$ = 10 mM would be sufficient to observe a Pb chemical shift further downfield, an indication of more Pb(S-cys)$_3$ formed. In this Pb(II)-cysteine solution, if $[HCys^-/Cys^-]_{coord.}$ = 30 mM to give a Pb(S-cys)$_3$ complex, $[HCys^-/Cys^-]_{free}$ = 120 mM. The Pb chemical shift observed for Pb(II)-cysteine solution G, remained near shifts observed for Pb(II)-cysteine solutions J - L, which have $[HCys^-/Cys^-]_{free} \approx$ 100 – 300 mM. ^{207}Pb NMR was reasonably useful in deducing possible Pb(II)-cysteine complexes present in solutions A – M, with the help of previously reported ^{207}Pb shifts of lead(II)-thiolates, ^{13}C and ^{1}H NMR, UV-Vis and ESI-MS. The information gained from techniques above, can be complimented with structural information obtained from XAS measurements collected for Pb(II)-cysteine solutions.

4.3.5 EXAFS spectroscopy

The EXAFS oscillations and corresponding Fourier Transforms (FT) for Pb(II)-cysteine solutions A – F and H - M are shown in Figure 41. The Pb L_{III}-edge X-ray Absorption Fine

Structure (EXAFS) oscillations for Pb(II)-cysteine solutions A- F and H - M were modeled using two different models: (I) using only one Pb-S path, and (II) including Pb-S and Pb-(N/O) paths. Regardless of the model used, average Pb-S and Pb-(N/O) bond distances consistently emerged in the range 2.63 – 2.67 Å and 2.43 – 2.46 ± 0.04 Å respectively (Table 15). The average Pb-S and Pb-(N/O) bond distances obtained were consistent with Pb(II)-cysteine complexes having PbS_2N_2 and PbS_3 coordination geometries, since Pb(II) complexes Pb-S and Pb-(N/O) distances are reported for lead(II)-thiolate complexes.[46,89,90,102,106,117–120] The Fourier Transform magnitudes were slightly lower for Pb(II)-cysteine solutions A and H compared to solutions B – F and I – M, suggesting less Pb-S coordination, or dampening of the FT amplitude due to unequal Pb-S bond distances. The average Pb-S (2.65 ± 0.04Å) and Pb-(N/O) (2.44 ± 0.04Å) bond distances obtained through curve fitting of k^3 weighted EXAFS oscillations are comparable to those reported for lead(II)-bis(aminoethanethiolate)$_2$: Pb-S_{ave} = 2.64 Å and Pb-N_{ave} = 2.59 Å, and Pb(II)-GSH: Pb-S_{ave} = 2.64 Å and Pb-N as found in the penicillaminatolead(II) crystal structure.[106,117] High disorder parameters obtained for Pb-(N/O) bond distances can be expected, if cysteine acts as a *(S,N)*-bidentate chelator as described in the crystal structure of lead(II)-bis(aminoethanethiolate)$_2$. The crystal structure, with no centre of symmetry contains two similar Pb-S bond distances (2.63 and 2.64 Å), and two different Pb-N bond distances (2.55 and 2.63 Å), commonly found in 4-coordinate PbS_2N_2 Pb(II) complexes.[117,121] At lowest H_2Cys/Pb^{2+} mole ratio 2.0, Pb(II)-cysteine solutions A and H fit with lower residuals for model I compared to model II. Fitting residuals of all other Pb(II)-cysteine solutions did not differ substantially, indicating the high probability of mixed Pb(II)-complexes in Pb(II)-cysteine solutions A – M. Pb(II)-cysteine solutions H – M consistently had overall better fitting residuals, for both models I and II. There was no strongly preferred coordination model for Pb(II)-cysteine solutions, even at

high ligand concentrations. The improved disorder of Pb-S bond lengths found using model II however, is an indicator that $Pb(S\text{-}cys)_3$ is more readily formed at higher free ligand concentrations.

Comparing EXAFS oscillations of Pb(II)-cysteine solutions A and H in Figure 42 demonstrate that both solutions have similar local structure around the Pb(II) centre. In addition, the slightly smaller FT amplitude of Pb(II)-cysteine solutions A and H are shown as a comparison with Pb(II)-cysteine solutions D and M (Figure 43).

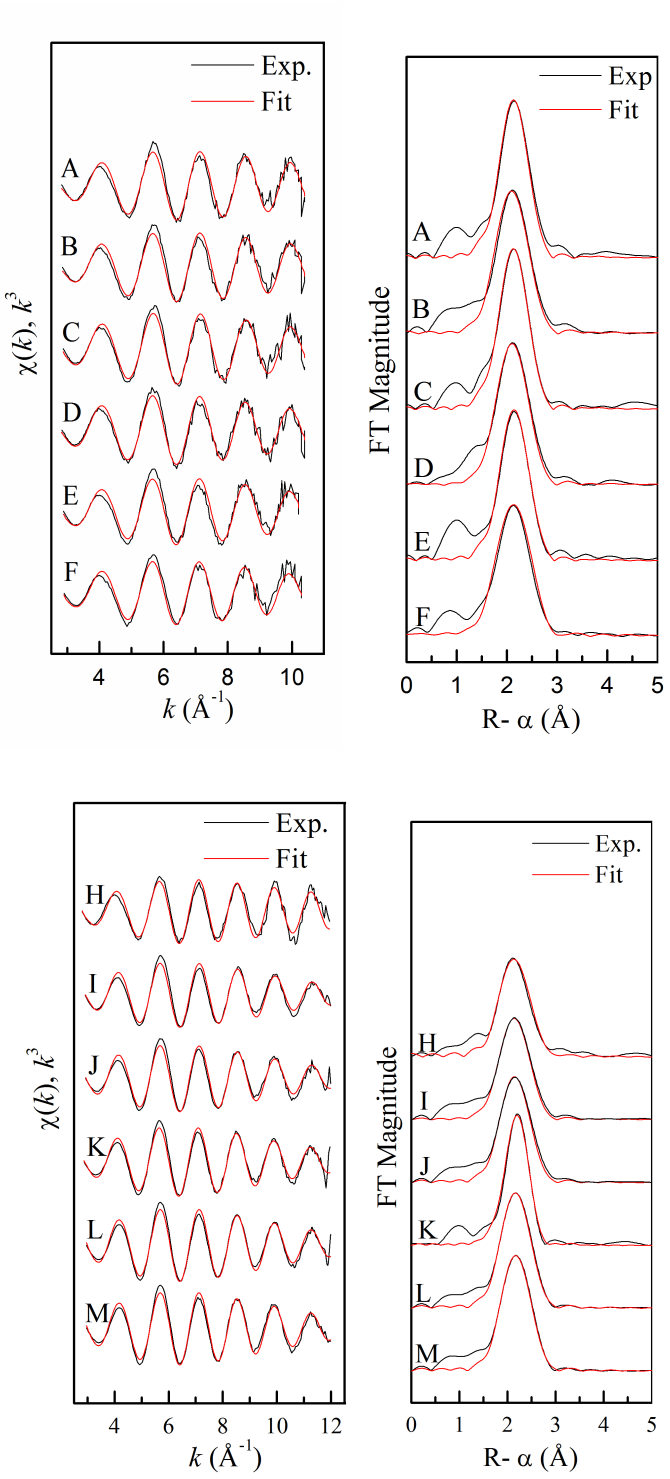

Figure 41: Curve fitting of Pb L_{III}-edge k^3-weighted EXAFS oscillations (left), and corresponding (non phase-shift corrected) Fourier Transforms (right) for Pb(II)-cysteine solutions A – F (top) and H – M (bottom) with fittings for Model II. Fittings with Model I shown for solutions A and H.

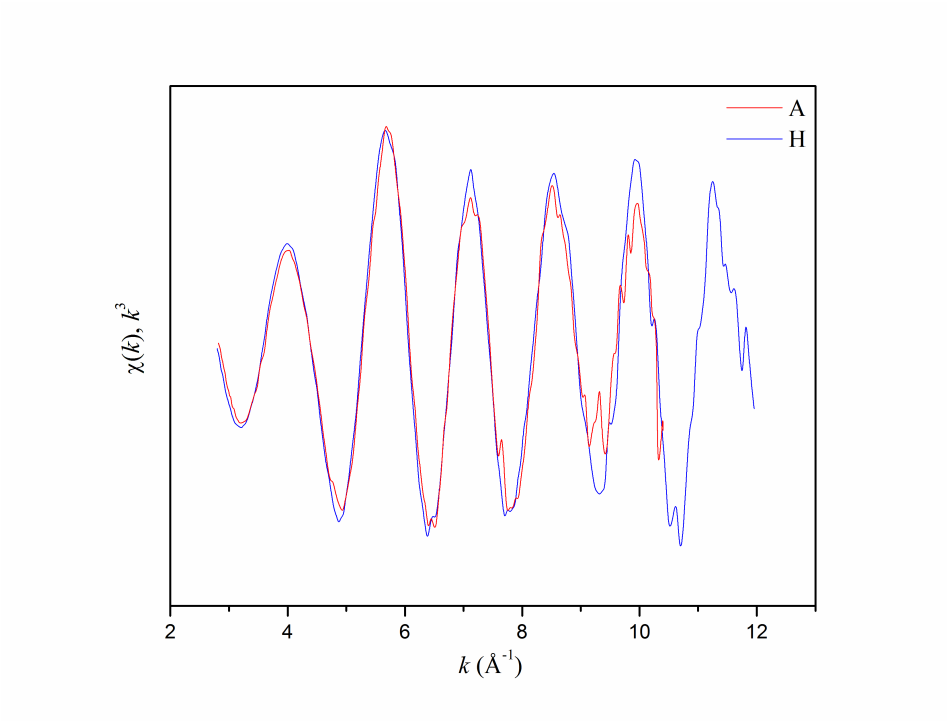

Figure 42: Comparing EXAFS oscillations of Pb(II)-cysteine solutions A and H.

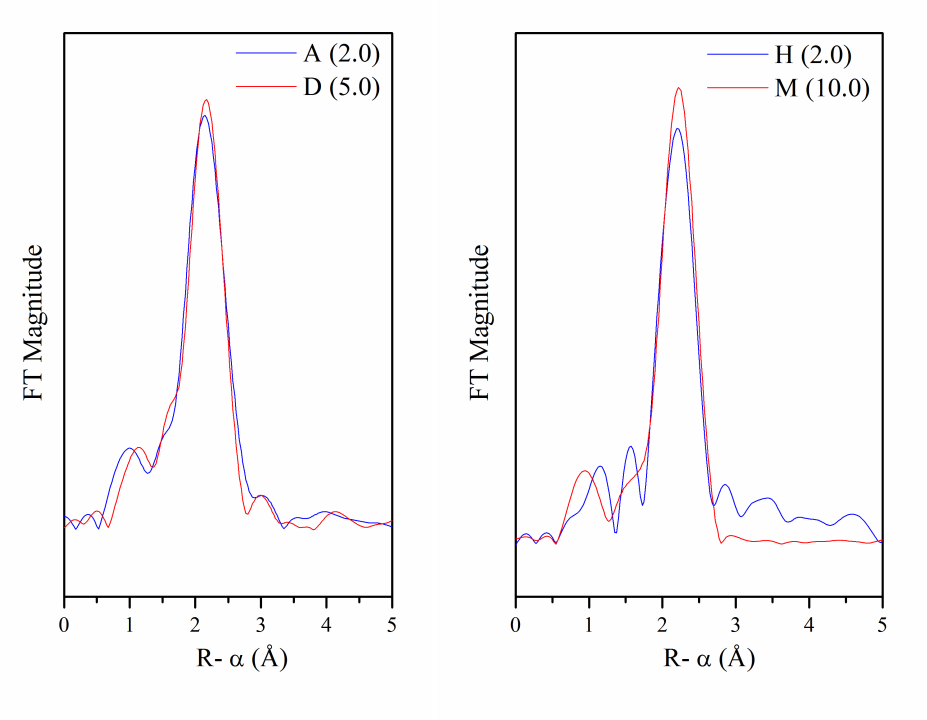

Figure 43: Comparing FT magnitudes of Pb(II)-cysteine solutions A and D and H and M.

Table 15: Least-squares curve fitting results for Pb L_{III}-edge k^3 EXAFS for Pb(II)-cysteine solutions A – M.[a]

			Pb-S		2 Pb-(N/O)		
Solution	Model	N	R (Å)	σ^2 (Å^2)	R (Å)	σ^2 (Å^2)	Residual
A	I	2.0 f	2.64	0.0054	2.43	0.028	25.5
B	I	2.0 f	2.64	0.0053	2.43	0.028	26.2
	II	2.6	2.63	0.0073			23.2
C	I	2.0 f	2.64	0.0056	2.44	0.022	26.5
	II	2.8	2.63	0.0080			22.6
D	I	2.0 f	2.66	0.0056	2.44	0.025	25.6
	II	2.8	2.63	0.0080			23.0
E	I	2.0 f	2.64	0.0055	2.44	0.025	31.0
	II	2.5	2.63	0.0077			26.5
F	I	2.0 f	2.65	0.0063	2.45	0.031	29.9
	II	2.7	2.64	0.0090			25.6
H	I	2.0 f	2.65	0.0042	2.45	0.022	21.4
I	I	2.0 f	2.66	0.0051	2.45	0.017	20.0
	II	2.9	2.64	0.0074			22.0
J	I	2.0 f	2.66	0.0048	2.45	0.016	18.8
	II	3.0	2.65	0.0074			21.5
K	I	2.0 f	2.67	0.0046	2.45	0.014	17.3
	II	3.1	2.65	0.0070			17.8

L	I	2.0 *f*	2.67	0.0045	2.46	0.012	16.9
	II	3.2	2.66	0.0070			17.1
M	I	2.0 *f*	2.67	0.0043	2.46	0.013	19.0
	II	3.2	2.66	0.0070			19.1

[a] $S_0^2 = 0.9$ fixed; *k*-range = 2.8 – 11.9 $Å^{-1}$; $R \pm 0.04$ Å; $\sigma^2 \pm 0.002$ $Å^2$; residual value reflects the deviation between theoretical and experimental EXAFS oscillations.

4.4 Conclusions

Using a combination of information obtained NMR, UV-Vis, and ESI-MS, the Pb(II)-cysteine complexes in solutions A – M are proposed in Figure 44. The position of the wavelength at maximum absorbance in UV-Vis λ_{max} = 298 – 300 nm, and the formation of a shoulder for Pb(II)-cysteine solutions D – G in the 325 – 350 nm region, indicate Pb(II)-cysteine complexation from two to three lead(II)-thiolate interactions, although three-coordinate lead(II)-thiolate is minor at ($[Pb^{2+}]$ = 10 mM). Maximum absorption of LMCT bands for Pb(II)-penicillamine have been found at ~299 nm, suggesting at low concentration, Pb(II)-cysteine possesses a similar coordination tridentate environment (Pb-S_2NO). However, at higher concentrations, three-coordinate Pb(II)-cysteine complexes will form similar to Pb(II)-GSH and Pb(II)-finger protein complexes (Pb-S_3). Low intensity mass peaks observed for Pb(II)-cysteine metal-to-ligand 1:2 and 1:3 complexes is also indicative of the difficulty for more cysteine residues to bind at low concentrations. As increased cysteine becomes available in solution, bis-thiolate, bidentate Pb(II)-cysteine complexes form (Figure 44, centre) and finally, a three-coordinate monodentate Pb(II)-cys_3 complex is formed ($H_2Cys/Pb^{2+} \geq 3.0$).

Using ^{207}Pb NMR as a foundation, and building with EXAFS curve-fitting results using two different models, average Pb-S and Pb-(N/O) distances varied over 2.63 – 2.68 Å and 2.48 – 2.53 Å respectively. Mean Pb-S and Pb-(N/O) distances emerged over smaller ranges when only considering Pb(II)-cysteine solutions H – M, where ^{207}Pb NMR resonances appeared sharper, indicative of fast ligand-exchange on the NMR time-scale. Furthermore, ^{13}C NMR supports the proposed structures, showing a significant $\Delta\delta$ (^{13}C) = 5.0 ppm for Pb(II)-cysteine solution A, and drastically dropping to $\Delta\delta$ (^{13}C) = 1.4 ppm in Pb(II)-cysteine solution B. The changes observed relative to free ligand in ^{13}C NMR suggest a drastic decrease in COO^- coordination as H_2Cys/Pb^{2+} mole ratio is increased from 2.0 to 3.0, while C_2 and C_3 s $\Delta\delta$ (^{13}C) values do not decrease as significantly.

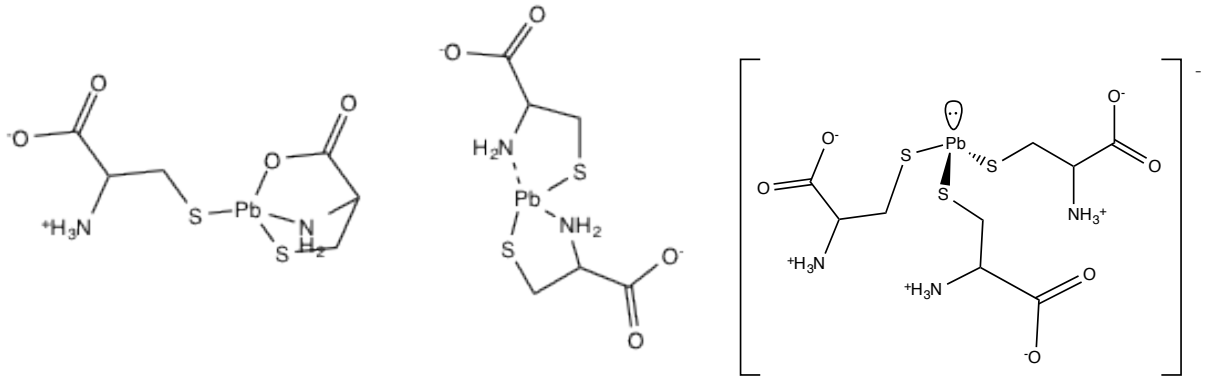

Figure 44: Proposed structure for Pb(II)-cysteine mixture in aqueous solution for Pb(II)-cysteine solutions A and H (left), and B – F and I – M (centre and right) with H_2Cys/Pb^{2+} = 2.0 and ≥ 3.0 respectively.

These spectroscopic results revealed that due to the nature of cysteine as a chelate, it will not favour a specific type of coordination to Pb(II) over the concentrations and mole ratios investigated in this study ([Pb^{2+}] = 10 and 100 mM; H_2Cys/Pb^{2+} = 2.0 – 10.0. ^{207}Pb NMR spectra of Pb(II)-cysteine solutions H – M demonstrated that at higher concentrations, cysteine will form

more Pb(II)-cysteine complexes similar to the Pb(II)-GSH system with PbS_3 coordination geometry, but does not predominantly form the three-coordinate Pb(II)-cys_3 complex, as the chemical shift remains 200 ppm upfield for Pb(II)-cysteine solution M compared to Pb(II)-GSH solution (2793 ppm).[81]

Chapter Five: Conclusions and Future work

Studying Pb(II) complexes with *D*-penicillamine, *N*-acetyl-*L*-cysteine (NAC) and *L*-cysteine gives insight into different modes of chelation to the heavy metal, and elucidation of its behaviour in aqueous alkaline solution. The ^{207}Pb chemical shifts have been obtained, along with structural investigation via X-ray absorption spectroscopy and UV-Vis, for these Pb(II) complexes in aqueous alkaline solution. The Pb(II) complexes proposed in this study differ from many other reports in small molecule Pb(II) systems, where the structures generally have a coordination number of 4 around the Pb(II) ion. A previous study has shown that in sulfur-rich coordination sites, Pb(II) generally avoids four-coordination and instead adopts 3-coordinate trigonal pyramidal or Pb(II)-$S_{5\text{-}8}$.[84]

5.1 Pb(II)-penicillamine system

The results obtained for the Pb(II)-penicillamine system gives further understanding into the chelation of *D*-penicillamine and will afford structural direction in the design of better chelating agents. Four Pb(II)-penicillamine solutions with $[Pb^{2+}]_{total} \approx 10$ mM with H_2Pen:Pb(II) molar ratios of 2.0 – 10.0 at pH 9.6 (pH 10.3 for H_2Pen:Pb(II) ratio 2.0) were investigated by multinuclear NMR, EXAFS and UV-Vis spectroscopy, and ESI-MS (H_2Pen:Pb(II) molar ratios 2.0 and 10.0). Pb(II)-penicillamine species $[Pb(HPen)]^+$, $Na[Pb(Pen)]^+$, and $[Pb(H_2Pen)(HPen)]^+$ were detected in the positive-ion mode ESI-MS spectra. Only one Pb(II)-pencillamine complex $[Pb(Hpen)(Pen)]^-$ was detected in negative-ion mode ESI-MS spectra. ESI mass spectra of

Pb(II)-pencillamine solutions indicate only 1:1 and 1:2 metal-to-ligand species were stable, even at increased ligand concentration, although neutral species are not detected. UV-Vis spectroscopy revealed a consistent ligand-to-metal charge-transfer (LMCT) band at λ_{max} = 299 nm. The LMCT band is comparable to λ_{max} values reported for Pb(II)-complexes with finger protein CP-CCHH (PbS_2N_2)[1] and CadC mutant ($PbS_2(N/O)$[2] at 310 nm and 325 nm respectively. ^{13}C NMR spectra revealed significant $\Delta\delta$ (^{13}C, ppm) values compared to free ligand, for carbon atoms directly bonded to possible coordination sites, for Pb(II)-penicillamine solutions with $H_2Pen:Pb^{2+}$ molar ratios 2.0 – 4.0. ^{13}C NMR resonances of Pb(II)-pencillamine solutions were deshielded compared to free ligand, verifying coordination via thiolate (S^-), amino (NH_2) and carboxylate (COO^-) groups to the lead(II) centre.

Four Pb(II)-penicillamine solutions with $[Pb^{2+}]_{total} \approx 100$ mM with H_2Pen:Pb(II) ratios of 2.0 – 10.0 at pH 9.6 (pH 11.0 for H_2Pen:Pb(II) ratio 2.0) were also investigated by ^{207}Pb NMR and EXAFS spectroscopy. Although the penicillaminatolead(II) crystal structure has been previously reported, the proposed four-coordinate solution-state complex has not been previously established. The average bond lengths obtained by EXAFS spectroscopy for the proposed Pb(II)-penicillamine complex Na[Pb(Pen)(HPen)] was determined by fitting the k^3-weighted experimental EXAFS oscillations using two Pb-S paths and two Pb-(N/O) paths to give an overall Pb-$S_2(N/O)_2$ coordination geometry. All eight aqueous Pb(II)-penicillamine solutions investigated by EXAFS spectroscopy had overlapping experimental EXAFS oscillations. A mean Pb-(N/O) bond distance of 2.45 Å 0.04Å is comparable to the distance found in the crystal structure, while the mean Pb-S distance of 2.64 Å ± 0.04Å falls in the range for lead(II)-thiolate Pb-S distances, but shorter than the distance found in the crystal structure.[3, 4]

^{207}Pb NMR strongly supported that the proposed four-coordinated Pb(II)-penicillamine complex Na[Pb(Pen)(HPen)] is the prevalent Pb(II)-penicillamine species in all eight aqueous solutions with overall Pb-*S_2NO* coordination. The ^{207}Pb resonances appear over the small range 1806 – 1873 ppm for all eight Pb(II)-pencillamine solutions. The slight downfield shift of ^{207}Pb resonances as ligand-to-metal concentration was increased, shows a deshielding of the lead(II) centre. Deshielding is due additional thiol coordination to the metal, from a three-coordinated Pb-(*S*-Pen)$_3$ species formed in minor amounts. The ^{207}Pb chemical shift range (1806 – 1873 ppm) of Pb(II)-penicillamine solutions is deshielded compared to the isotropic chemical shift of 902 ppm obtained for the pencillaminatolead(II) solid and further supports increased thiol coordination to the Pb(II) centre.

5.2 Pb(II)-*N*-acetyl-*L*-cysteine system

N-acetyl-*L*-cysteine is a non-chelating ligand, even at low concentrations. It has been used in conjunction with chelation therapy, to counteract reactive oxygen species created during lead(II) intoxication. Five Pb(II)-NAC solutions with $[Pb^{2+}]_{total} \approx 10$ mM with H_2NAC:Pb(II) molar ratios of 2.0 – 10.0 at pH 9.1, were investigated by multinuclear NMR, EXAFS and UV-Vis spectroscopy, and ESI-MS ($[H_2NAC]_{total}$ = 20, 30 and 100 mM). Five Pb(II)-NAC solutions with $[Pb^{2+}]_{total} \approx 100$ mM with H_2NAC:Pb(II) ratios of 2.0 – 10.0 at pH 9.1 were also investigated by ^{207}Pb NMR and EXAFS spectroscopy. Pb(II)-NAC species $[Pb(HNAC)]^+$, $Na[Pb(HNAC)_2]^+$, $Na_2[Pb(HNAC)(NAC)]^+$, were detected in all solutions; $Na_2[Pb(HNAC)_3]^+$, $Na_3[Pb(HNAC)_2(NAC)]^+$ (when $[H_2NAC]_{total} \geq 3.0$) were detected in positive-ion mode ESI-MS. Pb(II)-NAC complex $[Pb_2(HNAC)(NAC)]^+$ was detected for Pb(II)-NAC solution containing

$[H_2NAC]_{total}$ = 20 mM. No ions were detected in negative-ion mode. ESI mass spectra of Pb(II)-NAC solutions indicate three-coordinated Pb(II)-NAC complexes are stable in the gas-phase, and are formed when $[H_2NAC]_{total} \geq 30$ mM. This is supported by UV-Vis spectra of Pb(II)-NAC solutions. The LMCT band of Pb(II)-NAC solutions were observed from λ_{max} = 318 – 335 nm, shifting to higher wavelengths as the ligand concentration increased. The charge-transfer band of Pb(II)-NAC solutions with $[H_2NAC]_{total} \geq 40$ mM almost identical spectra were obtained, with λ_{max} =335 nm, while solutions with $[H_2NAC]_{total}$ = 20 and 30 mM appeared at 318 nm and 330 nm respectively. The UV-Vis spectra obtained for Pb(II)-NAC solutions were in parallel to the Pb(II)-GSH system.[5] The LMCT bands of the Pb(II)-GSH system were assigned to two lead(II)-thiolate interactions, to dominantly three S-donor atoms coordinated to Pb(II). Similarly, the LMCT bands of Pb(II)-NAC solutions can be assigned to two lead(II)-thiolate interactions when $[H_2NAC]_{total}$ = 20 mM, two to three S-donors when $[H_2NAC]_{total}$ = 30 mM, and mainly three Pb-S interactions when $[H_2NAC]_{total} \geq 30$ mM. Comparable LMCT bands reported for lead(II) complexes also appear in this range ~330 nm.[1, 2, 6-9]

^{13}C NMR spectra revealed that *N*-acetylcysteine is only weakly coordinating to Pb(II) through its COO^- group, if at all. Compared to the Pb(II)-Pen system ($\Delta\delta$-^{13}C = 1.4 – 6.0 ppm), the ^{13}C chemical shift of the carboxylate group shifts only $\Delta\delta(^{13}C)$ = 0.2 – 0.6 ppm with respect to the free ligand. The carbon atom directly bonded to the thiol group, experiences $\Delta\delta(^{13}C)$ = 0.8 – 3.1 ppm, meaning the thiolate (S^-) is coordinated to the Pb(II) centre. These results confirm that *N*-acetylcysteine only binds through the thiolate (S^-) and not through its carboxylate (COO^-) group.

^{207}Pb NMR resonances appeared over a very small range (2764 – 2792 ppm) for seven of the Pb(II)-NAC solutions with H_2NAC:Pb(II) ≥ 3.0. These chemical shifts fall in the same region

as reported for the Pb(II)-GSH system (2793 ppm), especially at higher free ligand concentration, strongly supporting three-coordinated Pb(II)-NAC complexes in these solutions. The ^{207}Pb chemical shift of Pb(II)-NAC solution with $[H_2NAC]_{total}$ = 20 mM appeared deshielded at 2886 ppm compared to the other Pb(II)-NAC solutions. At H_2NAC:Pb(II) mole ratio 2.0, deshielding occurred when a binuclear Pb(II)-NAC complex forms to give an overall PbS_2S' coordination environment.

EXAFS results also support the three-coordinated Pb(II) complexes found in Pb(II)-NAC solutions. Average Pb-S bond lengths obtained by EXAFS spectroscopy were determined by fitting the experimental k^3-weighted oscillations to a model with three Pb-S bonds. A mean Pb-S distance of 2.67 Å ± 0.02 Å obtained is comparable to the distance obtained in an EXAFS study of the Pb(II)-GSH system (2.65 Å).[10]

5.3 Pb(II)-cysteine system

The Pb(II)-cysteine system has promising applications in nanochemistry, especially in the development of nanofibres or membranes, where cysteine can be grafted or "coated" (polymerized) over a large surface area.[53]The ability for cysteine to bind in multiple modes to Pb(II) dependent on both the metal and ligand concentration, can be used as a tool to build various nanostructure morphologies. Six aqueous Pb(II)-cysteine solutions with $[Pb^{2+}]_{total} \approx 10$ mM with H_2Cys:Pb(II) molar ratios of 2.0 – 10.0 at pH 9.1 (pH 10.4 for H_2Cys:Pb(II) ratio 2.0) were investigated by multinuclear NMR, EXAFS and UV-Vis spectroscopy, and ESI-MS (H_2Cys:Pb(II) molar ratios 2.0 and 10.0). Six Pb(II)-cysteine solutions with $[Pb^{2+}]_{total} \approx 100$ mM and H_2Cys:Pb(II) ratios of 2.0 – 10.0 at pH 9.1 (pH 10.4 for H_2Cys:Pb(II) ratio 2.0) were also

investigated by ^{207}Pb NMR and EXAFS spectroscopy. Pb(II)-cysteine species $[Pb(HCys)]^+$, $Na[Pb(Cys)]^+$, $[Pb(HCys)_2(Cys)]^+$ and $[Pb(HCys)(Cys)]^-$ were detected by ESI-MS in positive and negative-ion modes. ESI mass spectra of Pb(II)-cysteine solutions indicate only 1:1 and 1:2 metal-to-ligand species were stable in the gas-phase at $[H_2Cys]_{total}$ = 20 mM ligand concentrations, while 1:3 metal-to-ligand Pb(II)-cysteine complexes are stable when $[H_2Cys]_{total}$ ≥ 30 mM. UV-Vis spectroscopy spectra revealed LMCT bands at λ_{max} ~ 300 nm, comparable to those obtained for Pb(II)-penicillamine solutions at λ_{max} = 299 nm. For Pb(II)-cysteine solutions with $[H_2Cys]_{total}$ = 50 and 80 mM, intensity of the LMCT bands decrease slightly, and Pb(II)-cysteine solution with $[H_2Cys]_{total}$ = 100 mM, the band intensity is decreased significantly. The decrease in LMCT band intensity is due to the formation of a three-coordinate Pb(II)-cysteine complex, which is also evidenced by the appearance of a shoulder in the UV-Vis spectra for Pb(II)-cysteine solutions with $[H_2Cys]_{total}$ = 80 and 100 mM at ~335 nm. Reported LMCT bands of coordinated cysteine residues decreasing from three to two show a shift from 330 to 315 nm.[1, 9]

^{13}C NMR spectra support tridentate coordination of cysteine in Pb(II)-cysteine solutions with Δδ (^{13}C, ppm) = 4.1 – 5.0 ($[H_2Cys]_{total}$ = 20 mM), similar to the Pb(II)-penicillamine system. ^{13}C NMR chemical shifts drastically decrease when $[H_2Cys]_{total}$ is increased to 30 mM, indicating weaker coordination of all three binding sites to the Pb(II) centre. This supports the formation of a three-coordinated Pb(II)-cysteine complex with an overall PbS_3 coordination environment as seen in Pb(II)-GSH and Pb(II)-NAC systems at increased ligand concentration.

EXAFS investigation of Pb(II)-cysteine solutions also support two thiolate coordination (tridentate and bidentate binding) at low ligand concentration to the formation of three-coordinated cysteine to the Pb(II) centre when ligand concentration is increased. Pb(II)-cysteine

solutions were studied by EXAFS using two models with different coordination geometries: Pb$S_2(N/O)_2$ and PbS_3. At lower $[H_2Cys]_{total}$ concentrations, the first model fits better to experimental EXAFS oscillations, while at higher $[H_2Cys]_{total}$ concentrations, the second three-coordinated Pb(II)-cysteine model is a better fit. Average Pb-S and Pb-(N/O) distances of 2.64 Å ± 0.02Å and 2.44 Å ± 0.02Å were obtained for the Pb$S_2(N/O)_2$ model respectively. An average Pb-S bond distance of 2.64 Å ± 0.02Å was obtained for the PbS_3 model, comparable to the distance found for the Pb(II)-GSH system.[5]

^{207}Pb NMR spectra were the strongest indicators of the Pb(II)-cysteine system forming proposed Pb$S_2(N/O)_2$ and PbS_3 coordination geometries that were dependent on free ligand concentration. Compared to the Pb(II)-penicillamine system (~1825 ppm), ^{207}Pb resonances of Pb(II)-cysteine solutions appeared downfield, and more deshielded (2005 – 2507 ppm). Compared to both Pb(II)-NAC and Pb(II)-penicillamine systems, Pb(II)-cysteine resonances appeared over a wider range, confirming more than one Pb(II)-cysteine speciation as ligand concentration is increased. At low ligand concentration (H_2Cys/Pb^{2+} = 2.0 – 5.0), four-coordinated lead species with tridentate and bidentate Pb(II)-cysteine complexes dominate. When $[H_2Cys]_{free}$ = 0 mM, each cysteine ligand is coordinated to the lead centre, in a similar fashion as found in the Pb(II)-penicillamine solution, with the presence of bidentate Pb(II)-cystein complexes causing deshielding. As ligand concentration is increased, especially in Pb(II)-cysteine solution where $[H_2Cys]_{free}$ = 700 mM, a narrow ^{207}Pb resonance observed furthest downfield is due to the dominant three-coordinated (monodentate) Pb(II)-cysteine complex with over all PbS_3 coordination geometry. For Pb(II)-cysteine solutions with $[Pb^{2+}]$ = 10 mM, free ligand concentrations $[H_2Cys]_{free}$ = 10 – 70 mM remain dominantly Pb$S_2(N/O)_2$ tridentate and

bidentate complexes. ^{207}Pb NMR indicate that the free ligand concentration present in Pb(II)-cysteine solutions largely affects the mode of coordination cysteine takes with the Pb(II) centre.

5.4 Future Work

In this study, Pb(II) complex formation with simple thiolate-containing molecules illustrated the different Pb(II) species formed based on available coordination sites. These results provide spectroscopic characterization useful for the study of other Pb(II) complexes with S, N and O donors. Future work can include the expansion to Pb(II) complex formation with larger biomolecules such as dipeptides containing thiol, amine and carboxyl groups. These Pb(II)-dipeptide complexes may give better understanding to Pb(II) speciation in physiological environments. Solid-state analysis via FT-IR or Raman spectroscopic techniques along with XAS and NMR studies of the three Pb(II) systems would give insight into coordination geometry and bond lengths.

N-acetylcysteine and *L*-cysteine can further benefit applications in nanomaterials. Both ligands can be used as precursors as sources of sulfur in PbS nanostructures, modifying nanoparticle morphologies as desired.[54,55] They can also be functionalized within nanostructures, to interact with lead(II) or other heavy metals. Decontamination of water by adsorption of heavy metals for example, can yield good efficiency, while operating at lower cost, if optimal ligand:metal ratios ($C_{Pb(II)} \sim 10 - 100$ ppm) are utilized.[51] Presently, many nanomaterials are produced in excess ligand conditions, and often ligands such as cysteine can self-polymerize undesirably.

Lastly, more effective chelators can be practically designed for the treatment of plumbism, using C-alkylation, and pairing S and N donors to improve chelate stability. The spectroscopic techniques in the study can facilitate the assignment of the coordination environment around the Pb(II) centre.

References

(1) Gross, J. *Mass Spectrometry A Textbook*; Second.; Springer: Heidelberg, 2011.

(2) Shimoni-Livny, L.; Glusker, J.; Bock, C. *Inorg. Chem.* **1998**, *37*, 1853–1867.

(3) Shahid, M.; Dumat, C.; Pourrut, B.; Sabir, M.; Pinelli, E. *J. Geochem. Explor.* **2014**.

(4) Giaccio, L.; Cicchella, D.; De Vivo, B.; Lombardi, G.; De Rosa, M. *J. Geochem. Explor.* **2012**, *112*, 218–225.

(5) Pearce, J. *Eur. Neurol.* **2007**, *57*, 118–119.

(6) Banna, S. *J. Chem. Educ.* **1985**, *62*, 197–198.

(7) McKelvey, D. *J. Chem. Educ.* **1983**, *60*, 112–116.

(8) Cornelis, R.; Caruso, J.; Crews, J.; Heumann, H. *Handbook of Elemental Speciation II: Species in the Environment, Food, Medicine & Occupational Health*; John Wiley & Sons, 2005.

(9) Wahsha, M.; Bini, C.; Fontana, S.; Wahsha, A.; Zilioli, D. *J. Geochem. Explor.* **2012**, *113*, 112–117.

(10) Walsh, A.; Watson, G. W. *J. Solid State Chem.* **2005**, *178*, 1422–1428.

(11) Patrick, L. *Altern. Med. Rev.* **2006**, *11*, 2–22.

(12) Miessler, G.; Tarr, D. *Inorganic Chemistry*; 3rd ed.; Pearson Education Inc.: Upper Saddle River, 2004.

(13) Wander, M.; Clark, A. *Inorg. Chem.* **2008**, *47*, 8233–8241.

(14) Persson, I.; Lyczko, K.; Lundberg, D.; Eriksson, L.; Placzek, A. *Inorg. Chem.* **2011**, *50*, 1058–1072.

(15) Richens, D. *The Chemistry of Aqua Ions*; John Wiley & Sons: Chichester, 1997.

(16) Cruywagen, J.; Van de Water, R. *Talanta* **1993**, *40*, 1091–1095.

(17) Sylva, R. N.; Brown, P. *Dalton Trans.* **1980**, 1577–1581.

(18) Grimes, S.; Johnston, S.; Abrahams, I. *Dalton Trans.* **1995**, 2081–2086.

(19) Seyferth, D. *Organometallics* **2003**, *22*, 2346–2357.

(20) Perera, N.; Hefter, G.; Sipos, P. *Inorg. Chem.* **2001**, *40*, 3974–3978.

(21) Crea, F.; Falcone, G.; Foti, C.; Giuffre, O.; Materazzi, S. *New J. Chem.* **2014**, *38*.

(22) Harrison, R. *Pollution: Causes, Effects and Control*; Fourth.; The Royal Society of Chemistry: Cambridge, 2001; pp. 353–355.

(23) Ji, W.; Yang, T.; Ma, S.; Ni, W. *Energy Procedia* **2012**, *16*, 21–26.

(24) Godwin, H. *Curr. Opin. Chem. Biol.* **2001**, *5*, 223–227.

(25) Ahamed, M.; Siddiqui, M. K. J. *Clin. Nutr.* **2007**, *26*, 400–408.

(26) Philip, A.; Gerson, B. *Clin. Lab. Med.* **1994**, *14*, 423–444.

(27) Gidlow, D. a. *Occup. Med-C* **2004**, *54*, 76–81.

(28) Flora, S.; Tandon, S. *Toxicology* **1990**, *64*, 129–139.

(29) Papanikolaou, N.; Hatzidaki, E.; Belivanis, S.; Tzanakakis, G.; Tsatsakis, A. *Med. Sci. Monitor.* **2005**, *11*, RA329–336.

(30) Dongre, N.; Suryakar, A.; Patil, A.; Hundekari, I.; Devarnavadagi, B. *Indian Journal of Clinical Biochemistry* **2013**, *28*, 65–70.

(31) Soriano, A.; Pallares, S.; Pardo, F.; Vicente, A.; Sanfeliu, T.; Bech, J. *J. Geochem. Explor.* **2012**, *113*, 36–44.

(32) Brookes, P. *Biol. Fert. Soils* **1995**, *19*, 269–279.

(33) Seyferth, D. *Organometallics* **2003**, *22*.

(34) Needleman, H. *Annu. Rev. Med.* **2004**, *55*, 209–222.

(35) Farfel, M.; Chisolm, J. *Environ. Res.* **1991**, *55*, 199–212.

(36) Canfield, R.; Henderson, C.; Cory-Slechta, D.; Cox, C.; Jusko, T.; Lanphear, B. *N. Engl. J. Med.* **2003**, *348*, 1517–1526.

(37) Chisolm, J. *J. Pediatr.* **1968**, *73*, 1–38.

(38) Piomelli, S. *Pediatr. Clin. N. Am.* **2002**, *49*, 1285–1304.

(39) Flora, G.; Gupta, D.; Tiwari, A. *Interdisciplinary Toxicology* **2012**, *5*, 47–58.

(40) Lowry, J. Oral Chelation Therapy for Patients with Lead Poisoning, 2010, 1–13.

(41) Kwong, W. T.; Friello, P.; Semba, R. D. *Sci. Total Environ.* **2004**, *330*, 21–37.

(42) Kasperczyk, A.; Prokopowicz, A.; Dobrakowski, M.; Pawlas, N.; Kasperczyk, S. *Biol. Trace Elem. Res.* **2012**, *150*, 49–50.

(43) Erskine, P.; Norton, E.; Cooper, J.; Lambert, R.; Coker, A.; Lewis, G.; Spencer, P.; Sarwar, M.; Wood, S.; Warren, M.; Shoolingin-Jordan, P. *Biochemistry* **2001**, *312*, 133–141.

(44) Warren, M.; Cooper, J.; Wood, S.; Schoolingin-Jordan, P. *Trends Biochem. Sci.* **1998**, *23*, 217–221.

(45) Erskine, P.; Senior, N.; Awan, S.; Lambert, R.; Lewis, G.; Tickle, I.; Sarwar, M.; Spencer, P.; Thomas, P.; Warren, M.; Shoolingin-Jordan, P.; Wood, S.; Cooper, J. *Nat. Struct. Biol.* **1997**, *4*, 1025–1031.

(46) Bridgewater, B.; Parkin, G. *J. Am. Chem. Soc.* **2000**, *122*, 7140–7141.

(47) Bressler, J.; Kim, K.; Chakraborti, T.; Goldstein, G. *Neurochem. Res.* **1999**, *24*, 595–600.

(48) Weiss, K.; Thurik, F.; Gotthardt, D.; Schafer, M.; Teuful, U. *Clinical Gastroenterology and Hepatology* **2013**, *11*, 1028–1035.

(49) Hancock, R. *Chem. Rev.* **1989**, *89*, 1875–1914.

(50) Chandra, S.; Saleem, H.; Sebastian, S.; Sundaraganesan, N. *Spectrochim. Acta.* **2011**, *A*, 1515–1524.

(51) Tolani, S.; Mugweru, A.; Craig, M.; Wanekaya, A. K. *J. Appl. Polym. Sci.* **2010**, *116*, 308–313.

(52) Li, L.; Wu, J.; Zhao, M.; Wang, Y.; Zhang, H.; Zhang, X.; Gui, L.; Liu, J.; Mair, N.; Peng, S. *Chem. Res. Toxicol.* **2012**, *25*, 1948–1954.

(53) Yang, R.; Aubrecht, K. B.; Ma, H.; Wang, R.; Grubbs, R. B.; Hsiao, B. S.; Chu, B. *Polymer* **2014**, *55*, 1167–1176.

(54) Salavati-Niasari, M.; Sobhani, A.; Khoshrooz, S.; Mirzanasiri, N. *J. Clust. Sci.* **2014**, *25*, 937–947.

(55) Emadi, H.; Salavati-Niasari, M. *Superlattices Microstruct.* **2013**, *54*, 118–127.

(56) Xiong, S.; Xi, B.; Xu, D.; Wang, C.; Feng, X. *J. Phys. Chem. C* **2007**, *111*, 16761–16767.

(57) Cao, H.; Wei, M.; Chen, Z.; Huang, Y. *Analyst* **2013**, *138*, 2420–2426.

(58) Dong, Y.; Tian, W.; Ren, S.; Dai, R.; Chi, Y.; Chen, G. *Appl. Mater. Interfaces* **2014**, *6*, 1646–1651.

(59) Choi, A.; Cho, S.; Desbarats, J.; Lovric, J.; Maysinger, D. *Journal of Nanobiotechnology* **2007**, *5*, 1–13.

(60) Willmott, P. *Introduction to Synchrotron Radiation: Techniques and Applications*; Wiley: Hoboken, 2011.

(61) George, G.; George, S.; Pickering, I. EXAFSPAK, 2001.

(62) Rehr, J.; Kas, J.; Prange, M.; Sorini, A.; Takimoto, Y.; Vila, F. *C. R. Phys.* **2009**, *10*, 549–559.

(63) Fayon, F.; Farnan, I.; Bessada, C.; Coutures, J.; Massiot, D.; J.P, C. *J. Am. Chem. Soc.* **1997**, *119*, 6837–6843.

(64) Coleman, J. *Method. Enzymol.* **1993**, *227*, 16–43.

(65) Summers, M. *Coord. Chem. Rev.* **1988**, *86*, 43–134.

(66) Walshe, J. *Am. J. Med.* **1956**, *21*, 487–495.

(67) Corrie, A.; Walker, M.; Williams, D. *J. Chem. Soc. Dalton* **1976**, 1012–1015.

(68) Kianoush, S.; Balali-Mood, M.; Mousavi, S.; Moradi, V.; Sadeghi, M.; Dadpour, B.; Rajabi, O.; Shakeri, T. *Basic Clin. Pharmacol. Toxicol.* **2012**, *110*, 476–481.

(69) Shannon, M.; Townsend, M. *Ann. Pharmacother.* **2000**, *34*, 15–18.

(70) Kuchinskas, E.; Rosen, Y. *Arch. Biochem. Biophys.* **1962**, *97*, 370–372.

(71) Ohlsson, W. *Brit. Med. J.* **1962**, 1454–1456.

(72) Goldberg, A.; Smith, J.; Lochhead, A. *Brit. Med. J.* **1963**, 1270–1275.

(73) Beattie, A. D. *P. Roy. Soc. Med.* **1977**, *70*, 43–45.

(74) Delangle, P.; Mintz, E. *Dalton Trans.* **2012**, *41*, 6359–6370.

(75) Doornbos, D.; Faber, J. *Pharm. Weekblad.* **1964**, *99*, 289–316.

(76) Andersen, O. *Chem. Rev.* **1999**, *99*, 2683–2710.

(77) Abu-Dari, K.; Karpishin, T.; Raymond, K. *Inorg. Chem.* **1993**, *32*, 3052–3055.

(78) Freeman, H.; Stevens, G.; Taylor, I. *J. Chem. Soc. Chem. Comm.* **1974**, 366–367.

(79) Schell, A. C.; Parvez, M.; Jalilehvand, F. *Acta crystallographica, Section E: Structure Reports Online* **2012**, *68*, m489–90.

(80) Rehr, J.; Albers, R. *Rev. Mod. Phys.* **2000**, *72*, 621–654.

(81) Mah, V.; Jalilehvand, F. *Inorg. Chem.* **2012**, *51*, 6285–6298.

(82) Willans, M.; Demko, B.; Wasylishen, R. *Phys. Chem. Chem. Phys.* **2006**, *8*, 2733–2743.

(83) Mason, H.; Hirner, J.; Xu, W.; Parise, J.; Phillips, B. *Magn. Reson. Chem.* **2009**, *47*, 1062–1070.

(84) Magyar, J.; Weng, T.-C.; Stern, C.; Dye, D.; Payne, J.; Bridgewater, B.; Mijovilovich, A.; Parkin, G.; Zaleski, J.; Penner-Hahn, J.; Godwin, H. *J. Am. Chem. Soc.* **2005**, *127*, 9495–9505.

(85) Burnett, T.; Dean, P.; Vittal, J. *Can. J. Chem.* **1994**, *72*, 1127–1136.

(86) Rupprecht, S.; Langemann, K.; Lugger, T.; McCormick, J.; Raymond, K. *Inorg. Chim. Acta* **1996**, *243*, 79–90.

(87) Andersen, R.; DiTargiani, R.; Hancock, R.; Stern, C.; Goldberg, D.; Godwin, H. *Inorg. Chem.* **2006**, *45*, 6574–6576.

(88) Briand, G.; Smith, A.; Schatte, G.; Rossini, A.; Schurko, R. *Inorg. Chem.* **2007**, *46*, 8625–8637.

(89) Hardin, S.; Healy, P.; Mumme, W.; White, A.; Winter, G. *Aust. J. Chem.* **1982**, *35*, 2423–2433.

(90) Appleton, S.; Briand, G.; Decken, A.; Smith, A. *Dalton Trans.* **2004**, 3515–3520.

(91) Bharara, M. S.; Parkin, S.; Atwood, D. a. *Inorg. Chim. Acta* **2006**, *359*, 3375–3378.

(92) Clark-Baldwin, K.; Tierney, D.; Govindaswamy, N.; Gruff, E.; Kim, C.; Berg, J.; Koch, S.; Penner-Hahn, J. *J. Am. Chem. Soc.* **1998**, *120*, 8401–8409.

(93) Guzeloglu, S.; Yalcin, G.; Pekin, M. *J. Organomet. Chem.* **1998**, *568*, 143–147.

(94) Picquart, M.; Abedinzadeh, Z.; Grajcar, L.; Baron, M. *Chem. Phys.* **1998**, *228*, 279–291.

(95) Jalilehvand, F.; Leung, B.; Izadifard, M.; Damian, E. *Inorg. Chem.* **2006**, *45*, 66–73.

(96) Wagner-Roos, L.; Zahn, H.; Sequaris, J.; Valenta, P. *Toxicol. Environ. Chem.* **1989**, *22*, 77–90.

(97) Busenlehner, L.; Weng, T.-C.; Penner-Hahn, J.; Giedroc, D. *J. Mol. Biol.* **2002**, *319*, 685–701.

(98) Rupprecht, S.; Franklin, S.; Raymond, K. *Inorg. Chim. Acta* **1995**, *235*, 185–194.

(99) Neupane, K.; Pecoraro, V. *Angew. Chem., Int. Ed.* **2010**, *49*, 8177–8180.

(100) Aramini, J.; Hiraoki, T.; Yazawam, M.; Yuan, T.; Zhang, M.; Vogel, H. *J. Biol. Inorg. Chem.* **1996**, *1*, 39–48.

(101) Arsenault, I.; Dean, P. *Can. J. Chem.* **1983**, *61*, 1516–1523.

(102) dean, P.; Vittal, J.; Payne, N. *Inorg. Chem.* **1984**, *23*, 4232–4236.

(103) Kozlowski, H.; Urbanska, J. *Polyhedron* **1990**, *9*, 831–837.

(104) Rousselot-Pailley, P.; Sénèque, O.; Lebrun, C.; Crouzy, S.; Boturyn, D.; Dumy, P.; Ferrand, M.; Delangle, P. *Inorg. Chem.* **2006**, *45*, 5510–5520.

(105) Neupane, K. P.; Pecoraro, V. L. *J. Inorg. Biochem.* **2011**, *105*, 1030–1034.

(106) Mah, V.; Jalilehvand, F. Heavy Metal Complex Formation with Glutathione, University of Calgary: Calgary, 2009, Vol. PhD, p. 276.

(107) Duan, J.; Jiang, X.; Ni, S.; Yang, M.; Zhan, J. *Talanta* **2011**, *85*, 1738–1743.

(108) Kramer, R. *Angew. Chem., Int. Ed.* **1998**, *37*, 772–773.

(109) Wang, Y.; Hemmingsen, L.; Giedroc, D. *Biochemistry* **2005**, *44*, 8976–8988.

(110) De Silva, P.; Gunaratne, N.; Gunnlaugsson, T.; Huxley, A.; McCoy, C.; Rademacher, J.; Rice, T. *Chem. Rev.* **1997**, *97*, 1515–1566.

(111) Gockel, P.; Vahrenkamp, H. *Helv. Chim. Acta* **1993**, *76*, 511–520.

(112) Wrathall, D.; Izatt, R.; Christensen, J. *J. Am. Chem. Soc.* **1964**, *86*, 4779–4783.

(113) Li, N.; Manning, R. *J. Am. Chem. Soc.* **1955**, *77*, 5225–5228.

(114) Payne, J. C.; Ter Horst, M. a; Godwin, H. A. *J. Am. Chem. Soc.* **1999**, *121*, 6850–6855.

(115) Kane-Maguire, L.; Riley, P. *J. Coord. Chem.* **1993**, *28*, 105–120.

(116) Wrackmeyer, B. *Annu. Rep. NMR Spectrosc.* **2002**, *47*, 1–37.

(117) Fleischer, H.; Schollmeyer, D. *Inorg. Chem.* **2004**, *43*, 5529–5536.

(118) Agre, V.; Shugam, E. *Russian Journal of Structural Chemistry* **1971**, *12*, 84–88.

(119) Perez, R.; Sousa, C.; Vankeersbilck, T.; Machado, M.; Soares, E. *Curr. Opin. Microbiol.* **2013**, *67*, 300–305.

(120) Dance, I.; Guerney, P. *Aust. J. Chem.* **1981**, *34*, 57–64.

(121) Fleischer, H.; Dienes, Y.; Mathiasch, B.; Schmitt, V.; Schollmeyer, D. *Inorg. Chem.* **2005**, *44*, 8087–8096.